Materials Research Institute

FY 1998 Annual Report

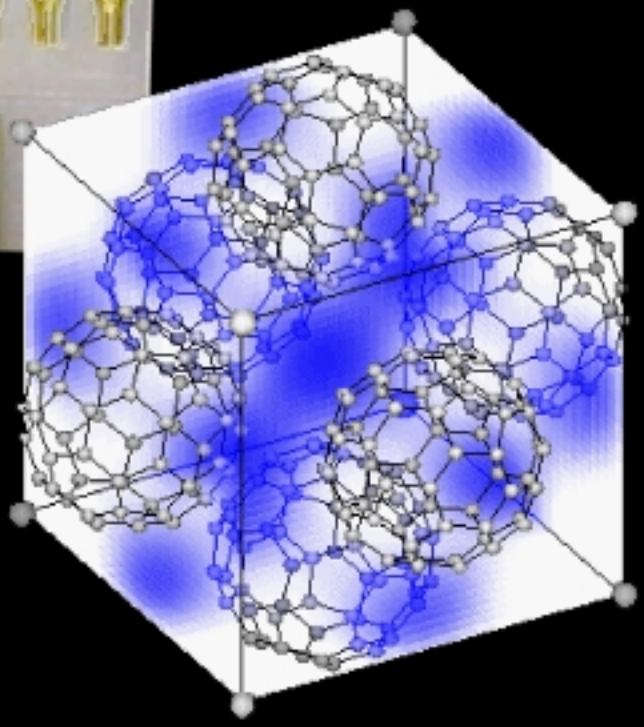

MATERIALS RESEARCH MRI INSTITUTE

University of California
Lawrence Livermore National Laboratory
UCRL-LR-136428

AUSPICES

This work was performed under the auspices of the U.S. Department of Energy by University of California Lawrence Livermore National Laboratory under contract No. W-7405-Eng-48. **UCRL-LR-136428**

Materials
Research
Institute

FY 1998
Annual Report

Edited by

Harry B. Radousky

Materials Research Institute
Lawrence Livermore National Laboratory

Acknowledgments:

Scientific Editor – Harry B. Radousky

Publication Coordinator – Karen Fink

Publication Editor/Graphics – Marsha McInnis

Copy Edit – Jan Tweed

About the Cover:

The cover illustrates a project from each of the three topical areas within the MRI. From left to right: Biomaterials – 3-D surface of the void spores in bone, showing the canal networks and fine details of the surfaces; Electro/Optical Materials – Blue LED based on Si Nanocrystals; Metal/Organic Materials – Positron distribution in C_{60}.

Table of Contents

OVERVIEW

PROJECTS

APPENDICES

MRI Director's Message

The Materials Research Institute (MRI) is the newest of the University/LLNL Institutes and began operating in March 1997. The MRI is one of five Institutes reporting to the LLNL University Relations Program (URP), all of which have as their primary goal to facilitate university interactions at LLNL. This report covers the period from the opening of the MRI through the end of FY98 (September 30, 1998). The purpose of this report is to emphasize both the science that has been accomplished, as well as the LLNL and university people who were involved. The MRI is concentrating on projects, which highlight and utilize the Laboratory's unique facilities and expertise. Our goal is to enable the best university research to enhance Laboratory programs in the area of cutting-edge materials science.

The MRI is focusing on three primary areas of materials research: **Biomaterials** (organic/inorganic interfaces, biomemetic processes, materials with improved biological response, DNA materials science); **Electro/Optical Materials** (laser materials and nonlinear optical materials, semiconductor devices, nanostructured materials); and **Metals/Organics** (equation of state of metals, synthesis of unique materials, high explosives/polymers). In particular we are supporting projects that will enable the MRI to begin to make a distinctive name for itself within the scientific community and will develop techniques applicable to LLNL's core mission. This report is organized along the lines of these three topic areas.

A fundamental goal of the MRI is to nucleate discussion and interaction between Lab and university researchers, and among Lab researchers from different LLNL Directorates. This is accomplished through our weekly seminar series, special seminar series such as Biomaterials and Applications of High Pressure Science, conferences and workshops, our extensive visitors program and MRI lunches. We are especially pleased to have housed five graduate students who are performing their thesis research in residence at the MRI, and to have supported seventeen additional graduate students who are performing their thesis work on campus in collaboration with a LLNL researcher. One of the main objectives of the MRI is to use its portfolio to help develop the next generation of materials scientists in LLNL's areas of competency. As the MRI continues to grow, we look forward to continually expanding and strengthening the variety of collaborations, which form the basis of the MRI's research activities.

Harry B. Radousky,
Acting Director – Materials Research Institute
Deputy Director – University Relations Program

HIGHLIGHTS:

MATERIALS RESEARCH INSTITUTE

The MRI is focusing on three primary areas of materials research: Electro/Optical Materials, Biomaterials, and Metals/Organics. In this section we highlight several projects within each area that have made significant advances. All the projects described in this report are characterized by a strong collaboration between university and Lab researchers.

Our goal is to collaborate with the best university researchers to enhance Lab programs in cutting-edge materials science areas. In particular we support projects that utilize the Laboratory's unique facilities and expertise in material sciences.

Metals/Organics

New Theoretical Framework for Computing Positron Annihilation Characteristics

Positrons are a sensitive probe of open volume defects in materials including vacancies and vacancy clusters, dislocations, and grain boundaries. Theoretical calculations of positron observables are essential for interpreting positron experimental data. We have collaborated with UC-Davis and developed a new computer program using the general Finite Element (FE) approach for calculating positron lifetimes and distributions in materials that is suitable for very large systems and for both open- and close-packed geometries. It is now an established tool for calculating positron lifetimes in the Positron Group at LLNL.

The reliability of this program was tested by calculating the positron lifetime for 23 elemental metals and a number of elemental vacancies in metals, and obtained excellent agreement with both previous calculations and experimental data. A three-dimensional (3-D) representation of the positron distribution in pure C60 is shown in Figure 1, the result of a calculation on a 240-atom-unit cell structure.

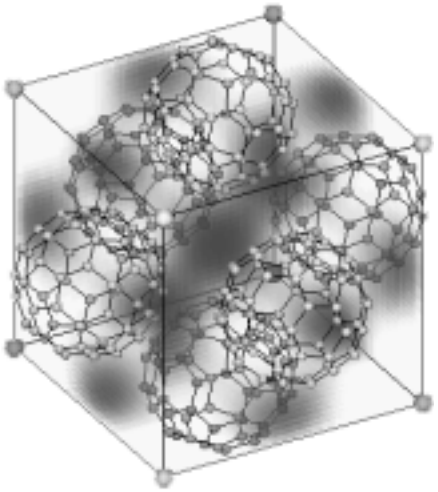

Figure 1. Positron distribution in crystalline C60. For clarity, only the face-centered C60 molecules are shown.

Extreme States of Matter on Nova

Dynamic diffraction experiments to diagnose shocked solid-state lattices on intense lasers have been developed. We collaborated with UC-San Diego, Univ. of Oxford, and Los Alamos Nat'l Laboratory to successfully develop dynamic diffraction experiments on (111) and (400) Silicon lattices, both on the Nova laser and on the Trident laser.

The goal of this endeavor was to technically assess whether dynamic diffraction could be developed into a robust diagnostic of solid-state lattices under shock loading. Successful observation of shock-compressed lattices in the direction of shock propagation in Si has been observed. Development of a diagnostic to observe the transition to 3-D is ongoing, with this work continuing on the Omega and Trident lasers.

Biomaterials

Micromechanical Modeling of Cortical Bone Deformation

Cortical bone is an extremely variable biological composite material system capable of adaptive structural changes in response to the types and quantities of loading experienced. The elastic stiffness and fatigue strength of cortical bone have been shown to vary with anatomic site, age, strain rate, and loading direction. The fatigue of bone under normal physiological loading conditions increases with age and could cause microdamage accumulation. Understanding the deformation models of cortical bone requires precise tissue level properties and microstructural detail.

To study the three-dimensional nature of microstructure and the locations where damage is initiated, we utilized four experimental techniques: x-ray tomographic microscopy (XTM), atomic force microscopy, electron microscopy, and mechanical deformation) to generate data as model input parameters. In collaboration with UC-San Francisco, we were able to identify the mineralization state associated with the bone remodeling process, architectural length scales, and variations in mineralization with age from the XTM data. The approach to be explored further in the future is incorporation of the tomographic data into finite element models.

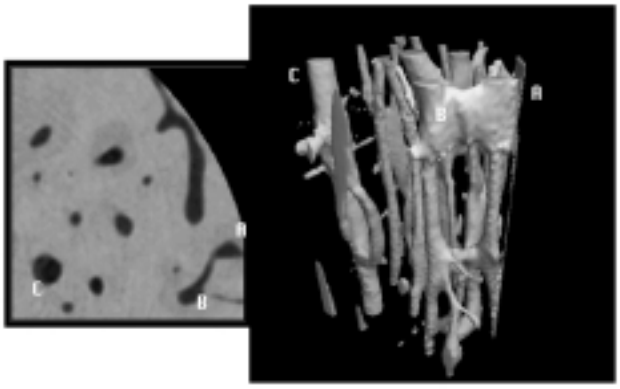

Figure 2. Sites of remodeling in the active mineralization phase in the osteon (tomographic cross-section on the left); The three-dimensional surface of the void spaces (at a constant mineral content) show the canal networks orientation and fine details of the surfaces. Locations A, B, and C in the tomographic cross-section are mapped onto the tissue surface.

Center for Laser Imaging and Cancer Diagnostics

The objective of this research effort is to develop a subsurface imaging system that can offer enhanced imaging depth (up to 1 cm) based on the spectral polarization difference imaging technique (SPDI). This technique requires the use of different illuminating wavelengths in combination with polarization techniques to obtain images of subsurface tissue structures at different depth zones based on their difference in absorption, scattering and depolarization. This project is part of a DOE Center for Excellence in Laser Medicine, which is based at City College of New York, (CCNY), and is hosted at LLNL within the MRI.

For the coming year, we will apply the knowledge gained in recent experiments to an imaging system being built to be used at the pathology room at the UC-Davis Cancer Center. This system will be computer controlled and user friendly. The aim is to investigate the usefulness of this technology in

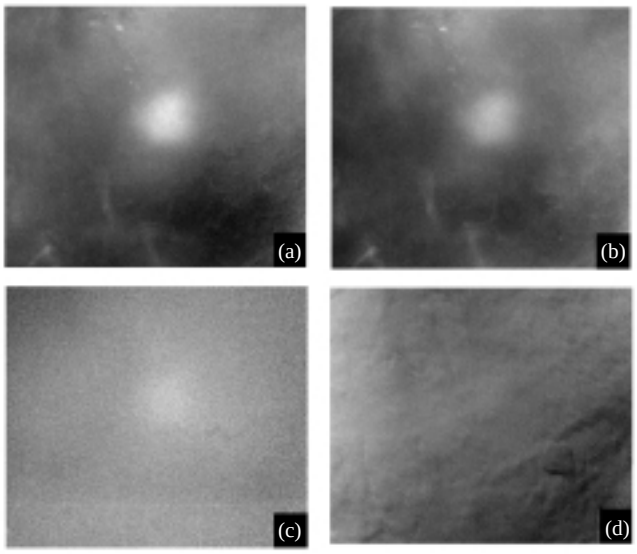

Figure 3. Subsurface images of a high scattering object located 1-cm underneath the surface of chicken breast tissue using the spectral polarization difference imaging technique and 600 nm, 690 nm, 770 nm and 970 nm illumination. (a) [970-600] nm SPDI image, (b) [970-770] nm SPDI image, (c) [770-690] nm SPDI image and d) [690-600] nm SPDI image.

a clinically relevant environment.

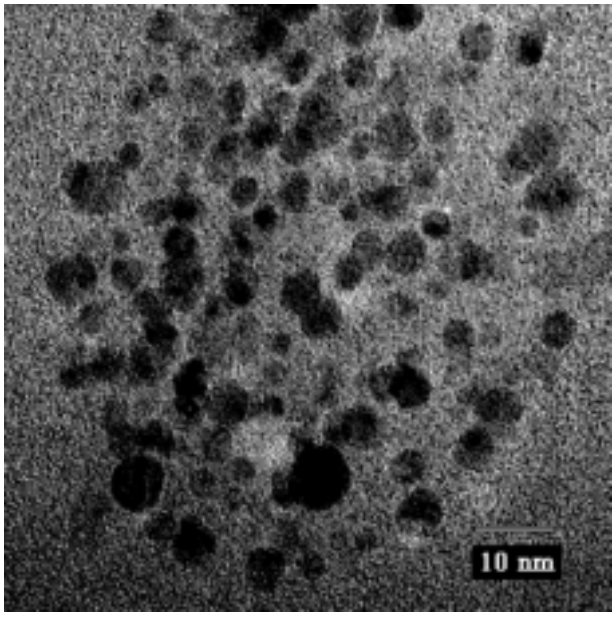

Figure 4. The HRTEM image for silicon nanoclusters terminated with methyl.

Electro/Optical Materials

The Study of Photoluminescence and Device Applications of Si Quantum Dots

In conjunction with UC-Davis, we investigated Mg_2Si as a reagent to prepare Si nanoclusters. We also showed that these nanoclusters can be prepared without oxygen on the surface. In accompanying figure, we show a micrograph for the methyl-terminated silicon nanoclusters, which contains a large number of nanoclusters. This is produced from a reaction starting with Mg_2Si. For some of the larger nanoclusters (5 nm), the outline of a hexagonal shape can be discerned. The sizes range from 1 nm to 4-5 nm for a typical synthesis with only one lattice fringe orientation visible. Lattice fringes are measured from the negatives and are consistent with the {111} crystal plane of Si. We have also developed a convenient and versatile technique for the synthesis of a variety of alkyl-terminated silicon nanocrystallites. These nanoclusters photoluminesce strongly in the blue, providing the basis for a new generation of opto-electronic devices.

Nanoscale Study of Strain and Strain Dynamics in Nonlinear Optical Materials

Strain and fracture dynamics is an exploding new area of physics. In collaboration with UC-Riverside we are studying surface stress and strain dynamics in optical components (laser materials and nonlinear optical materials) with nanometer resolution using a variety of scanning microscopes such as the Near-Field Scanning Optical Microscope (NSOM), Atomic Force Microscope (AFM) and Scanning Tunneling Microscope (STM). The stresses in optical components are associated with defects incorporated during fabrication of the optical components, especially the cutting and polishing stages. These nanoscale stresses and strains will exacerbate failure mechanisms in the optical components. Also, given the high intensity optical beams that are transmitted through the optical components, even small phase differences and/or polarization rotations that are introduced by the nanometer scale defects could eventually result in a loss of coherence in the transmitted optical beam. We have used a NSOM and AFM to identify and characterize nanometer- sized surface and subsurface defects in optical components at LLNL.

BIOMATERIALS

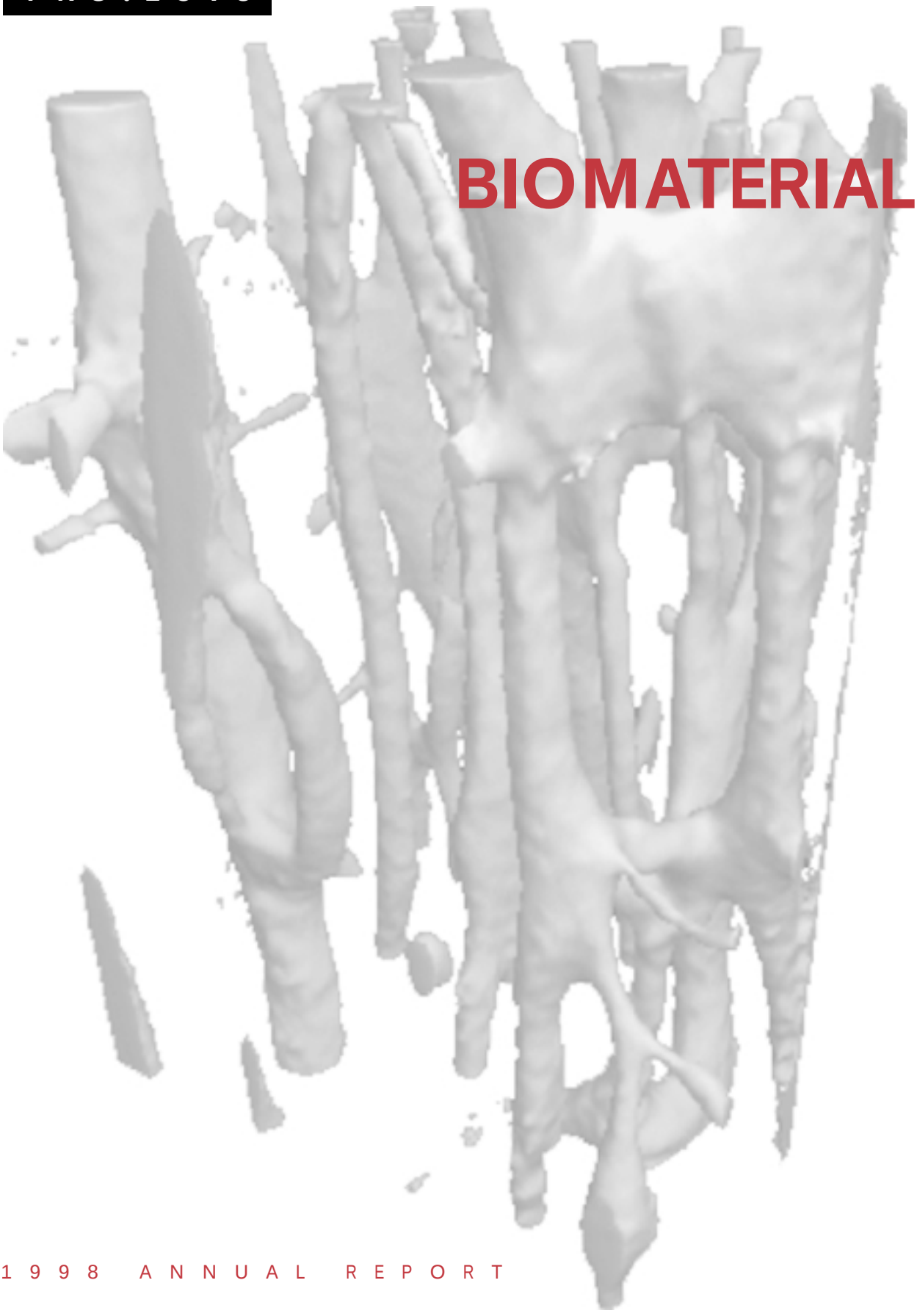

Device Miniaturization Through Self-Assembly: An *In Situ* AFM Study of Molecular Scaffolds

UC Principal Investigator: *Professor G. Taynas R. Palmore, UC-Davis*
LLNL Collaborator: *James De Yoreo*
Students: *Mary McBride, Tracie Martin, Tzy Jian (Mark) Luo, UC-Davis*

Although the manipulation of individual molecules into large aggregates with well-defined shapes is masterfully demonstrated in nature,[1] the deliberate control of molecular orientation in solids by researchers is still in its infancy.[2] Efforts have begun, however, to exploit the strength, directionality and selectivity of hydrogen bonds to control the orientation of molecules in the solid state.[3-6] Our approach to engineering the structure of crystalline solids is to design molecules to self-assemble into one- and two-dimensional aggregates that serve as scaffolds with which to control three-dimensional structure. To this end, we are using derivatives of 2,5-diketopiperazines (DKPs) as our molecular building blocks (Figure 1a).[7] The selection of DKPs is based on several criteria that include: the presence of a pair of secondary amides held in cis conformation, which should promote the formation of a robust, one-dimensional aggregate we refer to as "tapes" (Figure 1b); the near planarity and conformational rigidity of the six-membered ring, which should decrease the occurrence of polymorphism caused by conformational mobility in the backbone of the tapes; the relative ease of synthesis; and avenues for systematic variation of molecular properties such as size, shape, symmetry, hydrogen-bonding ability and hydrophobicity through changes in X.

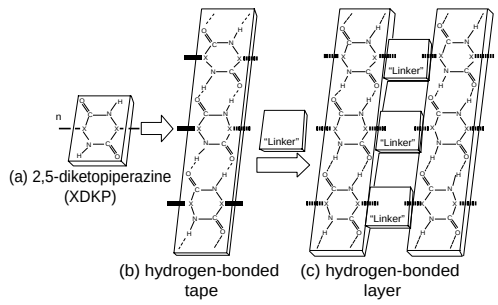

Figure 1. a) Generic 2,5-diketopiperazine (XDKP) where X represents a substituted carbon atom. b) Tape that results when each XDKP forms a pair of hydrogen bonds (dashed lines) with two adjacent XDKPs. c) The layer that results when adjacent parallel tapes are cross-linked either directly through functional groups on X or indirectly through co-crystallization with "linker" molecules. Linker molecules provide an avenue for introducing optical, magnetic, and conductive properties into the solid.

Our interests in molecules that form tapes are based on the following rationale: First, tapes are one-dimensional aggregates. Engineering solid-state structure based on the manipulation of a robust aggregate has the advantage of limiting the number of ways a molecule can pack in the crystal, thus improving our ability to predict the structure of a crystal. Second, tapes are good systems for examining how molecular structure and symmetry influences crystalline structure. For example, non-symmetrical or chiral derivatives should influence the relative orientation of these molecules within a tape and consequently, the relative orientation of tapes with respect to each other. Third, parallel tapes can function as scaffolds for controlling the position of guest molecules within the solid (Figure 1c), which can be the source of new properties in the bulk phase.[8-9,10] Fourth, crystalline solids that contain tapes are ideal for *in situ* AFM studies. The presence of tapes in crystalline solids of related molecular structure suggests that the mechanisms of nucleation and growth are similar (tapes often pack with their long axes parallel and the periodicity of DKPs within a tape are nearly invariant). Consequently, tapes are a unique structural motif that can be systematically modified in the direction perpendicular to the long axes of the tape (i.e., by changing X in the DKPs). These changes to X will influence the energetics of the surfaces orthogonal to the long axis of the tape and their kinetics of crystal growth, which we can observe and quantify with *in situ* AFM.

Our program of research addresses some of the critical issues surrounding crystallization. These issues include: (1) The effect of variations in molecular structure on growth mechanisms and the kinetics of crystal growth, (2) the influence of molecular structure on the morphology of crystals, and (3) the relationship between crystallization conditions and defect structure in crystals.

Accomplishments

During the past year, the collaboration between the Palmore (UC-Davis) and De Yoreo (LLNL) laboratories has resulted in the establishment of an AFM facility at UC-Davis in which *in situ* atomic-force microscopy studies

can be conducted, the training of two UC-Davis graduate students in the use of this technique, and the completion of *in situ* AFM experiments on the glycine derivative of 2,5-diketopiperazine (GLYDKP) at a level suitable for publication. The results obtained from these experiments have been presented at numerous conferences and are described in two manuscripts, one of which is published and the second of which is in preparation. In addition, the Palmore group has published four other manuscripts on amide chemistry and diketopiperazines that are related to the work accomplished through the UCD-LLNL collaboration.

We have investigated nucleation, step dynamics, evolution of surface morphology and generation of defects during solvent-mediated crystallization of the glycine derivative of 2,5-diketopiperazine (GLYDKP). This solid is the simplest member in the series of molecular solids that we are studying (Figure 2). Each solid in this series is different in terms of the structure of its molecular constituents, but in all of these solids the tape motif is maintained in the crystalline lattice. By using the AFM, we determined how step morphology, step speed, nucleation rates, terrace widths and step-step interactions in GLYDKP depend on solution and solute composition. From these experiments, we determined the values of the energetic and kinetic factors controlling the growth of GLYDKP. The remaining four solids have been synthesized and characterized crystallographically and presently are being imaged during their growth to determine the effect that their structural variations have on the energetics and kinetics of crystal growth. For example, we expect the size of the terraces in GLYDKP to be quite different from those of ASPDKP due to the protic nature of X in ASPDKP. Establishing a correlation between molecular structure and the thermodynamics and kinetics of crystal growth is the solid-state equivalent to the solution studies of Hammett,[11] who developed the theory used to predict the reactivity of a molecule in a given reaction based on its molecular structure. Our studies aim to establish this correlation and may provide parameters with which to predict the structure and

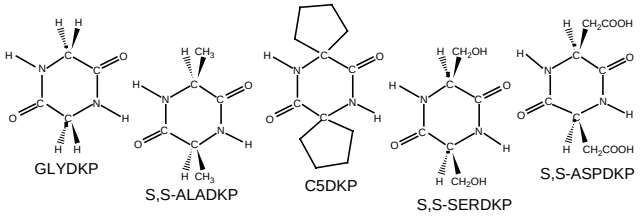

Figure 2. Crystalline solids of these molecules will be studied by in situ AFM. Each molecule contains the DKP molecular fragment responsible for tape formation. X is systematically changed in terms of its size, shape, stereochemistry, hydrophobicity, and ability to form hydrogen bonds.

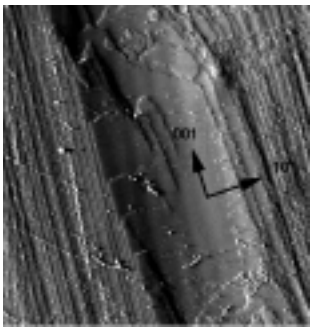

Figure 3. AFM image (50 μm x 50 μm) of a crystal of GLYDKP. Elliptically-shaped hillock illustrates the anisotropy in the kinetics of crystal growth at the 001 and -101 surfaces.

morphology of crystalline solids based on knowledge of molecular structure.

We have established that crystals of GLYDKP grow in a narrow range of concentrations (0.16–0.18 M at room temperature) and consequently, must be monitored for the presence of microcrystals during the *in situ* AFM experiments. Crystals of GLYDKP grow anisotropically resulting in elliptically shaped hillocks (Figure 3) with steps advancing along the direction of the hydrogen bonded tapes {001} at rates that are ~6x's faster than those perpendicular to the direction of the tapes {–101}. This difference in kinetics of crystal growth at the two different faces may result from either a greater sticking coefficient for molecules attaching at the end of the tapes (to form hydrogen-bonds) or the presence of a pathway for fast diffusion along the long axis of the tapes. Two-dimensional nucleation is not observed on the surface of a growing crystal of GLYDKP. Growth of a crystal of GLYDKP appears to initiate exclusively from complex screw dislocations generating two types of step edges, straight (–101) and jagged (001).

The velocity at which the {–101} step-edge of GLYDKP advances was measured at nine different concentrations (Figure 4a). From this data, the equilibrium concentration of GLYDKP was extrapolated (0.1589 M or 10^{20} molecules ml^{-1}), and from the slope of a plot of step velocity versus supersaturation (Figure 4b), the value of the kinetic coefficient, β, was determined. This fundamental materials parameter reflects the height of the barriers (i.e., $\Delta G‡$) for the adsorption, diffusion and incorporation of molecules of GLYDKP into the crystalline lattice at the –101 face. Large values for β indicate that the barriers to these processes are low; small values for β indicate that the barriers are high. The value of β for growth at the –101 face of GLYDKP is 3×10^{-3} cm^2 s^{-1}, which is considerably smaller than that found for ionic solids such as KH_2PO_4 or $CaCO_3$ (i.e., β = 0.1–0.3 cm^2 s^{-1}) but larger than that found for crystals of macromolecules (e.g., β for canavalin is 1×10^{-4} cm^2 s^{-1}). Due to the nature of the crystalline lattice of GLYDKP, molecules diffuse to the 001 face

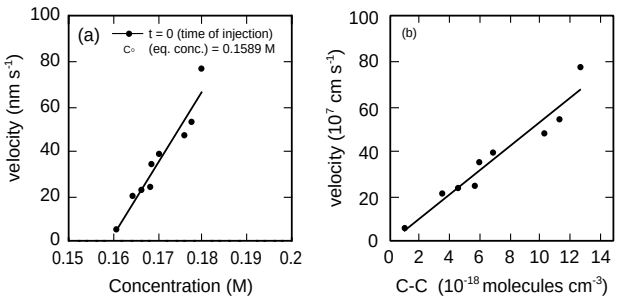

Figure 4. (a) Velocity of step advancement (-101) vs. concentration. This data is used to extrapolate the equilibrium concentration (C°) of GLYDKP at v = 0; (b) Velocity data plotted as a function of supersaturation (C-C°) to determine the value of β (is 3 x 10^{-3} cm^2 s^{-1}).

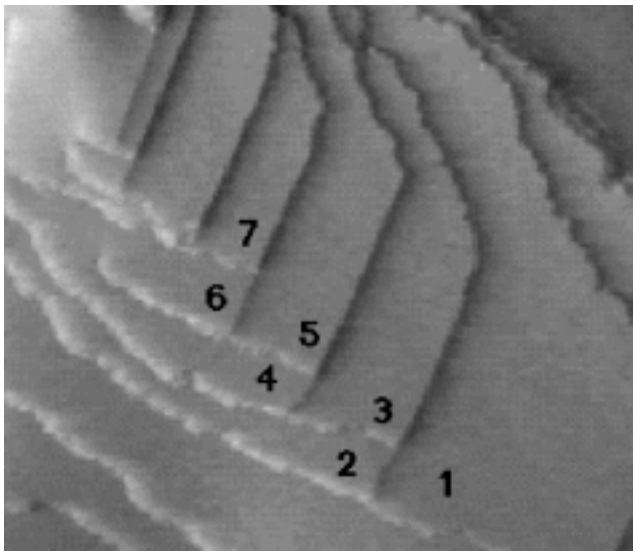

Figure 5. Interlacing in a growing crystal of GLYDKP. Layers of growth are labelled sequentially 1–7. All step edges in the image advancing to the northeast are 11.64 Å in height due to pinning by slower underlayer. The height of the step edge advancing to the southwest between layers 2 and 3 is monomolecular (5.87 Å) due to faster underlayer.

along the long axes of the tapes (i.e., analogous to a train on a track) as compared to the pathway for diffusion to the -101 face, which runs perpendicular to the long axes of the tapes. Moreover, the incorporation of molecules at these faces results in interactions that are energetically different (i.e., N-H–O hydrogen bonds at the 001 face vs. C-H–O hydrogen bonds at the –101 face). Consequently, the value of β for growth at these two faces should reflect the different pathways for diffusion and incorporation of solute. It should be noted that the measured value of β for GLYDKP is the first of its kind, and that predictions on the value of β for other molecular solids comprised of small organic molecules would be premature at this time.

The energy of the –101 step edge of GLYDKP (α) was determined and found to be 200 ergs cm^{-2}, which is equivalent to 10 kcal mol^{-1}. This value is consistent with published values for a dimer of C-H–O hydrogen bonds and van der Waal contacts between cyclic compounds, which are the interactions that occur between molecules on the –101 face of GLYDKP.

Growing crystals of GLYDKP exhibit "interlacing," an interesting kinetic phenomenon recently predicted by van Enckevort and Bennema for molecular solids that exhibit either screw-axis or glide-plane symmetry. In essence, the presence of a screw-axis in the symmetry of a molecular solid changes the orientation of molecules and their chemical functionality at the step edge from one layer of growth to the next (e.g., interactions between incoming solute and step edges of ⇑vs.⇓ would be different). This change in orientation alternates back and forth from one layer of growth to the next and results in adjacent layers growing at different rates (Figure 5). If the layer on the bottom of two layers grows faster than the layer on top, then step-splitting occurs to give, for example in GLYDKP, step heights that correspond to a single molecule. If, on the other hand, the layer on the bottom of two layers grows slower than the layer on top, then the faster top layer is "pinned" by the slower bottom layer to give step heights that correspond to two molecules. GLYDKP crystallizes in the $P2_1/a$ space group, which possesses a glide-plane parallel to the a-axis and a two-fold screw-axis parallel to the b-axis. Interlacing is observed in growing crystals of GLYDKP at both the –101 and 001 faces. We do not observe interlacing in C5DKP or expect to observe it in ASPDKP (cf. Figure 2), both of which crystallize in the P-1 space group.

Due to the underlying structural similarity in crystalline solids of XDKPs (i.e., the presence of tapes), this group of solids is an ideal model system with which to develop an understanding of the mechanisms and physical parameters controlling the process of crystallization. By comparing the results obtained from AFM studies of crystalline solids of XDKP, we can quantify the interplay between solution chemistry, surface chemistry and the processes of nucleation and crystal growth that forms the physical basis of crystallization. Results from this work have the potential to impact micro- and nanotechnological enterprises, in both the near term and the long term.

References

1. Addadi, L. and Weiner, S. Angew, *Chem. Intl. Ed. Engl*., **31**, 153, 1992.

2. (a) Douglas, T., Dickson, D. P. E., Betteridge, S., Charnock, J., Garner, C. D. and Mann, S., *Science*, **269**, 54, 1995. (b) Archibald, D. D. and Mann, S., Nature, **364**, 430, 1993. (c) Brisdon, B. J., Heywood, B. R., Hodson, A. G. W., Mann, S. and Wong, K. K. W., *Adv. Mater.*, **5**, 49, 1993. (d) Heywood, B. R. and Mann, S., *J. Am. Chem. Soc.*, **114**, 4681, 1992. (e) Mann, S., Heywood, B. R., Rajam, S. and Birchall, J. D., *Nature*, **334**, 692, 1988. (f) Mann, S., *Nature*, **332**, 119, 1988. (g) Weiner, S., *CRC Critical Reviews in Biochemistry*, **20**, 365, 1986.

3. Palmore, G. T. R. and McBride, M. T., *Acta Cryst.*, **C53**, 1904, 1997.

4. **Recent Reviews:** (a) Palmore, G. T. R. and MacDonald, J. C., in *Structure, Energetics and Reactivity in Chemistry*, Eds. A. Greenberg, C. Breneman and J. Liebman 1998, in press. (b) Russell, V. A. and Ward, M. D., *Chem. Mater.*, **8**, 1654, 1996. (c) MacDonald, J. C. and Whitesides, G. M., *Chem. Rev.*, **94**, 2383, 1994. (d) Subramanian, S. and Zaworotko, M. J., Coord. Chem. Rev., **137**, 357, 1994.

5. **Selected Examples:** (a) Simanek, E. E., Tsoi, A., Wang, C. C., Whitesides, G. M., McBride, M. T. and Palmore, G. T. R., Chem. Mater., **9**, 1954, 1997. (b) Schwiebert, K. E., Chin, D. N. and MacDonald, J. C., *J. Am. Chem. Soc.*, **118**, 4018, 1996. (c) Kane, J. J., Liao, R.-F., Lauher, J. W. and Fowler, F. W., *J. Am. Chem. Soc.*, **117**, 12003, 1995. (d) Toledo, L. M., Lauher, J. W. and Fowler, F. W., *Chem. Mater.*, **1,** 1222, 1994. (e) Brown, M. E. and Hollingsworth, M. D., *Nature*, **376**, 323, 1995. (f) Zerkowski, J. A., MacDonald, J. C., Seto, C. T., Wierda, D. A. and Whitesides, G. M., *J. Am. Chem. Soc.*, **116**, 2382, 1994. (g) Russell, V. A., Etter, M. C. and Ward, M. D., *J. Am. Chem. Soc.*, **116**, 1941, 1994. (h) Chang, Y. L., West, M. A., Fowler, F. W. and Lauher, J. W., *J. Am. Chem. Soc.*, **115**, 5991, 1993. (i) Reddy, D. S., Panneerselvam, K., Pilati, T. and Desiraju, G. R, *J. Am. Chem. Soc.*, *Chem. Commun.*, 661, 1993. (j) Aakeroy, C. B. and Seddon, K. R., *Chem. Soc. Rev.*, 397, 1993. (k) Zerkowski, J. A., Seto, C. T. and Whitesides, G. M., *J. Am. Chem. Soc.*, **114**, 5473, 1992. (l) Garcia-Tellado, F., Geib, S. J., Goswami, S. and Hamilton, A. D., *J. Am. Chem. Soc.*, **113**, 9265, 1991. (m) Simard, M., Su, D. and Wuest, J. D., *J. Am. Chem. Soc.*, **113**, 4696, 1991. (n) Zerkowski, J. A., Seto, C. T., Wierda, D. A. and Whitesides, G. M., *J. Am. Chem. Soc.*, **112**, 9025, 1990. (o) Zhao, X., Chang, Y.-L., Fowler, F. W. and Lauher, J. W., *J. Am. Chem. Soc.*, **112**, 6627, 1990. (p) Etter, M. C. and Adsmond, D. A., *J. Am. Chem. Soc.*, *Chem. Commun.*, 589, 1990. (q) Lehn, J.-M. Angew., *Chem. Int. Ed. Engl.*, **27,** 89, 1988. (r) Leiserowitz, L. and Schmidt, G. M. J., *J. Chem. Soc.*, **A**, 2372, 1969.

6. Etter, M. C., *J. Phys. Chem.*, **95**, 4601, 1991.

7. Palacin, S., Chin, D. N., Simanek, E. E., MacDonald, J. C., Whitesides, G. M., McBride, M. T. and Palmore, G. T. R., *J. Am. Chem. Soc.*, **119**, 11807, 1997.

8. (a) Kitaigorodskii, A. I., "Organic Chemical Crystallography", Consultants Bureau: New York, 1961. (b) Perlstein, J., *J. Am. Chem. Soc.*, **116**, 455, 1994.

9. Palmore, G. T. R. and McBride, M. T., *Chem. Commun.*, 145, 1998.

10. Perlstein, J., *J. Am. Chem. Soc.*, **116**, 455, 1994.

11. Hammett, L. P., *J. Am. Chem. Soc.*, **59**, 96, 1937.

DOE Center for Laser Imaging and Cancer Diagnostics

LLNL Principal Investigators: *Stavros Demos, H. B. Radousky*
University Collaborator: *Professor R. R. Alfano, City College of New York*

This Center is one of the DOE Centers of Excellence in Laser Medicine, and is based at the City College of New York (CCNY). The objective of the LLNL research effort as part of the Center is to develop a subsurface imaging system that can offer enhanced imaging depth (up to 1 cm) based on the spectral polarization difference imaging technique. This technique requires the use of different illuminating wavelengths in combination with polarization techniques to obtain images of subsurface tissue structures at different depth zones based on their difference in absorption, scattering and depolarization.

During this research period, two imaging systems have been built and tested. The experimental layouts of these systems are shown in Figure 1. The main difference between these two systems is the source of the illumination light, which in the first case is derived from diode lasers while in the second case is from a white light source. The illumination assembly that utilizes inexpensive 3–mW diode lasers operating at 633-nm, 670-nm, 820-nm and 970-nm is shown on the inset on the left-hand side of Figure 1. The output laser beam is coupled into the input of a fiber to be delivered on the sample. A polarizer (P) located at the output of the fiber ensures linearly polarized illumination of the sample. The collection of the backscattered light from the sample is achieved using a 50–mm camera lens (CL). A polarizer (P) in front of the camera lens is used to record only the perpendicular polarization image component using a liquid-nitrogen-cooled CCD detector. The alternative illumination assembly, which utilizes a white light source, is shown on the inset on the right-hand side of Figure 1. The white light is coupled into a fiber bundle and delivered into the sample. Using appropriate optical filters (F) at the output of the fiber, illumination of the sample with light at different wavelengths is achieved. These filters may be narrow-band interference filters, relatively broad-spectral band filters, or long-pass interference filters. A polarizer (P) positioned after the optical filters ensures polarized illumination of the sample. The image collection assembly is the same as the one described before.

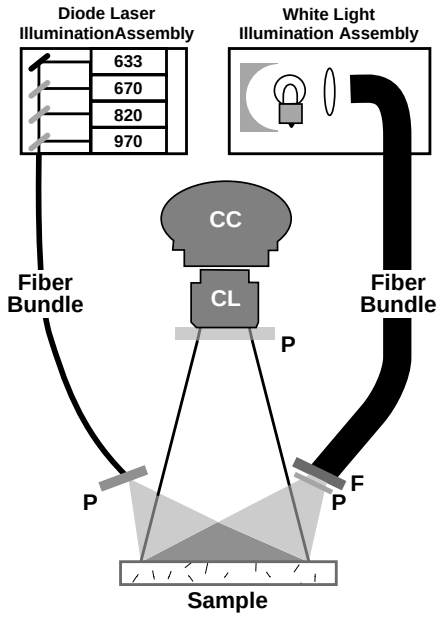

Figure 1. *Schematic diagram of the experimental setup of the SPDI system. The illumination assembly involves diode lasers (left) or a white light source (right). The illumination is delivered into the sample using fibers.*

A demonstration of the ability of the technique and our experimental system to image tissue components at different depth is provided in Figure 2. An imaging system utilizing white light and subsequent wavelength selection was used. The sample was prepared using chicken breast tissue as a model medium. In the middle of the front surface of a 5 x 4 x 1 cm^3 (1-cm thick) chicken breast tissue layer, there was positioned a 4-mm diameter, 1-mm thick object, which exhibits high light scattering, that was used as the "interesting" target to be imaged. Another 1-cm thick layer of chicken breast tissue was then positioned on the top of the object containing the chicken breast layer so that the object was sandwiched between the two thick breast tissue layers. The sample was placed between two glass plates and was slightly compressed to a uniform thickness.

The perpendicular polarization images of the sample were recorded using the white-light-illumination assembly and four narrow–band interference filters to select monochromatic illumination of the sample at 600-nm, 690-nm, 770-nm and 970-nm. The exposure time of the CCD camera

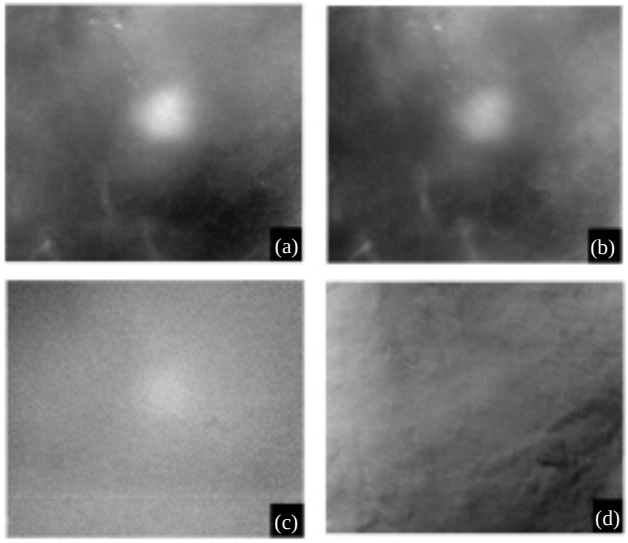

Figure 2: *Subsurface images of a high scattering object located 1-cm underneath the surface of breast chicken tissue obtained using the spectral polarization difference imaging technique and 600- nm, 690-nm, 770-nm and 970-nm illumination. (a) [970-600] nm SPDI image, (b) [970-770] nm SPDI image, (c) [770-690] nm SPDI image and (d) [690-600] nm SPDI image.*

to record the image for each illumination wavelength was adjusted so that the digitized image intensity at an arbitrary point at the lower-right part of the image was approximately the same. The images were then subtracted (a second image recorded using a shorter illumination wavelength from a first image recorded using a longer illumination wavelength) to obtain a set of new images. Figure 2a shows the spectral polarization difference image obtained following subtraction of the 970-nm image from the 600-nm image. Similarly, figures 2b, 2c and 2d show the SPDI images obtained from the subtraction of the 970-nm image from the 770-nm image, the 770-nm image from the 690-nm image, the 690-nm image from the 600-nm image, respectively.

The object is viewed with maximum contrast in the images shown in figures 2a and 2b where the 970-nm illumination was used to record the first direct image. This is due to the maximum photon penetration depth achieved for the longest wavelength illumination. The object is also visible in the image shown in Figure 2c where the 770-nm illumination was used to record the first direct image. Figure 2d indicates that when shorter illumination wavelengths are used to obtain the first direct image, the object is no longer visible because the backscattered photons cannot reach the object located 1-cm underneath the surface of the tissue to carry its image information.

The above results demonstrate that subsurface imaging at different depth zones can be achieved using the Spectral and Polarization Difference Imaging (SPDI) technique and that the selection of the appropriate illumination wavelengths is of critical importance. For the coming year, we will apply the knowledge obtained from this work to an imaging system we are currently building to be used at the pathology room at the UC-Davis Cancer Center. This system will be computer controlled and user friendly. The aim is to investigate the usefulness of this technology in a clinically relevant environment.

Micromechanical Modeling of Cortical Bone Deformation

UC Principal Investigator: *Professor Thomas M. Breunig, UC-San Francisco*
LLNL Collaborator: *John H. Kinney*

Cortical bone is an extremely variable biological composite material system, which is capable of adaptive structural changes in response to the types and quantities of loading experienced. The elastic stiffness and fatigue strength of cortical bone have been shown to vary with anatomic site, age, strain rate, and loading direction. In order to test the hypothesis that accurate deformation models of cortical bone will require precise tissue level properties and microstructural detail, it is essential to understand the three-dimensional nature of microstructure and the locations where damage is initiated. The tissue level properties of cortical bone are not well understood, and modeling efforts have not been able to fully investigate the role of architecture on structural response. During physiologic activity, cortical bone is subject to fatigue conditions. It has been suggested that micro-damage accumulation, caused by fatigue of bone under normal physiological loading conditions, increases with age,[1, 2] strain range,[3, 4] strain rate,[5, 6] and density.[7, 8] Compact bone within the mid-diaphyseal region of long bones has been shown to experience peak strains in the range of 1,500 - 2,000 με, and there may be a critical damage strain threshold above which there is increased crack growth.[4] The strain threshold is above normal physiologic levels, but is within the range used for mechanical testing procedures.

To test our hypothesis, we utilized four experimental techniques (x-ray tomographic microscopy [XTM], atomic force microscopy [AFM], electron microscopy, and mechanical deformation) to generate data as model input parameters. The combination of these techniques allowed us to probe the cortical bone's microstructure and mechanical properties at a variety of length scales. During this project we were able to identify the mineralization state associated with the bone remodeling process, architectural length scales, and variations in mineralization with age from the XTM data. We obtained tissue level properties and microstructural information from the AFM indicating that significant variations exist at this anatomic site. The presence and growth path of fatigue microcracks were identified in equine cortical bone and are in agreement with results previously reported in the literature. The concentric cylinders modeling approach proved to be inadequate for cortical bone because of the number of architectural and mineralization variations present. In the following paragraphs, examples of the results obtained will be presented.

A total of 10 specimens were examined from four human femurs and the equine third metacarpal. The human femur specimens were fabricated from the central diaphysis on the lateral side and approximately in the middle of the cortical wall. The endosteal and periosteal surfaces were left intact to orient the samples for tomographic imaging. The wedge-shaped sections were approximately 40-mm long, with the central 6-mm region reduced to a 3-mm diameter. The equine specimens were provided by colleagues from the UC-Davis Orthopedics Research Laboratory. These specimens had been fatigue tested in three-point bending to determine stiffness loss properties. All of the specimens were imaged with the XTM in an *in vivo* wet cell on Beam Line 10-2 at the Stanford Synchrotron Radiation Laboratory. The sample hydration state was maintained to prevent dimensional changes from shrinkage and to preserve their mechanical integrity.

When tomographic data is collected, the projected image of the specimen must fit into the field-of-view of the imaging system. To obtain the highest spatial resolution possible for these specimens, a 6.86-μm pixel size was selected. As a result, the in vitro cell was larger than the imaging system's field-of-view. To correct for potential errors in the x-ray attenuation maps produced by the tomographic reconstruction, a region-of-interest correction was performed on each data set prior to reconstruction. The correction was checked by evaluation of the x-ray attenuation values in the saline solution surrounding the bone during data collection. The reconstructed XTM data sets each contained approximately 360 million volume elements. The data sets were reduced by extracting a volume that contained the bone and a small volume of the saline solution surrounding the bone.

The equine cortical bones, imaged with the XTM, were found to contain fatigue cracks. The fatigue cracks were located on the tensile and compressive surfaces of the three-point bend specimens. In a three-point bending configuration, the maximum stress is located at the central

loading point. The cracks were nucleated at the machined surfaces and propagated straight inward until an osteonal cement line was encountered. The cement line has a slightly higher mineral content and is poorly bonded to the interstitial matrix and the osteon. As a result, the crack growth path was deflected along the weak interface where a greater amount of energy can be dissipated. These observations are in agreement with the bone and composite materials literature.

Fatigue testing of the human femur specimens was performed in tension to determine fatigue life and damage formation. The central portion of each specimen was approximately 3 mm in diameter and 6 mm long. The specimens were stored frozen and followed established protocols for these tissues. We imaged each specimen with the XTM in the mechanical testing gage section prior to fatigue testing. Availability of x-ray beam time precluded examination of the specimens after fatigue testing. In the tomographic data sets, we were unable to locate any micro-damage in the interstitial or osteonal bone. Cracks were located in the shoulder region transitioning from the gage section diameter to the natural cortical bone's thickness. These cracks were clearly generated by the process of fabricating the fatigue specimens. Each crack identified was located at the cement line between the interstitial bone and osteonal remodeled bone. The literature suggests that this region has lower shear strength than the surrounding bone.

The fatigue life of eight human femur specimens was highly dependant upon the bone mineralization and architecture. The fatigue lives ranged from less than 10,000 to greater than 400,000. The very short fatigue life specimens were from donors with very low bone mass and were identified as being osteopenic but not yet osteoporotic. A maximum load required to produce a fatigue strain of 2,500 με (.0025 mm/mm) was determined on the first cycle. The fatigue tests were then performed in load control. As expected, the strain increased rapidly during the first 100 cycles and the rate of increase was very small by 1,000 cycles. The changing strain was due to generation of damage in the structure that caused a decrease in the stiffness. The fatigue damage process observed was very similar to fatigue damage characteristics of metal matrix composite materials.[9]

Four of the samples failed during fatigue testing. The failure process was characterized by a very rapid loss of stiffness in the final few cycles. In future work we will attempt to relate this rapid loss of stiffness to a critical scaling behavior[10] of the damage features associated with the failure process. In one of the samples that did not fail, the load was increased several times to determine the effect on the bone's measured stiffness. As expected in a composite material system, the stiffness decreased rapidly with the introduction of damage and stabilized at a new level within 1,000 cycles. We also used one specimen to verify the fatigue damage threshold in human cortical bone. To determine the fatigue damage threshold, the stiffness change during the first 1,000 cycles was monitored at an initial fatigue strain of 1,500 με, 2,000 με, and 2,500 με. The measured stiffness did not change until the fatigue loading was adequate to generate 2,500 με. The critical fatigue damage threshold is, therefore, 2500με for human cortical bone at the central dyaphysis.

The XTM data sets were used to quantify various features within the cortical bone structure. The types of features quantified were: volume fractions of phases present; the distribution and mean diameter of Haversian canals, Volkmann's canals, and osteons; the surface area to volume ratios for the Haversian and Volkmann's canals; surface orientation distribution functions; preferred orientations; distribution and mean spacing of features; etc. The ability to examine these parameters for inter- and intra-sample variations, which may have significant effects on the macromechanical properties measured, will be a major advance in our understanding of the parameters required for accurately modeling cortical bone's mechanical deformation response. The mean porosity associated with the canal networks varied from 5.7 % to 12.5 %. The inter-specimen mean canal radii varied from 36 μm to 85 μm, with the low bone mass sample having a standard deviation of 40 μm. The canal size distribution for the low-bone-mass sample contained the central distribution for healthy bone and had many more canals with a significantly larger size. The greater number of features with a larger size may be reflective of a decrease in osteoblast activity. (The osteoblasts deposit new bone.)

The arrangement of Haversian canals was found to be highly ordered and hexagonal in nature. We have not been able to find this characteristic reported in the literature for cortical bone. The mean center-to-center spacing of the Haverisan canals was 265 μm in all of the samples except those with low bone mass. The low-bone-mass samples had a mean spacing of 310 μm. Even though there is a relatively large difference between these mean values, there is no statistical significance in these differences.

A skeletonization routine was used to identify the branching characteristics of the Haversian structure. We found that there are three branches connected at each node identified. This would indicate that the remodeling process does not activate from a large number of sites.

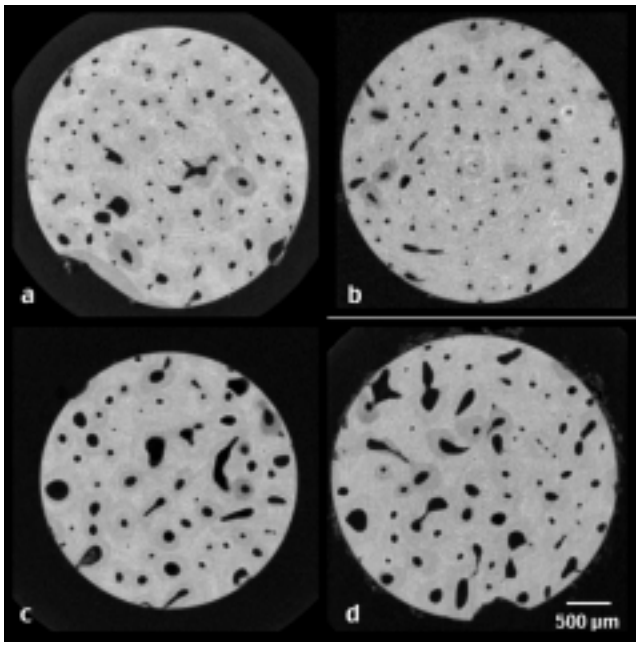

Figure 1. Representative tomographic cross-sectional images from the four human femurs examined in this project. The ages and sex of the donors are: (a) 37-year-old female, (b) 55-year-old male, (c) 45-year-old female, and (d) 80+ year old female. The color scale represents the mineral content with darker being lower levels and brighter being higher levels.

The mineral distributions were also determined from the XTM data. We have been able to identify variations between the each femur, but not between the two samples from each femur. Figures 1 and 2 are representative tomographic images from the samples examined in this study. In these figures the color scale is representative of the mineral content with black being very low and white being the highest. All of the images have been scaled with the same maximum mineral content. Figure 1 shows representative cross-sections from each of the human femurs examined. The femur shown in Figure 1d is from the low-bone-mass subject. The structure in this image has fewer small canals and greater overall porosity than the other specimens. Examination of the complete data sets reveal a great deal of variability with location. In Figure 2, images a and b are located 2.6 mm apart vertically in the same specimen. Figure 2c is from the same femur and is located approximately 1.5 cm circumferentially from 2a and 2b. The need to examine and characterize multiple three-dimensional volumes from each femur is apparent based on the variations observed. These spatial variations also indicate the source for the statistical variations in the measurements of architectural features discussed above.

Several interesting features from Figure 1b are shown in Figure 3. The Haversian canal sizes and mineralization patterns allow the primary osteons, associated with the initial growth process, and secondary osteons, associated with the remodeling process, to be identified. The mineralization pattern surrounding a primary osteon is not significantly different than the interstitial matrix at the length scale of these images. The mineral content of a secondary osteon is lower than the interstitial matrix and can be seen clearly around several canals. A hyper-mineralized cement line has been identified in this specimen. Figure 3b is a vertical section through this feature. The hyper-mineralized region extends over a short length of the osteon. There is very little in the literature describing the frequency and extent of this type of feature in cortical bone.

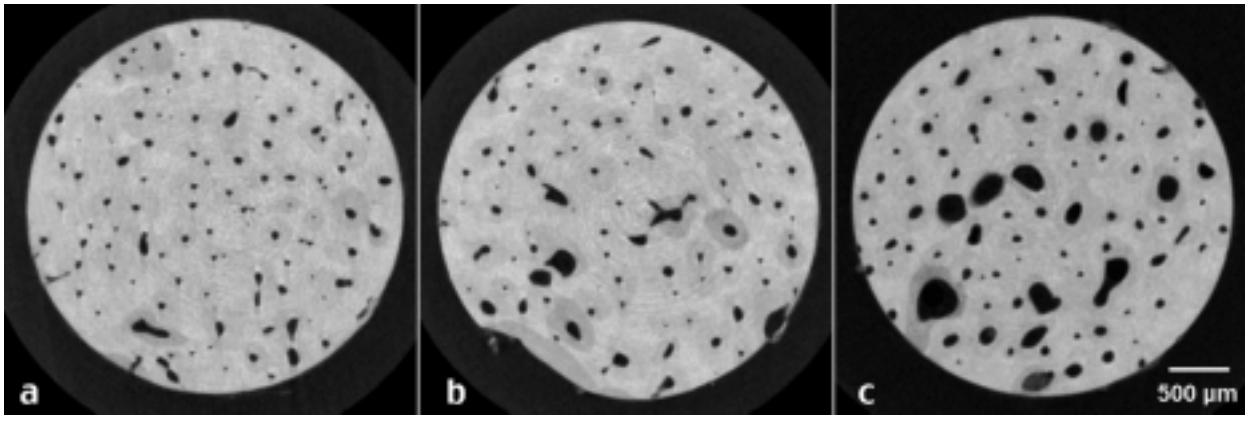

Figure 2. Tomographic cross-sections from the same cortical bone donor as Figure 1b illustrating the variability of structure and mineralization level with position. Figures 2a and 2b are separated vertically be 2.6 mm, while Figure 2c is located approximately 1.5 cm circumferentially from 2a and 2b.

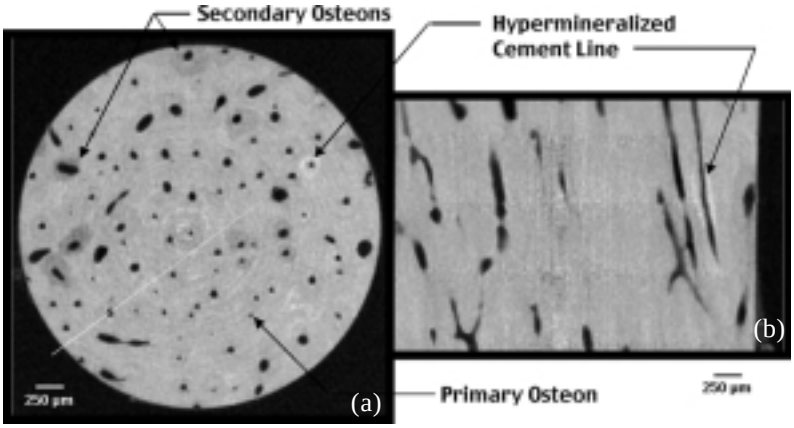

Figure 3. Mineralization pattern in cortical bone of a 55-year-old male. Features of interest identified in the tomographic data are the primary and secondary osteons around the haversian canals. A location of a hypermineralized cement line has been highlighted and its longitudinal extent illustrated by extracting a vertical section from the three-dimensional tomographic data set.

The sensitivity of the XTM data to variations in mineral content allowed us to identify the features associated with the remodeling process in cortical bone. There are three stages required for remodeling: activation, resorption, and mineralization. Figures 4 and 5 highlight the capabilities of the XTM data sets for characterizing these complex structures and their various stages of repair during a normal life cycle. Figure 4 shows a three-dimensional surface rendering of a resorption site that is 1.37 mm long. In histologic sections, osteoclast cells are associated with relatively smooth surfaces created as the bone matrix is demineralized. The resorption site was identified by the rapid decrease in mineral content from the surrounding matrix and its smooth surface. There is no partially demineralized layer identifiable with the 6.8-µm voxel size used for these experiments.

The mineralization phase follows resorption in the remodeling process. Figure 5 shows a typical region where mineralization is actively taking place. The ostoblast cells that form new bone deposit layers of collagen that the mineral will be deposited into and connected to. These layers of collagen and mineral form the secondary osteons. We can identify these features by their lower mineral content than the interstitial matrix. From the surface rendering it is possible to visualize the connectedness of the Haversian network. The mineral level used to create the surface rendering image is relatively low. The osteoblasts sit in small depressions on the newly forming bone surfaces. It is possible to identify these sites in the surface rendering as small bumps on the surfaces of the Haversian canals.

The statistical significance of age, sex, anatomic site, and disease state cannot be determined with the limited sample size examined in this study, but will be variables

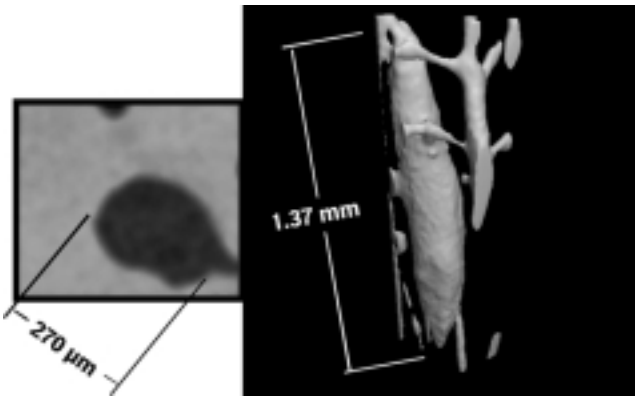

Figure 4. Site where the remodeling process is in the resorption phase. Resorption sites are characterized by their rapid decrease in mineral content from the matrix level. In histologic sections, osteoclast cells are associated with relatively smooth surfaces created as the bone matrix is demineralized. The resorption site is 270-µm wide, shown in the tomographic section on the left, and is 1.37-mm long as shown in the surface rendering on the right. In the surface rendering shown, the surfaces are smooth.

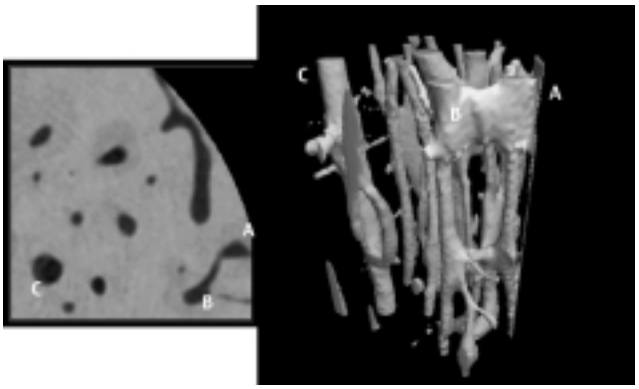

Figure 5. Site where the remodeling process is in the active mineralization phase. A mineralizing site can be characterized by the transition from the matrix mineral level to a lower mineral content in the osteon as seen in the tomographic cross-section on the left. From three-dimensional surface renderings of the void spaces (at a constant mineral content), it is possible to visualize the canal network's orientation and fine details of the surfaces. The locations labeled A, B, and C in the tomographic cross-section are indicated in the surface rendering.

included in the NIH proposal being prepared from these preliminary results.

The tissue level properties were measured with the AFM in the hypo-mineralized osteonal regions and the interstitial bone as a function of position. The modulus measured in the interstitial bone ranged from 16-28 GPa, and the osteonal bone had a modulus below 14 GPa. These stiffness values were highly dependent on their location within microstructure. As bone is deposited a lamellar structure is formed. The tissue level properties in lamella are higher than in the interlamellar regions. The tissue level properties in the secondary osteons where new bone is forming are reflective of the stage of remineralization and differences in collagen content in the newly forming bone. The tissue level properties we measured are similar to those measured with micro-hardness techniques. Our maximum modulus measured is higher than noted in the literature and may be due to the smaller interaction volume associated with the AFM's μN force compared to a microhardness force ranging from 50 mN – 500 mN. In the samples with low bone mass, the interstitial bone stiffness fell within the range of the bones with normal bone mass. Further testing will be required to determine if there are significant differences in these tissue level properties when osteoporosis is more advanced. The variations with gender, age, anatomic site, and disease state are variables that need to be further examined.

The concentric cylinders modeling approach used to predict cortical bones mechanical deformation response was not as successful as we had hoped. This modeling approach is at a continuum level and requires a homogenization of the architecture present. As a result, it is not able to reflect local changes associated with the remodeling process. The continuum nature of this modeling technique also limits the ability to incorporate damage parameters. The current method used for incorporation of damage is to decrease the structural stiffness of various cylinders. This will not account for interactions of damage with the architecture features. The approach to be explored further in the future is incorporation of the tomographic data into finite element models similar to the approach of Kinney.[11] While the finite element approach will allow incorporation of tissue level properties and damage characteristics, the computational time will be very significant for a relatively small volume of material.

Summary of University - LLNL Interaction

During the course of this grant, there was significant interaction between people at the UC-San Francisco campus and LLNL. The availability of office space at LLNL provided a location to focus the literature evaluation and modeling portion of this project. In addition, access to other locations at the LLNL site provided contact with people for the exchange of ideas on how to approach various aspects of this project. While the XTM data collection was performed at the Stanford Synchrotron Radiation Laboratory, using unique equipment available through LLNL, all of the data reduction was performed in Dr. Kinney's laboratory. The data analysis was performed at both facilities.

The AFM and Hysitron nano-mechanical experiments used equipment at LLNL and on campus. Mehdi Balooch of LLNL assisted in performance of these experiments and provided additional information about evaluation of tissue level properties measurements in biomaterials.

A remote terminal was purchased for use in this project by the Materials Research Institute for this project. The willingness of the Materials Research Institute to provide facilities and equipment for successful completion of this project and others is greatly appreciated by the University investigators.

Future

The information generated from this grant will form the basis for a National Institutes of Health R01 grant application. The central hypothesis to be tested is that the mechanical properties of cortical bone vary with anatomic site. To evaluate the central hypothesis, we will test the hypothesis that the tissue level properties depend upon anatomic site and are affected by factors such as age, gender, and ethnicity. We will use the XTM to evaluate the mineral density at various anatomic sites and to determine if there are differences in micro-crack nucleation and growth characteristics associated with fatigue damage. We will establish a correlation between the mineral density present and the tissue modulus measured with the AFM. The collaboration between investigators at UC-San Francisco and Lawrence Livermore National Laboratory will be a key factor for the successful evaluation of this complex biological phenomenon.

References:

1. Courtney, A. C., Hayes, W. C. and Gibson, L. J., "Age-Related Differences in Post-Yield Damage in Human Cortical Bone Experiment and Model", *J. Biomech.*, V**29**: 1463-1471, 1996.

2. Schaffler, M. B., Choi, K. and Milgrom, C., "Aging and Matrix Microdamage Accumulationin Human Compact Bone", V**7**: 521-525, 1995.

3. Zioupos, P., Wang, X. T. and Currey, J. D., "Experimental and Theoretical Quantification of the Development of Damage in Fatigue Tests of Bone and Antler", *J. Biomech.*, **29**: 989-1002, 1996.

4. Pattin, C. A., Caler, W. E. and Carter, D. R., "Cyclic Mechanical Property Degradation During Fatigue Loading of Cortical Bone", *J. Biomech.*, V**29**: 69-79, 1996.

5. Schaffler, M. B., Radin, E. L. and Burr, D. B., "Long-Term Fatigue Behavior of Compact Bone at Low Strain Magnitude and Rate, Bone", V**11**: 321-226, 1990.

6. Schaffler, M. B., Radin, E. L. and Burr, D. B., "Mechanical and Morphological Effects of Strain Rate on Fatigue of Compact Bone", V**10**: 207-214, 1989.

7. Schaffler, M. B. and Burr, D. B., "Stiffness of Compact Bone: Effects of Porosity and Density", *J. Biomech.*, V**21**: 13-16, 1988.

8. Currey, J. D., "The Effects of Porosity and Mineral Content on the Young's Modulus of Elasticity of Compact Bone", J. Biomech., V**21**: 131-139, 1988.

9. Johnson, W. S., "Fatigue Testing and Damage Development in Continuous Fiber Reinforced Metal Matrix Composites", NASA TM100628, June 1988.

10. Stauffer, D. and Aharony, A., "Introduction to Percolation Theory", 2nd Edition (Taylor and Francis, London, 1992).

11. Ladd, A. J. C., Kinney, J. H. and Breunig, T. M., "Deformation and Failure of Cellular Materials", *Phys Rev E*, V**55**: 55-59, 1997.

ELECTRO/OPTICAL MATERIALS

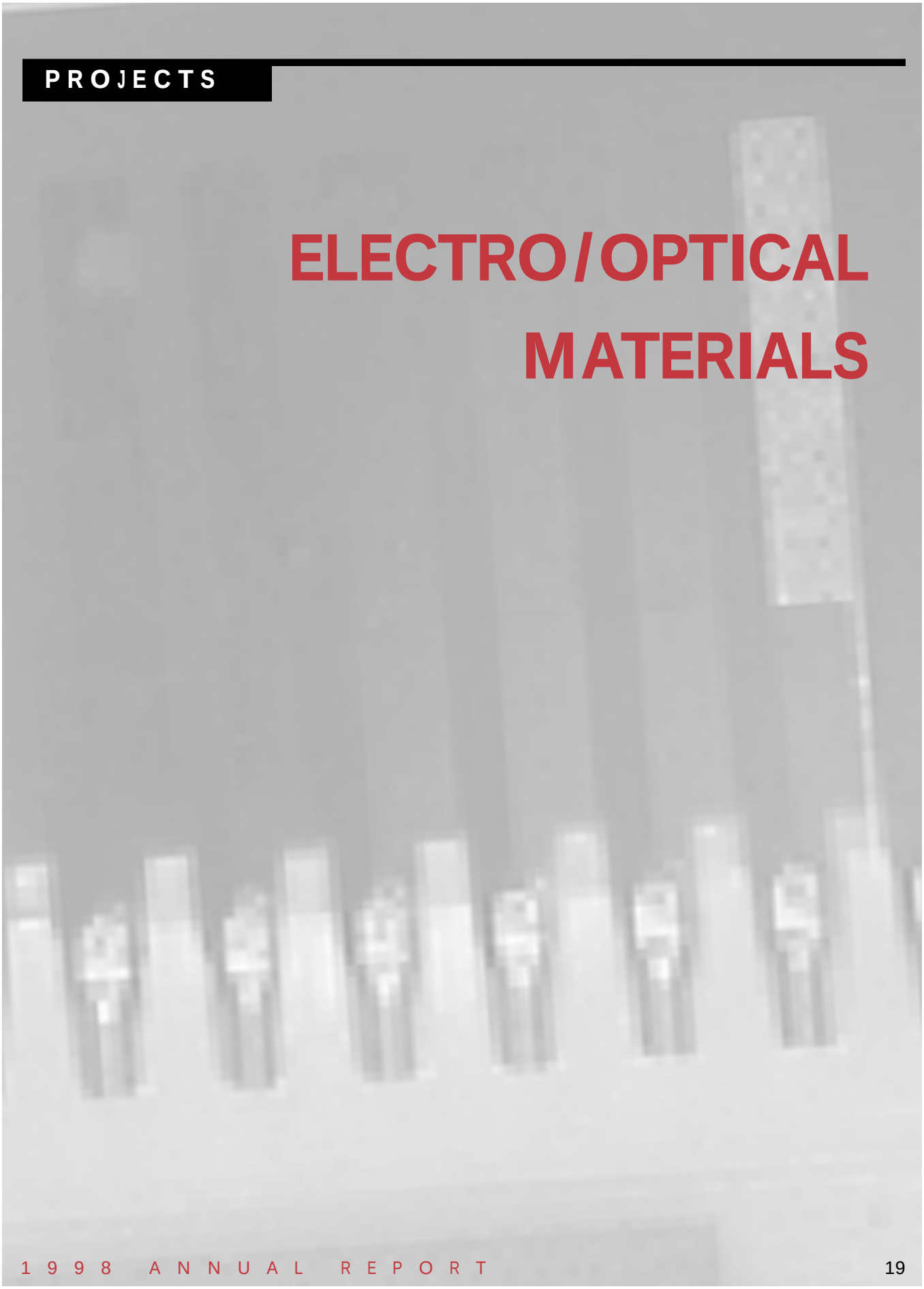

Fundamental Studies and Applications of Semiconductor Nanocrystals

UC Principal Investigator: *Professor Susan M. Kauzlarich, UC-Davis*
LLNL Principal Investigator: *Howard W. H. Lee*
Student: *Boyd Taylor, UC-Davis*

Nanocrystals are particles with physical dimensions of a few nanometers and typically contain a few thousand atoms or less. At sufficiently small sizes, three dimensional quantum confinement (QC) of electrons and holes gives rise to optical and electrical properties that are highly-size and shape-dependent and dramatically altered from their bulk counterparts. This is manifested, for example, as enhanced light emission and optical nonlinearity, shifts in the optical spectra to greater energies than the bulk, and localization and modifications in the density of electronic states.

Extensive research has been conducted on direct band gap nanocrystals; however, except for Si, relatively little has been performed on indirect bandgap nanocrystals. Interband radiative relaxation in bulk indirect bandgap semiconductors requires phonon assistance, which is inefficient and undesirable for many optoelectronic and photonic applications. Quantum confinement offers an intriguing method to modify the optical and electronic properties of indirect bandgap materials, thus providing material systems with different and desirable properties from the bulk.

The fascination with light emission from Si and Ge nanocrystals derives from: (1) scientific interest in efficient and above-bandgap light emission from an indirect bandgap material where such emission is inherently inefficient due to the need for phonon intervention, and (2) the drive for higher performing optoelectronic and photonic systems that are compatible with mature Si-based microelectronics. The observation of efficient visible luminescence from porous silicon (PSi) in 1990[1] initiated intense worldwide research into the mechanism of light emission from PSi and nanocrystalline silicon and the applications that this would enable. Many theories attribute at least some portion of the visible emission, particularly in the red, to QC.[2] Defects, impurities, molecular species, amorphous Si, and surface states have also been proposed.[2] Nevertheless, in spite of the enormous amount of research into their optical properties, the origin and nature of the visible luminescence from nanocrystalline Si and Ge, and the new applications that they will enable, remain controversial and continue to receive intense worldwide attention.

We have made several significant contributions to this field: (1) pioneered the only synthetic solution method to produce Si and Ge nanocrystals with surfaces that are well-terminated with oxides or organic alkyl groups[3], (2) observed for the first time a broad and continuously tunable light emission (ultraviolet to visible) from Si and Ge nanocrystals[4], (3) developed a definitive model for the physics of light emission from these nanocrystals[4], and (4) designed and fabricated the first and only blue light emitting LED based on these Si and Ge nanocrystals[5]. Optical studies include absorption, photoluminescence (PL), PL excitation (PLE), size-selective spectroscopy, femtosecond spectroscopy, power dependent spectroscopy, and nonlinear optical spectroscopy.

Our results provide a comprehensive understanding of the origin and nature of light emission from isolated Si and Ge nanocrystals.[4] A key manifestation of quantum confinement is a size-dependent PL energy. We observe light emission that can be continuously tuned from the ultraviolet (UV) to throughout the visible by changing the nanocrystal size (Figure 1).

This is the first observation of such a broad (UV to visible) and continuously tunable light emission from isolated Si and Ge nanocrystals. The mechanism for this light emission can be separated into quantum confinement (QC) and non-quantum confinement (non-QC) contributions. We can differentiate between QC and non-QC effects by appropriate spectroscopic studies. Our results indicate that QC in Si and Ge nanocrystals is responsible for this broadly tunable emission. Similar optical properties are observed for nanocrystals with different surface terminations, confirming that the QC luminescence arises from the nanocrystalline core. Our results also resolve the long-standing question of whether the UV-blue-green PL originates from the surface oxide layer, as long believed. Our observation of this PL from nanocrystals with and without an oxide layer unequivocally establishes that this PL originates from the nanocrystalline core. In addition, it is generally believed that as the particle size decreases, the band structure becomes more

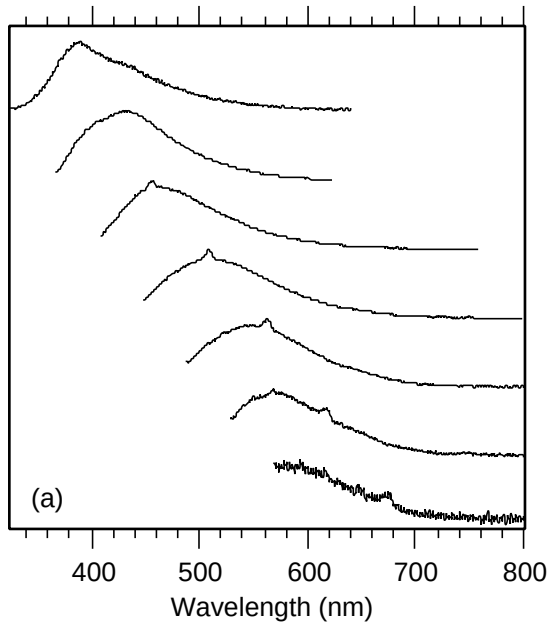

Figure 1a. Broadly tunable PL from different size Si nanocrystals.

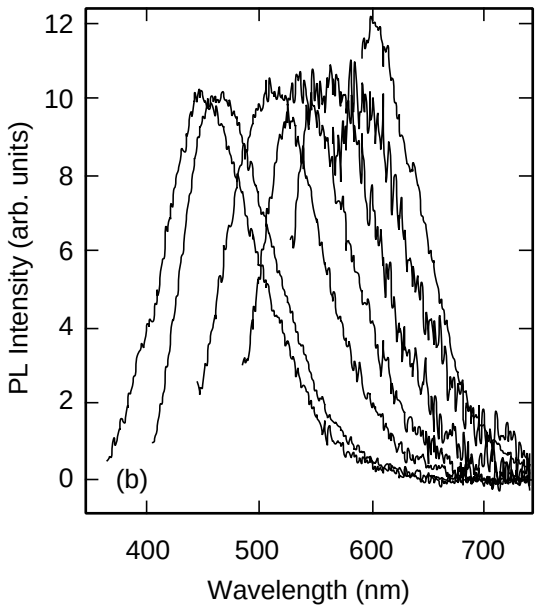

Figure 1b. Broadly tunable PL from different size Ge nanocrystals.

dispersionless and hence more direct-like. Surprisingly, our results also show that this QC luminescence maintains an indirect character even down to small diameters (≤ 2 nm). This is confirmed by our observation of phonon replicas in the resonant PL spectra and phonon absorption and emission in the PLE spectra (Figure 2). Phonon intervention is required for light emission in spite of quantum confinement, even for small nanocrystals.

Another key manifestation of QC is a size-dependent energy gap. We observed and characterized such a size-dependent energy gap associated with Si and Ge nanocrystals. Our results also show similar energy gaps

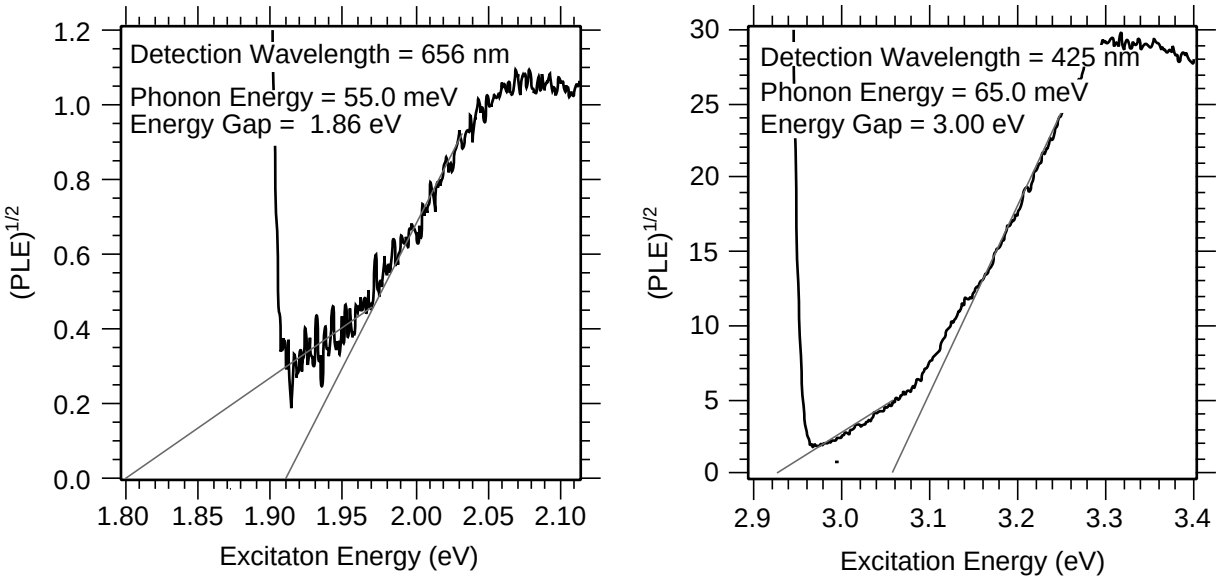

Figure 2. Observation of phonon absorption and emission in the PLE spectra of Si nanocrystals.

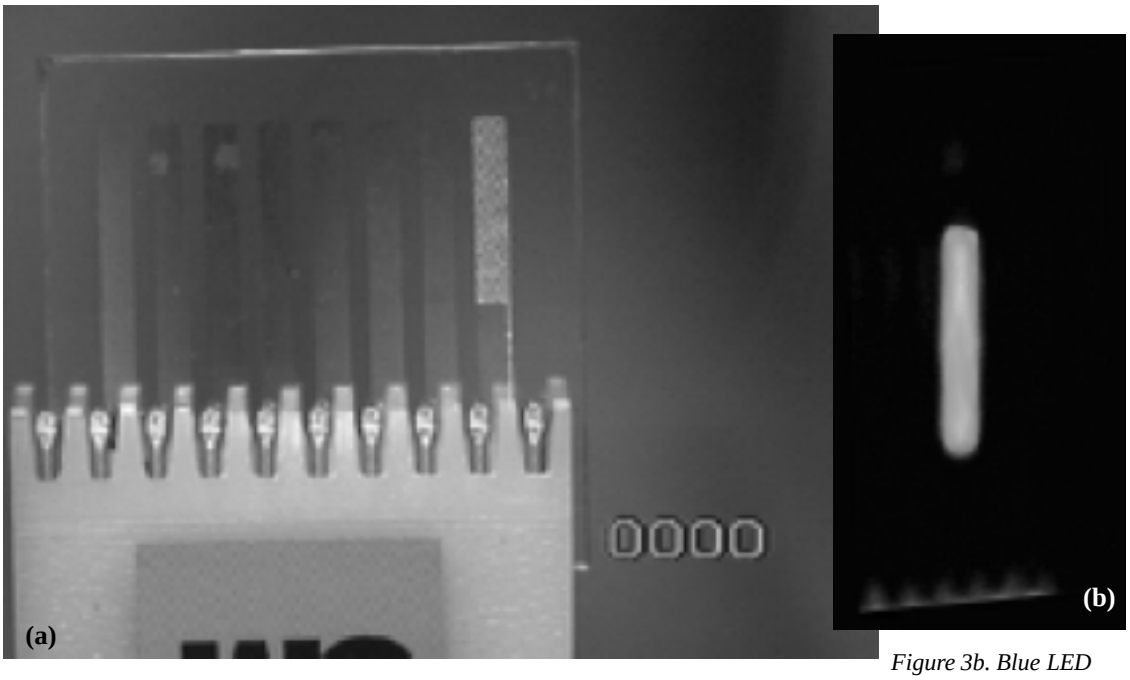

Figure 3a. Blue LED based on Si nanocrystals.

Figure 3b. Blue LED based on Ge nanocrystals.

for nanocrystals with the same size but different surface terminations. This strongly indicates that the effective energy gap derives from the nanocrystalline core. Many theories predict a size-dependent energy gap of the form

$$E_g(d) = E_g(\infty) + \frac{C}{d^n}$$

where $E_g(\infty)$ is the bulk bandgap, C is a constant that depends on material properties, d is the nanocrystal diameter, and n is a constant that generally varies between 1 and 2. Simple effective mass theories[6] predict $n = 2$, which does not agree with our data. Our results on Si nanocrystals give $n = 1.4 \pm 0.1$, $C = 115 \pm 27$ (d in Angstrom), and $E_g(\infty) = 1.15$ eV $\pm$ 0.05. These values agree well with more sophisticated tight binding[7] and with pseudopotential calculations.[8] Our results establish that: (1) QC plays an important role in these nanocrystals, (2) the size-selective PLE spectra represent absorption from different sized QC nanocrystals, and (3) the broadly tunable PL directly results from this QC. Our results indicate that $n = 1.4$ for Ge nanocrystals as well.

Non-QC luminescence is also observed and involves mainly localized trap emission. This non-QC luminescence occurs at trap-specific energies in the visible and may be mistaken for QC emission. Through saturation spectroscopy, we identified these traps as defects in the oxide surface layer. For Si nanocrystals, these emissions occur in the red (1.8-2.0 eV), green (2.5 eV), and blue-green (2.7 eV) spectral regions and may be mistaken for QC luminescence. These non-QC mechanisms that give rise to visible emission (particularly the red) underline the caution required for the interpretation of visible light emission from nanostructured Si and Ge. In light of our results, many reports of QC luminescence from Si and Ge nanocrystals are now understood to results from non-QC origins. Nanocrystals terminated with organic alkyl groups show only QC luminescence. Trap emission is not observed. This attests to the complete and defect-free nature of the alkyl surface termination in our synthesis process.

Based on our new understanding of these nanocrystals, we designed and fabricated the first and only blue-light-emitting device (LED) using semiconductor nanocrystals as the active material. Figure 3 shows operating blue LEDs using Si and Ge nanocrystals.

References

1. Canham, L. T., *Appl. Phys. Lett.*, **57**, 1046, 1990.

2. See for example, Cullis, A. G., Canham, L. T. and Calcott, P. D. J., *J. Appl. Phys.*, **82**, 909, 1997.

3. (a) Yang, C-S., Bley, R. A., Mayeri, D., Kauzlarich, S. M., Lee, H. W. H. and Delgado, G. R., *J. Am. Chem. Soc.;* (b) Bley, R. A. and Kauzlarich, S. M., *J. Am. Chem. Soc.*, **118**, 12461, 1996; (c) Bley, R. A. and Kauzlarich, S. M., "Synthesis of Silicon Nanoclusters"; (d) Fendler, J. H.; Ed.; (e) Wiley-VCH: Weinheim, pp 101, 1998; (f) Bley, R. A. and Kauzlarich, S. M., "A New Solution Phase Synthesis for Silicon Nanoclusters"*;* (g) Fendler, J. H. and Dékány, I., Ed. Kluwer Academic Press: The Netherlands, pp 467, 1996.

4. Lee, H. W. H., Thielen, P. A., Delgado, G. R., Kauzlarich, S. M., Yang, C-S. and Mayeri, D., *Science*, submitted.

5. Lee, H. W. H., patent disclosure.

6. (a) Takagahara, T. and Takeda, K., *Phys. Rev. B*, **46**, pp. 15578-81, 1992; (b) Woggon, U., "Optical Properties of Semiconductors Quantum Dots", **136**: Springer, 1997; (c) Yoffe, A. D., *Advances in Physics*, **42**, pp. 173-266, 1993; (d) Banyai, L. and Koch, S. W., *Semiconductor Quantum Dots*. Singapore: World Scientific, 1993.

7. (a) Dellerue, C., Allan, G. and Lannoo, M., *Phys. Rev.* B, **48**,11024, 1993; (b) Dellerue, C., Allan, Martin, E. and Lannoo, M., in *Porous Silicon Science and Technology*; (c) Vial, J. C. and Derrien, J., Eds. New York: Springer-Verlag, pp. 91-110, 1995.

8. (a) Wang, L. W. and Zunger, A., *Phys. Rev. Lett.*, **73**, 1039, 1994; (b) Wang, L.W. and Zunger, A.; in "Semiconductor Nanoclusters-Physical, Chemical, and Catalytic Aspects", **103**; (c) Kamat, P. V. and Meisel, D., Eds. Amsterdam: Elsevier, pp. 161, 1997.

NanoCrystalline Si Produced by Shock Compression

UC Principal Investigator: *Professor Subash Risbud, UC-Davis*
LLNL Principal Investigators: *W. J. Nellis, Howard W. H. Lee*
Student: *Michael Paskowitz, UC-Davis*

Introduction

The optical properties of nanocrystalline Si (n-Si) are of great scientific interest because they are tunable by choice of the particle size of n-Si. The issue remains as to the mechanism by which the optical properties are sensitive to particle size. The two competing ideas are quantum confinement, in which the properties depend only on particle size, and chemical passivation of the outer layers of n-Si by oxygen.

Conventional methods of making n-Si using wet chemistry and chemical impurities in the process are always issues as to what causes the optical properties to vary. In this project we are making n-Si by the physical process of shock compression, in which heterogeneous deformation of SiO_2 causes n-Si to nucleate and grow for ~1 microsec within an initial SiO_2 crystal.

The observation that n-Si can be made by shock compression was made because the dynamic deformation of minerals has been of interest in the geological community for determining the behavior of these materials at extreme pressures and high strain rates, such as occur in cometary impacts. In the past, dynamic shock experiments on quartz have been performed in steel capsules. Instead, Fiske, *et al*[1] shocked the quartz in an aluminum fixture to allow greater strain in the material and correspondingly greater heterogeneous shock temperature rise. The shockwave transforms the initial single-crystalline quartz samples into quartz crystallites containing diaplectic glass with < 400 nm regions of diamond-phase silicon in the grain boundaries interspersed with tiny aluminum particles. Under laser illumination for Raman spectroscopic investigations, the sample showed an intense red luminescence.[2] Current interest in the shock processing of quartz in aluminum fixtures is to find the mechanism for the formation of n-Si, such as the dependence on the magnitude and duration of the shock pulse, and to find a way of controlling the n-Si size for application as semiconductor quantum dots.

Project Update

It was suspected that aluminum oxide was present in the structure, but it could not be identified through previous x-ray or electron diffraction studies. Observation of the solid state 27-Al NMR signal corresponding to a four-fold coordination confirmed aluminum incorporation into the silicate network.

A peak corresponding to six-fold coordination was also found. Aluminum within a silica matrix shows a change in coordination from four-fold to six-fold coordination at high pressures. This coordination is quenched when the glass is rapidly brought to lower temperatures. The greater intensity of the six-fold peak in the NMR signal may be due to the quenched in higher coordinated aluminum or it may be due to oxidized aluminum present from atmospheric oxidation of bulk aluminum left within the sample. At present, it is not possible to distinguish from which of these two potential sources the six-fold coordinated Al signal comes. The presence of the four-fold coordinated signal provides evidence of aluminum incorporation into the glass.

Previous processing of the samples included infiltrating the post-shocked sample with canada balsam. This slowed efforts to get meaningful photoluminescence (PL) data from the sample since the canada balsam luminesced in the region of interest. Metallic aluminum incorporated into the sample during shock processing increased sample reflectivity, also causing problems with PL data collection.

A region of red luminescence was detected visually, but we were not able to characterize this region by spectroscopic techniques before the sample area ceased luminescing.

Future sample preparation will use a UV-transparent epoxy, which will pass the wavelengths necessary to characterize the samples with PL and PLE. Sample integrity will be maintained, while permitting efficient optical data collection.

References

1. Fiske, P. S., Nellis, W. J., Lipp, M., Lorenzana, H., Kikuchi, M. and Syono, Y., "Pseudotachylites Generated in Shock Experiments: Implications for Impact Cratering Products and Processes", *Science*, **270** (5234), pp. 281-283,1995.

2. Lorenzana, H., Fiske, P. S. and Nellis, W. J., (unpublished).

Nanoscale Study of Strain and Strain Dynamics in Laser Materials and Nonlinear Optical Materials

Principal Investigator: *Professor Umar Mohideen, UC-Riverside*

LLNL Principal Investigator: *Ming Yan*

Student: *T. J. Yang, UC-Riverside*

Strain and fracture dynamics is an exploding new area of physics, which has gained tremendous impetus from large-scale molecular dynamics simulations. However, a lack of detailed microscopic experimental investigations of strain dynamics has severely handicapped new theoretical advances. We propose to study surface stress and strain dynamics in optical components (laser materials and nonlinear optical materials) with nanometer resolution using a variety of scanning microscopes such as the Near-Field Scanning Optical Microscope (NSOM), Atomic Force Microscope (AFM) and Scanning Tunneling Microscope (STM). In the first year of the program, we have used a NSOM and AFM to identify and characterize nanometer-sized surface and subsurface defects in optical components at LLNL. This project will have a large impact on the basic physics of strain dynamics while fulfilling a programmatic need at Lawrence Livermore National Laboratory.

The first stage of the research has been partly accomplished during the first year of this grant. We were involved in the identification of the nature of surface defects in optical components at LLNL. We adapted a large-area AFM to perform NSOM scans of full-size fused silica optical components. This research has resulted in two publications. Next we will perform quantitative measurement of the strain, through the associated birefringence, and the relationship of the surface morphology to the strain. We now plan to integrate an STM with the NSOM in order to facilitate chemical identification of the defects.

Some of these studies have been conducted on actual optical components used in the laser program at LLNL. While the components do undergo a variety of optical tests at LLNL during fabrication, all of them are macroscopic and limited to a resolution of a few thousand angstroms. This will the first study of the nanometer-scale optical defects introduced in the fabrication. These studies will be based on our experience studying the strain associated with domain walls in nonlinear optical materials like $LiTaO_3$ and $LiNbO_3$. In the case of $LiTaO_3$ we have used the measured strain at the domain walls to calculate the domain wall energy and the associated internal electric field.

The stresses in optical components are associated with defects incorporated during fabrication of the optical components, especially the cutting and polishing stages. These nanoscale stresses and strains will exacerbate failure mechanisms in the optical components. Also, given the high intensity optical beams that are transmitted through the optical components, even small phase differences and/or polarization rotations that are introduced by the nanometer scale defects could eventually result in a loss of coherence in the transmitted optical beam. This decoherence can also lead to eventual self-focusing and serious damage to optical components in the beam path.

The surface topography measured with the AFM and the NSOM will be correlated with optical features detected by the NSOM. This will be the first quantitative study of strains and their dynamics in optical components on a nanometer scale. Additionally this study is tailormade to understand the optical defects in optical components fabricated at LLNL for use in the laser program. The results of the study can be used to better understand the failure mechanisms in optical components fabricated at LLNL. These will be the first submicroscopic experiments in the new evolving field of fracture and strain propagation.

Experimental Methodology and Technical Progress

We are using a NSOM[2,3] with a spatial resolution of 50 nm. This has allowed investigation of local and dynamic strains with unprecedented spatial resolution. In our experiment, the strain has been detected with nanometer scale resolution by the following two methods:

1. Polarization rotation of the transmitted light coupled in the near-field.
2. Near-field coupling of defect-perturbed evanescent modes.

Polarization rotation of the transmitted light coupled in the near-field

Strains of 10^{-5} have been measured with a spatial resolution of 100 nm using this technique on ferroelectric domain walls in $LiTaO_3$.[4-7] These strains were associated with the reorientation of the ferroelectric dipole at domain walls in optically polished single crystals. The strains are detected using the associated birefringence at the domain walls. The experiments were done at room temperature by detecting the transmitted light polarization rotation (from the birefringence[6]). A CW Ar ion laser with a wavelength of 514 nm was used. The light transmitted through the sample was passed through an analyzer, which was set for minimum transmission in an isotropic region of the crystal at the start of the scan. When the fiber probe is scanned over a domain wall, the birefringence associated with the strain produces a rotation of the polarization of the transmitted light. The resultant increased transmission through the analyzer is detected by a cooled photomultiplier tube.

Near-field coupling of defect-perturbed evanescent modes

This experimental method is more suited for detection of surface and subsurface (within 100nm of surface) defects and strains. A 1-mm diameter, l-mW laser is totally internally reflected from the surface to be investigated. The fiber probe of the NSOM is placed in the near-field of the surface (5 nm from the surface) using the shear force technique[2]. The evanescent field is coupled into the fiber tip (photon tunneling).[3] This coupling is drastically modified by any surface and subsurface refractive index perturbations such as from strain and defects. These refractive index perturbations can be correlated with the topographic image obtained from the shear-force technique and the AFM to yield definitive identification of the nature of the defect such as scratches, imbedded impurity, void, or strain field. We have used this technique to map the strain field around subsurface impurities with 20 nm resolution in optical components at LLNL.[8]

Accomplishments of the Past Year

In the first year of this grant, we were involved in the identification of the nature of surface defects in optical components at LLNL. We adapted a large-area AFM to perform NSOM scans of full-size fused silica optical components. We correlated the optical signal from the NSOM to the surface features detected with the AFM. In the case of nonlinear optical materials such as $LiTaO_3$, we were able to quantitatively measure the strain at single domain walls. We also studied the pinning of domain walls due to defect centers by observing the profile of the wall under an applied DC field. The above accomplishments have resulted in four publications[5,7-9] (two submitted).

Present LLNL – University Interactions

We have a strong ongoing research program with the Materials Division at LLNL. In the past year we have collaborated on the design of a special NSOM to handle large samples (full-size optical components). The experience at UC-Riverside in NSOM along with the large-area scanning capabilities at LLNL with the AFM were integrated to design the large-area NSOM. The large-area NSOM is now operational and has been used to obtain some of the results on defects in optical components.[8]

References:

1. Marder, M. and Fineberg, J., *Physics Today*, p. 24, September 1996.

2. Betzig, E. and Trautman, J.K., *Science*, **257**, 189, 1992

3. Pohl, D.W. and Courjon D., "Near-Field Optics", *Kluwer Academic Publishers*, Karlsruhe, Ge, 1993.

4. Yang, T. J. and Mohideen, U., "Near-field Microscopy of Ferroelectric Domain Walls", *Applied. Phys. Lett.*, **71**, 1960, 1997.

5. Yang, T. J. and Mohideen, U., "Nanoscale Measurement of Strain at Ferroelectric Domain Walls", submitted to *Applied Phys. Lett.*

6. Narshimamurthy, "Photoelastic and Electro-optic Properties of Crystals", *Plenum Press*, New York, 1981.

7. Yang, T. J. and Mohideen, U., "Nanoscale Study of Domain Wall Mobility", submitted to *Ferroelectrics*.

8. Yan, M., Wang, L., Siekhaus, W., Kozlowski, M., Yang, T. J. and Mohideen, U., "Proceedings of Laser Induced Damage in Materials", *SPIE* vol. 3244, p. 268, 1997.

9. Wang, Li, Yan, M., Siekhausm, W. and Oberhelman, S., "Probing Narrow Defects in Fused Silica by Near-field Scanning Optical Microscopy", submitted to *Applied Phys.*

Novel Approaches to Surface Analysis and Materials Engineering Using Highly Charged Ions

LLNL Principal Investigators: *Alex Hamza, Thomas Schenkel, Alan Barnes*

Students: *Mike Newman, Univ. of Conn.; Marcus Schneider, Cal Poly, San Luis Obispo; Mirko Hattlass, Geothe Univ., Frankfurt; Guillamme Machicoane, Thomas Niedermayr, Univ. of Paris*

Overview

We are developing the use of slow, highly charged ion (SHCI)-surface interactions for sensitive surface analysis. The unique competitive advantage of SHCIs over conventional, singly charged ions is the extreme, high-energy- density that is deposited into a nanometer-sized near-surface volume at impact of a single HCI. For example, a Au^{69+} ion deposits ~0.5MJ/cm^3. The high-energy-density causes the emission of large numbers of secondary particles, which are probes of the energy dissipation mechanism. The yields and energy of the emitted particles are also of technological significance; they lead to the development of SHCI-based analysis techniques (such as secondary ion mass spectroscopy) boosting sensitivity limits to $<10^9$ atoms/cm^2. This surface sensitivity and quantification can be and is being applied to Laboratory missions in enhanced surveillance and nonproliferation.

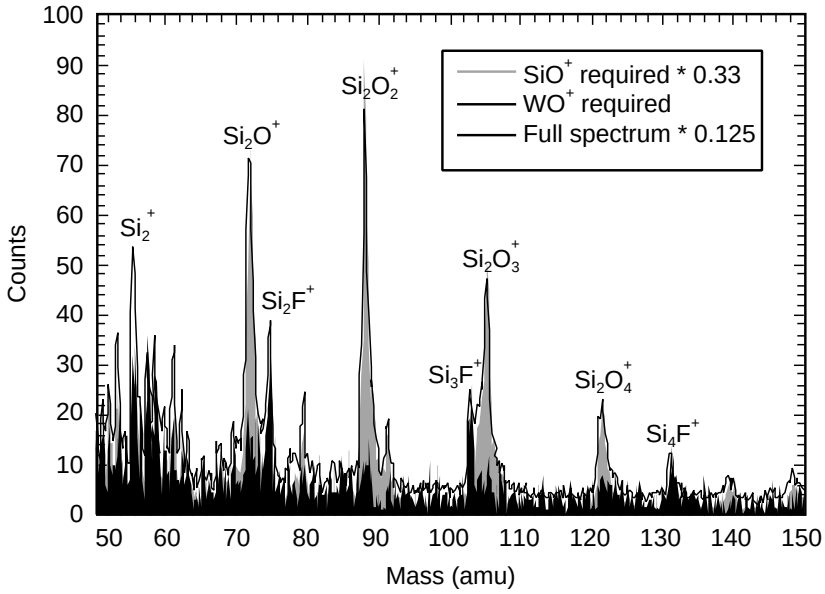

Figure 1. *Coincidence counting time-of-flight positive secondary ion mass spectrum from W/SiO_2/Si test wafer with a Th^{75+} primary beam with 262.5 keV incident energy. The black line is the full spectrum divided by 8. The SiO^+ coincidence spectrum divided by 3 is shown in yellow and the WO^+ coincidence spectrum is shown in red. The spectra are scaled based on the relative number of sweeps used to build each spectrum.*

Technical Progress 1998

More than one secondary ion can be detected from the impact of individual highly charged ions like Th^{75+} on surfaces. By accumulating time-of-flight cycles in secondary ion mass spectrometry (SIMS) event by event, we can differentiate impact events requiring the presence of characteristic fingerprint ions. Building spectra with characteristic requirements, we can now see correlation of secondary ions that were emitted from single primary ion impacts. We estimate the emission area of secondary ions to be only ~10 nm x 10 nm. The uniquely high secondary ion yields enable the probing of chemical structure and homogeneity of complex target surfaces on a nanometer scale. An example is given in Figure 1. The full spectrum shows signatures of tungsten oxide and silicon dioxide from a W/SiO_2 test wafer. Tungsten was deposited by reduction of WF_6 in disilane. A byproduct of this process is silicon fluoride compounds, most of which are volatile (SF_4). Requiring the presence of tungsten features, we find a very strong correlation with Si_xF ions. This indicates the presence of silicon fluoride on the tungsten areas. Requiring the presence of a SiO_2 feature reveals that no silicon fluoride is present on the SiO_2 areas of the test structure. The information gained can be fed back into optimization of process parameters. Highly charged ions are a unique tool for probing the chemical structure on a nanometer length scale. We are exploring the potential of this new technique in studies of materials

with programmatic significance such as hydrogen getter technology and high explosive mixtures.

We have designed and constructed a low-magnification, proof-of-principal, SHCI-based SIMS microscope. Images of test wafers were collected in several runs at the electron beam ion trap facility at LLNL. Contrast provided by the number of emitted electrons, secondary ion time-of-flight, and total emitted intensity was demonstrated at the micron scale. We will use this device as a testbed during development of components needed for the full instrument. In FY 98 we used the proof-of-principle device to attack three aspects of the project: the high bandwidth data acquisition system; the image processing and presentation software; and the quantification of the compositional information. The data from the test microscope is guiding the decisions for the final design. Figure 2 shows a SHCI-emission microscope image of copper lines on SiO_2.

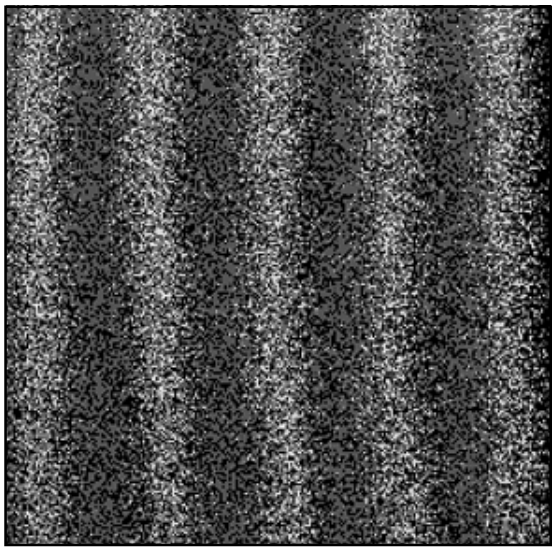

Figure 2. Slow, highly charged ion emission microscope image of 5 micron copper lines in SiO_2. The copper line spacing is 15 microns center-to-center. Red and yellow correspond to the higher pulse height events, hence higher electron emission. Events are also filtered based on the secondary ion time-of-flight.

We have also measured the sputter yields of uranium oxide and GaAs interacting with highly charged ions. Up to 70 uranium atoms and 1400 Ga and As atoms are removed by Th^{70+} ions. Sputter yields are fundamental characteristics of the interaction of highly charged ions with surfaces. Important new insights into atomistic mechanisms of the interaction are based on our results.

The Study of Photoluminescence and Device Applications of Si Quantum Dots

UC Principal Investigator: *Professor Susan M. Kauzlarich, UC-Davis*
LLNL Collaborator: *Howard Lee*
Students: *Daniel Mayeri, Chung-Sung Yang, UC-Davis*

During the past year, we have investigated Mg_2Si as a reagent to prepared Si nanoclusters. In addition, we showed that these nanoclusters can be prepared without oxygen on the surface. More work is necessary to prove a quantum confinement model.

Figure 1 shows a micrograph for the methyl-terminated silicon nanoclusters, which contains a large number of nanoclusters. This is produced from a reaction starting with Mg_2Si. Unlike reactions with ASi, we obtain a larger distribution of sizes. The number of nanoclusters, shapes and variety of sizes were typical for all preparations with Mg_2Si and similar micrographs were obtained regardless of surface termination. For some of the larger nanoclusters (5 nm), the outline of a hexagonal shape can be discerned. All the reactions that use Mg_2Si as a reagent produced particles that showed similar shapes. This is also quite distinct from our reactions with ASi, where we obtain mostly small particles (1-2 nm) with spherical shape. In all cases, the SAED (selected area electron diffraction) and lattice fringes (Figure 2) are consistent with diamond structure Si. The sizes range from 1 nm to 4-5 nm for a typical synthesis with only one lattice fringe orientation visible. Lattice fringes are measured from the negatives and are consistent with the {111} crystal plane of Si. The average size of nanoclusters obtained from TEM data is 3.2(1.3), 3.1(1.9), 3.7(2.1) and 4.4 (2.4) nm for $-CH_3$, $-C_2H_5$, -n C_4H_9, and -n C_8H_{17} termination, respectively. The standard deviation in nanocluster size increases with the length of the alkyl chain. This suggests that the longer-chain alkyl surfaces promote solubility of the larger nanoclusters.

FTIR was used to identify and characterize the organic species on the cluster surfaces. Seven characteristic peak groups are observed for Si clusters terminated with methyl, ethyl, n-butyl, and n-octyl alkyl groups, i.e., 2960-2920, 2860-2840, 1460-1450, 1380-1370, 1270-1250, 1100-1000, and 780-740 cm^{-1}. These peaks are assigned to C-H stretching and Si-C bending modes. There is no evidence for Si-O in the FTIR, which suggests that these nanoclusters have well-controlled surfaces and are completely passivated with alkyl groups.

Optical absorption and photoluminescence (PL) spectroscopy were used to investigate the optical properties of these silicon nanoclusters. The UV-vis absorption spectra

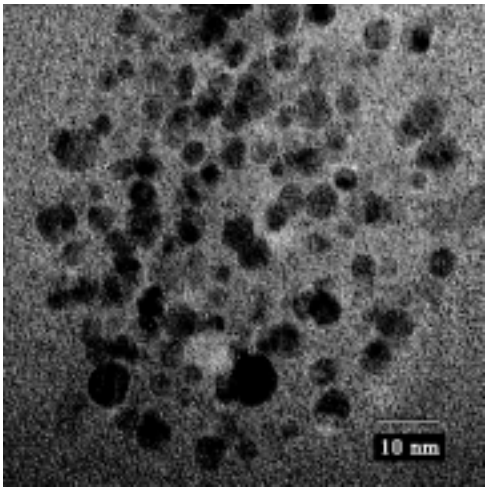

Figure 1. The HRTEM image for silicon nanoclusters terminated with methyl.

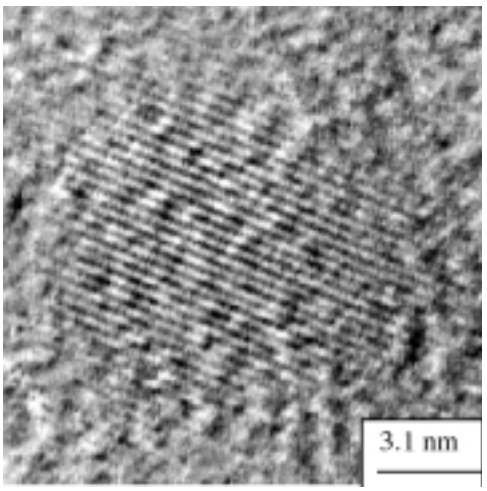

Figure 2. A HRTEM image showing lattice fringes of a Si nanocluster.

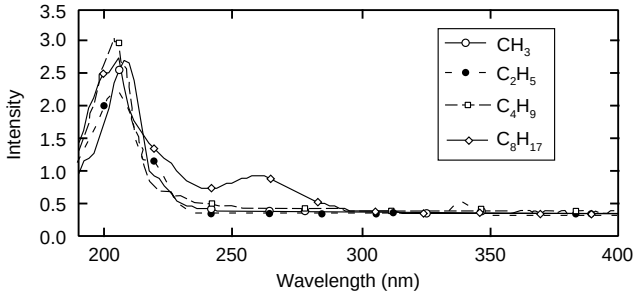

Figure 3. Optical spectra of Si nanoclusters terminated by various alkyl groups.

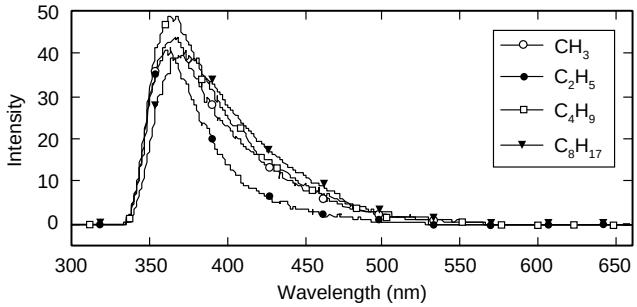

Figure 4. Photoluminescence spectra for alkyl-terminated Si nanoclusters. The emission spectra were collected from 300-800 nm with an excitation band width of 2.5 nm and excitation wavelength of 310 nm.

of various colloids are shown in Figure 3. The absorption of the solvent (hexane in this case) has been subtracted from each of the spectra. The nanocluster colloids showed similar features in the optical spectra. There is a small absorption at approximately 260 nm in the spectrum of the n-octyl-terminated sample. This feature is not assigned at the present time. An absorption edge appears at approximately 260 nm for the methyl-, -n butyl- and -n octyl-terminated samples and at 240 nm for the ethyl-terminated nanoclusters. This is considerably blue-shifted from the bandgap of bulk Si. The absorption edge shifts with nanocluster size in accordance with quantum confinement models and agrees with sizes observed in TEM images.

The photoluminescence spectra were measured at room temperature and are shown in Figure 4. One peak is observed for all four samples. To date, the origin of blue PL from nanocrystalline Si systems remains controversial.[6] This UV-blue peak is observed for all the samples regardless of surface termination, suggesting that the photoluminescence is intrinsic to the Si core. This UV-blue PL from these nanocrystallites occurs in a different spectral region than that from other blue emitters such as oxidized porous silicon (440-480 nm)[29] or silicon carbide (500-520 nm),[30] thus complementing the blue output performance. This result also suggests that these species are not the source of the blue emission that we observe from the Si nanocrystals.

We have developed a convenient and versatile technique for the synthesis of a variety of alkyl-terminated silicon nanocrystallites. This nanocluster photoluminesce strongly in the blue. The mechanism for the photoluminescence is still under investigation.

METALS/ORGANICS

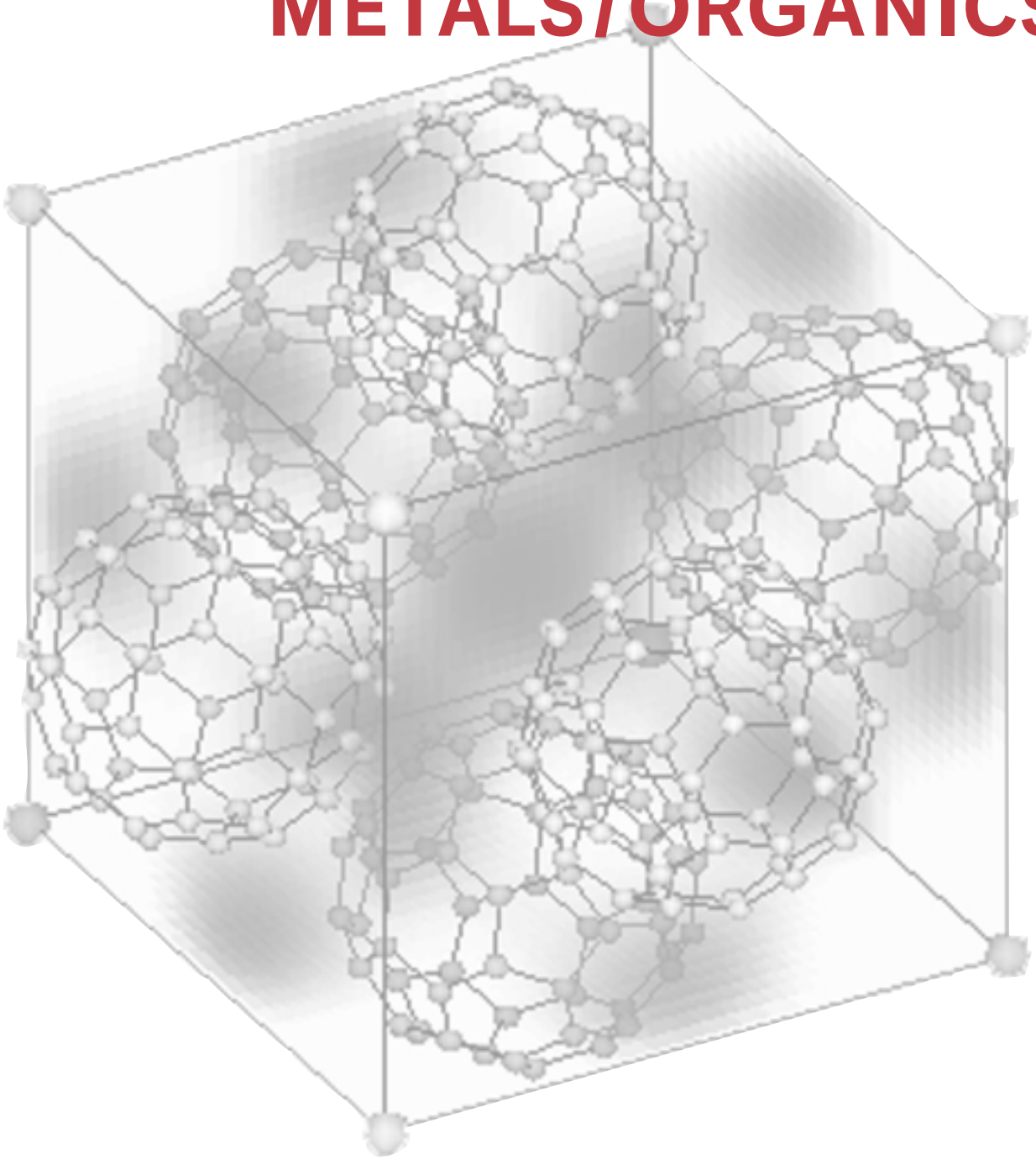

Dislocation Dynamics Simulations of Deformation Hardening In BCC Metals

UC Principal Investigator: *Professor Nasr M. Ghoniem, UC-Los Angeles*
LLNL Collaborator: *Tomas Diaz de la Rubia*
Post Docs: *Lizhi Sun, Shih-Hsi Tong, UC-Los Angeles*
Student: *Rudy Martinez, UC-Los Angeles*

Summary of Research Progress

Intensive experimental investigations of hardening mechanisms in both FCC and BCC alloys indicated that two types of phenomena govern the increase in flow stress: (1) source hardening and (2) friction hardening. Source hardening operates when the critical resolved shear-stress level is low and is increased slowly until dislocations are unpinned from the influence of small barriers to their motion. The phenomenon is common in BCC alloys, and is related to the fast diffusion rates of impurities, point defects, or other elements (e.g., carbon) to dislocation cores. Source hardening is manifest in a yield drop (from upper to lower yield points) and can be observed in unirradiated BCC alloys. Dislocation channels form in a manner similar to avalanche propagation, and the final result is the well-documented plastic instability in irradiated materials. Plastic deformation in this case is concentrated on slip planes, leading to premature fracture.

Deformation behavior of BCC metals, particularly Fe, is sensitive to temperature. Under neutron irradiation or high strain-rate deformation conditions, the flow stress in BCC metals increases, the DBTT shifts to higher values, and plastic deformation localizes, leading to premature fracture instabilities. Resistance to dislocation motion is known to increase as a result of increasing dispersed barriers through radiation-induced lattice defects. During the period covered by the research grant, we focused our efforts on the development of an accurate method for determination of stresses, forces, moments and interaction energies between slip dislocation loops and irradiation-induced defect clusters. In the following paragraphs, we describe our research accomplishments in these areas.

In DD simulations of plastic deformation, the computational effort-per-time step is proportional to the square of the number of interacting segments, because of the long-range stress field associated with dislocation lines. It is therefore advantageous to reduce the number of interacting segments during such calculations. Recent 3-D calculations of dislocation interactions using straight segments are based on analytical solutions of the elastic field of either mixed segments (e.g., Zbib, Rhee and Hirth, 1998 and Schwarz and LeGoues, 1997), or just screw and edge dislocation segments (e.g., DeVincre and Kubin, 1994). Zbib, Rhee and Hirth (1998) have shown that the length of each straight segment is roughly limited to the range of 50-200 units of Burgers vector. Longer segments may have substantial force variations, thus limiting the usefulness of one single equation of motion for the entire segment. Meanwhile, singular forces and stresses arise at sharp intersection points of straight segments, which results in divergence of the average force over the straight segment as the segment length is decreased. When the dislocation loop is discretized to either screw or edge components that move on a crystallographic lattice (Devincre and Kubin, 1994), the accuracy of strong dislocation interactions is compromised because line curvatures are crudely calculated. In addition, motion of dislocation segments on a fixed lattice produces inherent limitations to the accuracy of the overall dislocation dynamics.

Evaluation of the elastic field around an arbitrary-shape dislocation loop requires explicit development of the equations of elasticity for each finite segment. The procedure is quite lengthy, and is described in sufficient detail by Ghoniem and Bacaloni (1997). We developed a new procedure, by first rewriting Burgers displacement equation for a loop in index tensor form. The displacement vector is then differentiated to obtain the elastic strain in an isotropic material as a line integral. The stress tensor is computed from the linear relationship between the strain and stress in an isotropic elastic material. The line integral for each stress component is finally discretized by parametric segments, and the total stress field is computed by numerical quadrature integration over each segment. Summation of field contributions from loop segments is not required in these cases, because the entire loop is represented by one closed segment. Thus,

the stress tensor is evaluated by numerical integration of the following form:

$$\sigma_{ij} = \frac{Gb_n}{4\pi} \oint_c \left[\frac{1}{2} R_{,mpp} \left(\in_{jmn} dl_{i'} + \in_{imn} dl_{j'} \right) + \frac{m}{m-1} \in_{kmn} \left(R_{,ijm} - \delta_{ij} R_{,ppm} \right) dl_{k'} \right]$$

Ghoniem and Bacaloni (1997)-developed explicit forms for the stress field components in detail.

The interaction between slip-type dislocation loops and defect clusters has been determined in BCC metals. This is accomplished by development of equations for the interaction energy of a general dislocation loop and small _<111>-[111] prismatic defect clusters. Three levels of calculations have been performed: (1) full numerical evaluation of double-line integrals for the slip loop / defect cluster configuration, (2) an elastic dipole approximation and (3) a center of dilatation approximation for the cluster. The purpose of this investigation was to identify the main cause of decoration of slip loops by small irradiation-induced defect clusters, and to correlate the width of the interaction zone with experimental observations.

UCLA Campus–LLNL Collaboration

The UCLA team is composed of Professor Ghoniem, one graduate student, one undergraduate student and two post-doctoral students. Professor Ghoniem is leading the team by formulating new methodologies for dislocation dynamics and for the interaction of dislocations with irradiation-induced defects. The graduate student is helping him by performing tensor algebra and computer programming of the resulting equations. Dr. Shih-Shih Tong is an expert in computational geometry and is currently working with Professor Ghoniem to develop efficient techniques to represent dislocation topologies in 3-D. In addition, Dr. Lizhi Sun, who joined the group recently, is working with Professor Ghoniem to develop and implement the equations for the mechanical interaction between dislocations and defects. His background is in the area of micro-mechanics, and he is well suited to the tasks.

Dr. Tomas de la Rubia heads the LLNL team. The interaction between UCLA and LLNL comes naturally, because of the complementary nature of expertise between the two groups. The team at LLNL has extensive expertise in Molecular Dynamics (MD), while the team at UCLA is focusing mainly on 3-D Dislocation Dynamics. Dr. de la Rubia's group has been performing MD calculations for dislocation-defect interactions and for the migration of small-coupled crowdions in Fe. The research is complementary, because MD simulations can investigate defect behavior close to the dislocation core, where elasticity breaks down.

Significant Research Results

Representation of dislocation loops by parametric equations, coupled with a fast integration technique for field variables as line integrals, appear to have a number of potential advantages. These are summarized as:

- A complex dislocation loop (e.g., during the operation of a Frank-Read source, or during the process of cross-slip for non-planar loops) can be represented by a relatively few number of curved segments. The Peach-Koehler force resulting from the interaction of one loop with another can thus be numerically computed as a fast summation over those few curved segments. This can be quite advantageous in 3-D Dislocation Dynamics, because the force computation is proportional to the square of the number of segments. Thus, a reduction of two orders of magnitude in the number of segments will result in a four order-of-magnitude reduction in force calculations.

- Because of the high accuracy of curvature representation in the present method, the computation of self-forces and self-energies of individual segments within one loop is inherently accurate.

- When the P-K force and other elastic field quantities are required at distances greater than approximately 1/20–1/10 of a loop diameter from its core, very useful approximations of the loop can be advantageously used within the current line integral context. Thus, planar circles can readily approximate the core of small irregular loops, while dipolar loops can be treated as elongated ellipse, etc.

- Although two nodes bound each segment, the dislocation core is described by a continuous curve in-between. Thus, the segment has an infinite number of degrees of freedom. This particular aspect can be quite significant in a variational development of the equations of motion (see Ghoniem, 1998)). Other formulations of the equations of motion of straight

segments use an averaging scheme for force variations on the segment. Thus, when the segment is long, averaging of the P-K force at a central nodal position becomes less accurate.

- Since the dislocation loop is continuously described by a set of curves, updating the loop shape in Dislocation Dynamics can utilize the existence of such "shape functions." The need to artificially impose connectivity conditions where the straight pieces do not fit with one another upon updating the positions of their central nodes is thus alleviated.

Coupled dynamic crowdions produced by collision cascades have been shown to migrate at very low energies, on the order of 0.001–0.01 eV in Fe crystals. Once they migrate in one dimension, they interact with grown-in dislocations by elastic forces. We have studied the nature of this interaction in order that the conditions for locking grown-in dislocations can be clarified. In addition, we embarked on a joint effort with LLNL and RISO Materials Research Group (Denmark) to study the various factors, which lead to decoration of grown-in dislocations, and to the eventual absorption into the core region of such dislocations. This question is ultimately important to determine the onset conditions of dislocation channel formation in BCC metals. The findings of our work have been reported in the Workshop on the "Fundamental Differences Between FCC, BCC and HCP Metals," which was held in Congas de Onis, Spain, during the period: October 13-21, 1998. Our findings are summarized in the following:

- The "Dilatation Center Approximation" for the interaction of clusters is not adequate. It is weak by more than a factor of two and does not show the influence of cluster orientations.
- Interaction energy surfaces around slip loops show a significant dependence on cluster orientations.
- Four independent cluster orientations have been identified. The capture zone size at room temperature is ~ 10 nm for each one.
- Cluster mobility on crystallographic planes is constrained by their orientation on glide cylinders.
- Gliding clusters will be trapped below and above the slip plane. Maximum trapping occurs for near edge components, decreasing to zero near screw components.
- Trapped clusters will not get absorbed into slip loops, unless additional rotational work is done to change their BV orientation.
- Absorption zone for clusters is much smaller than the trapping zone, and is ~ 3 nm.
- Clusters produced from cascades in FCC crystals are generally sessile, because of dissociation into partials bound by stacking faults.
- The capture zone size in Cu is larger than in Fe, and is ~ 20 nm at RT.
- The absorption zone size in Cu is ~ 6 nm at RT.
- The temperature dependence of the capture zone in Cu is stronger than in Fe. The zone decreases by a factor of two from RT up to Tm/2.
- Conversion from Sessile to Glissile Clusters in FCC may occur only within ~ 6-10 nm away from the core of slip loops in Cu.

Elastic Constants of Ta at High Pressures and Temperatures Determined by Stress- and Angle-Resolved Synchrotron X-Ray Diffraction in a Diamond-Anvil Cell

LLNL Principal Investigators: *Hyunchae Cynn, Choong-shik Yoo*

University Collaborators: *Professor Yogi Gupta, Wash. St. Univ.; Professor Don Issak, UC-Los Angeles*

The elastic moduli C_{ij} of crystalline solids are of value for a wide range of important problems relevant to solid-state physics and geophysics. The C_{ij}'s provide fundamental information pertaining to interatomic potentials and are, therefore, essential parameters for guiding theoretical construction of exotic novel materials like low- compressible solids. Elastic moduli also provide information about macroscopic behavior, the bulk and shear modulus, and are required for a complete understanding of the thermoelastic properties of materials. Especially in geophysical applications, information on the elastic properties is essential for determining accurate equations of state and for computing the compressional and shear-wave velocities. Such information is fundamental to our understanding of the composition, structure, thermal properties, and evolution of the Earth.

We have developed a new experimental technique—a Stress and Angle-resolved X-ray diffraction (SAX; Figure 1), which is parallel to Stress and Energy-dispersive X-ray diffraction (SEX; Singh et al., 1998). The SAX utilizes a monochromatic synchrotron and an image plate detector. This combination allows a fixed geometry of a diamond-anvil cell (DAC) on the contrary to the SEX method, which requires rotation of a DAC.

The lattice strain of Ta was measured over 1 Mbar from a uniaxially compressed Ta sample supported by x-ray transparent gaskets. From the elliptically distorted x-ray powder diffraction patterns due to microscopic deviatoric stresses acting on each diffraction plane, and the knowledge of macroscopic stress obtained from the yield strength measurements and compressibility, the elastic constants C_{11}, C_{12}, and C_{44} for the bcc Ta were estimated as a function of pressure. The results indicate qualitative agreements with theory and the existing strength model.

As for the complimentary measurements, we have measured isothermal compressibility of Ta near to 2 Mbar (Figure 2) and the accurately confined pressure derivative of the compressibility of Ta places the equation of state of Ta to be the most precise pressure standard for static experiments using a diamond-anvil cell (Cynn and Yoo). We have also measured *in situ* thickness of uniaxially compressed Ta powder in cylindrical shape as a function of pressure to understand lattice strain and macroscopic plastic deformation. In order for this measurement, we used a submicron size synchrotron radiation at 10 keV (ALS) to measure x-ray absorption to reconstruct the sample dimension using tomographic image.

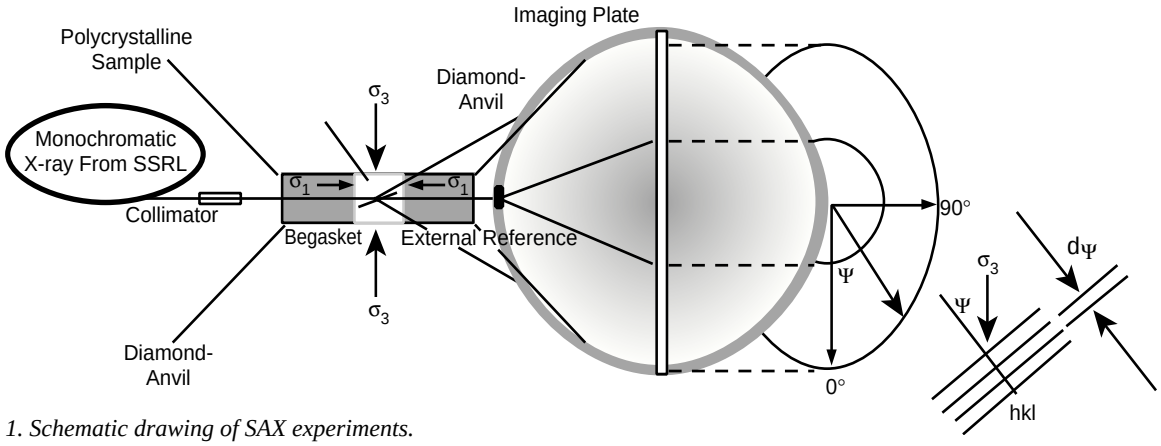

Figure 1. Schematic drawing of SAX experiments.

Yield strength of Ta was also directly measured by measuring x-ray absorption, which provides thickness and measuring volume compression. The latter provides the accurate pressure gradients. The direct absorption measurements yield better estimates of the thickness of the sample than other methods like estimating from a decompressed gasket using an equation of state.

References

1. Singh, A., Mao, H., Shu, J. and Hemley, R., "Estimation of Single-crystal Elastic Moduli from Polycrystalline X-ray Diffraction at High Pressure L Application to FeO and Iron", *PRL*, **80**, 1998.

2. Cynn, H. and Yoo, C., "Equation of State of Tantalum to 174 GPa", *PRB*, **59**, 1999.

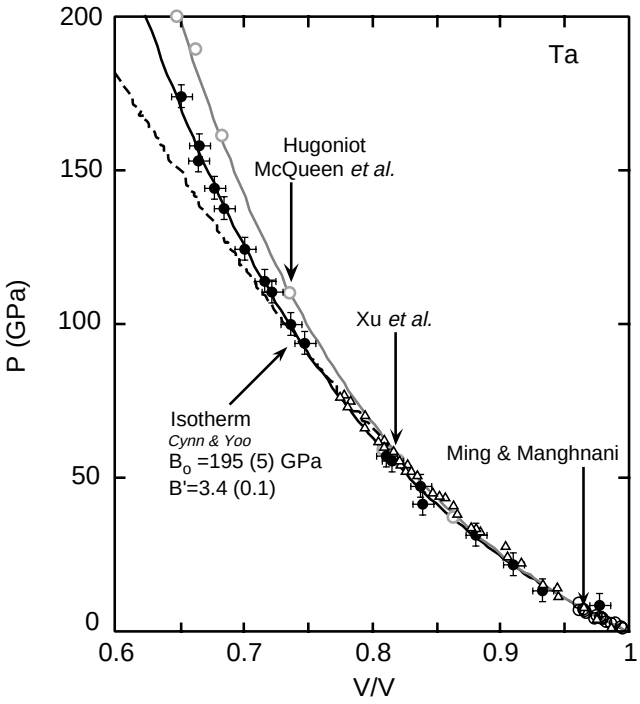

Figure 2. *Volume compression of Ta to 2 Mbar.*

Extreme States of Matter on Nova

LLNL Principal Investigators: *Bruce A. Remington, Dan Kalantar*

University Collaborators: *Professor Justin Wark, Univ. of Oxford; Professor Marc Meyer, UC-San Diego; Professor Tom Boehly, Univ. of Rochester*

Students: *Andrew Loveridge, Adrian Allen, Univ. of Oxford*

We have developed dynamic diffraction experiments to diagnose shocked solid-state lattices on intense lasers such as the Nova and Trident lasers. This was in collaboration with UC-San Diego, Univ. of Oxford, and Los Alamos National Laboratory. During this period, we have developed successful dynamic diffraction experiments on (111) and (400) Silicon lattices, both on the Nova laser and on the Trident laser. We also developed simultaneous transmission Bragg diffraction measurements off orthogonal lattice planes, to look for evidence of the transition to 3-D. No evidence for lateral lattice adjustment was observed for (400) Si, which is a theoretical puzzle still under active investigation.

These experiments have received high visibility, with several publications and 16 conference presentations, several of which were invited talks.

In anticipation of the closing of the Nova laser, we have successfully proposed transferring these dynamic diffraction experiments to the Omega laser at the Univ. of Rochester under the NLUF Program and will continue using the Trident laser at LANL.

The goal of this endeavor was to technically assess whether dynamic diffraction could be developed into a robust diagnostic of solid-state lattices under shock loading. Successful observation of shock-compressed lattices in the direction of shock propagation in Si have been observed. Development of a diagnostic to observe the transition to 3-D is ongoing, with this work continuing on the Omega and Trident lasers.

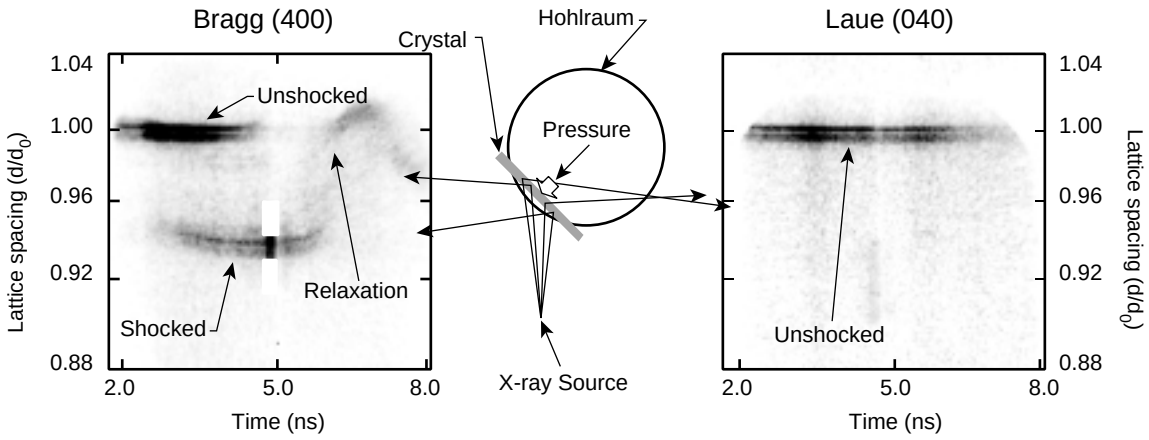

Figure 1. Diffraction from orthogonal lattice planes shows compression is uni-axial when shocked along the (400) direction at 115-135 kbar.

New Theoretical Framework for Computing Positron Annihilation Characteristics

UC Principal Investigator: *Philip A. Sterne, UC-Davis*
UC Co-Investigator: *Professor Barry M. Klein, UC-Davis*
LLNL Co-Investigator: *Richard H. Howell*
Student: *John E. Pask, UC-Davis*

Introduction

Lawrence Livermore National Laboratory has an active research effort in positron annihilation spectroscopy. Theoretical calculations of positron observables such as positron distributions and lifetimes are essential for interpreting positron experimental data. In the past, a program written by the PI was used for calculating positron observables in materials, but that program is not suitable for very large systems or for systems with very open structures like zeolites, fullerenes, and energetic materials like TATB. The goal of this project was to develop a new computer program for calculating positron lifetimes and distributions in materials that could be applied to very large systems and to both open-and close-packed geometries. This new computer program has been successfully developed and tested during this funding period and is now an established tool for calculating positron lifetimes at the LLNL Positron Facility.

Research

The Finite Element (FE) approach is widely used to solve general differential equations for arbitrary geometries in engineering and other applications. There have been relatively few FE applications to the solution of the Schrodinger equation in materials, but the success of the FE approach in other applications suggested that it could provide a full-potential electronic structure method with favorable scaling properties and no restriction on the unit cell geometry. The solution of the Schrodinger equation lies at the heart of both positron and electron calculations, so our intention is to develop a FE electronic structure program that can solve both electron and positron problems. In the past year we have made significant progress in this direction. The new positron program is a significant milestone in this work and it addresses an immediate need for large-scale calculations in the LLNL Positron Facility.

We solved a number of technical issues in developing this positron program. First, we formulated the mathematical approach required to solve the Schrodinger equation for a Bloch-periodic system within a FE approach and implemented this approach in a computer program. This program was tested by calculating electron bandstructures for an analytically solvable 3-D periodic Kronig-Penney model and an empirical Si pseudopotential. These tests confirmed the accuracy of the method and the validity of the mathematical approach and also demonstrated the variational nature of the solution, a significant advantage of this approach over other real-space methods.

The second challenge was to develop a general approach for providing an input positron potential for the calculations. This was addressed by developing a computer program to compute the charge density and potential at any point in the unit cell based on overlapping atomic calculations. This program has been tested extensively for positron potentials and will also be used in the coming year to generate initial electron potentials when we incorporate electron-charge self-consistency. The positron program currently does not take any charge density relaxation into account, and this, together with theoretical uncertainties in the electron-positron interactions, is the most significant limitation of the current approach.

Given an input potential, the FE method solves for the positron wavefunction. This, in turn, provides observables such as the positron distribution in the unit cell and the positron lifetime. We have validated our method by calculating the positron lifetime for 23 elemental metals and have obtained excellent agreement with both previous calculations and experimental data. Similar agreement was found for calculations on monovacancies in metals. The monovacancy calculations depend on the size of the periodic supercell used to model an isolated vacancy. We were able to go to unprecedented supercell sizes with this new method. Our previous positron computer program was limited to a maximum of about 150 atoms in the unit cell, but with the FE program we successfully calculated the positron lifetime and distribution in a much larger 863-atom supercell. Even larger calculations are feasible, and we plan to use this program in the

coming year to calculate positron lifetimes in dislocations in metals. This will require calculations on systems of 1000-5000 atoms.

Having validated the lifetime calculations in this approach, we computed lifetimes for a number of materials of immediate interest to LLNL. Calculations for bulk Pu and He-filled vacancies in Pu agreed with our previous calculations and confirmed previous interpretations of experimental lifetime measurements on aged Pu samples. Calculations on some insulator systems, including the scintillator crystal BaF_2 and the energetic material TATB, yielded different lifetime values, probably due to the limitations of the overlapping atomic approach, which we will address in the coming year. These calculations also indicated that the physical description of positrons in these systems may need to be amended to account for positronium formation, providing a significant theoretical challenge for the positron community.

The newly developed FE approach is able to provide positron distributions in real space, a significant advantage over our previous method. We illustrated this with calculations on potassium-doped fullerenes, where we could follow the positron redistribution in the unit cell due to increasing potassium doping. A 3-D representation of the positron distribution in pure C_{60} is shown in figure 1.

Two papers have been submitted for publication based on this year's work:

1. *A Real-Space Local Polynomial Basis for Solid-State Electronic-Structure Calculations: A Finite-Element Approach,* J. E. Pask, B. M. Klein, C. Y. Fong, and P. A. Sterne, submitted to Phys. Rev. B.

2. *Calculation of Positron Observables Using a Finite-Element-Based Approach,* P. A. Sterne, J. E. Pask, and B. M. Klein, submitted to Applied Surface Science.

In addition, presentations were given in talks at the APS March Meeting in Los Angeles and the SLOPOS-8 international workshop in Cape Town, South Africa, in September. A poster was presented at the Electronic Structure 1998 Conference in Philadelphia in May. The student, John Pask, also took part in a parallel computing workshop in San Diego in August where he presented some of this work as part of a group presentation on applications for parallel computers.

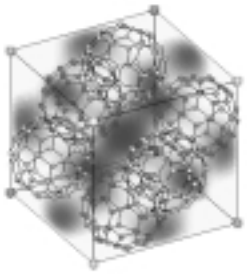

Figure 1. Positron distribution in crystalline C_{60}. For clarity, only the face-centered C_{60} molecules are shown; the cell-corner fullerene molecules are indicated as gray atoms. Note the positron charge buildup, represented as a shaded cloud, at the octahedral positions in the cell center and the edge centers.

Campus-LLNL Collaboration

This project involves a vigorous collaboration between LLNL and UC-Davis. John Pask, the student most directly involved in this work, has visited the Laboratory for two days a week regularly since June 1998. Prior to this, he made occasional visits to meet with LLNL personnel, including attendance at a Positron Workshop hosted by the Materials Research Institute in November 1997. His main contacts at LLNL have been with H-Division personnel because of the PI's close connections with that Division, but he has also recently interacted with personnel from the Center for Applied Scientific Computing (CASC) in the Computations Directorate. Future interactions with both of these divisions will be very helpful for the further development of the computer program for positron calculations.

Materials Research Institute

The MRI has provided an office for the student, John Pask, and another UC-Davis student, Gus Hart, when they visit LLNL for two days a week. This has been extremely valuable, both directly to the current project and indirectly to the intellectual vitality of the Laboratory and the Institute. They have both benefited from their frequent visits to the Laboratory through exposure to a wider range of materials-related and computational issues, and their interactions with other personnel have certainly been of benefit to LLNL.

Optically-Induced Structural Changes in Materials

UC Principal Investigator: *Professor Roger E. Falcone, UC-Berkeley*
LLNL Principal Investigator: *Troy W. Barbee, III*
Student: *Aaron Lindenburg, UC-Berkeley*

We are studying the structural changes that can be induced in crystalline materials by the optical excitation of carriers. In particular, short laser pulses can excite several percent of the bonding electrons in semiconductor crystals into the conduction band. This should result in a rapid phase transition, either to the amorphous state or to other (transient or metastable) structures. These phase transitions should be observable using newly developed, time-resolved x-ray scattering techniques.

Time-resolved x-ray scattering can be used to characterize rapidly evolving materials, where laser heated material can undergo rapid phase transitions (such as disordering, melting, cutting, or vaporization) and plasma dynamics (such as rapid ionization and hydrodynamic expansion). Dynamics of dense materials can be characterized by deeply probing x-rays in diffraction or other scattering techniques, such as EXAFS and other absorption measurements. The required, minimum time resolution for such experiments can be bounded by either the fundamental vibrational period of atoms in a crystal (0.1 ps) or the characteristic time scale of hydrodynamic expansion, often given by the optical skin depth (10 nm) divided by the sound speed (100 nm/ps) in a plasma (again, 0.1 ps).

We have developed a beamline at the Advanced Light Source (ALS) synchrotron at Lawrence Berkeley National Laboratory for time-resolved x-ray diffraction studies. The set-p[1] utilizes a synchrotron radiation x-ray source from a bending magnet beamline at the ALS. The bending magnet at beamline 10.3.2 emits a broad spectrum of x-ray radiation, extending to a useful photon energy of about 12 KeV. X-rays are monochromatized and focused using a bent crystal. A Ti:Al_2O_3-based laser system produced pulses with duration of about 100 fs at a repetition rate of 1 KHz; it has been synchronized to the x-rays from the electron storage ring. The delay between the laser and the x-ray pulse can be varied using an optical delay line in the laser beam path. The laser and x-ray beams are focused on a sample, which is mounted on a goniometric cradle and has a resolution and unidirectional repeatability of 5 mrad. Diffracted x-rays are detected by an x-ray-sensitive avalanche photodiode (APD) or streak-camera detector.

Synchrotron pulses are an excellent source for probing materials. With good collimation, a pulsed time structure, and uniform spectral intensity, the synchrotron provides a laser-like probe for experiments. For example, we detect 10,000 photons in a single x-ray diffraction spot from a silicon crystal at 5 KeV in a 70 ps pulse. The collimation is sub-millirad and the fractional bandwidth is 10^{-4}. The laser system (with pulses extending down to 100 fs) is synchronized to the synchrotron x-ray pulses, from single shot to a maximum repetition rate of 1 KHz. We can therefore heat material using the laser and subsequently probe its structure or absorption spectrum.

We are using time-resolved x-ray diffraction to study dynamics of radiation-heated materials. The properties of crystals following irradiation with ultrashort pulse lasers had been studied for nearly two decades. One motivation for this work has been the determination of the mechanism of ultra-fast disordering (melting) and other phase transitions, a still unsolved problem. Pump-probe techniques have generally been employed. On ultra-fast timescales (< 1 ps), these studies have involved time-resolved reflectivity and second-harmonic generation of optical light pulses. On longer timescales (> 1 ps to 10 ns), electron diffraction from surfaces and x-ray diffraction have provided additional insight into relevant phenomena, including thermal melting, shock propagation, heat diffusion, crystal regrowth, and annealing. These studies are not definitive since they (1) are limited by the rapidly changing optical properties of laser heated material, and (2) don't probe the structure of the material at the atomic (core) level. X-ray diffraction will allow use to probe the regularity of the lattice and thus determine accurately the order (or lack of order) of the illuminated material on a rapid time scale.

Theoretical studies[2] have suggested that excitation of 10% of the valence electrons in crystals should result in structural instability, which gives rise to a transition into a new ordered phase. Shown in Figure 1, calculations by Dr. Troy Barbee III show a structural instability in crystalline silicon is predicted when approximately 10% of the electrons are excited into the conduction band, a number that

we can approach using femtosecond laser excitation. It is this effect that we hope to measure in our experiments. In additional work, we plan to look for new transient or metastable structures, which would be manifested by new diffraction peaks.

We have previously demonstrated 2 ps resolution using both streak camera detection and cross-correlation measurements in preliminary work on x-ray scattering. In work covered under this proposal, we will employ a UC-Berkeley graduate student to apply the time-resolved x-ray technology to the specific measurement of the disordering time of laser-illuminated crystals using the ALS beamline, and compare these measurements to calculations on laser-illuminated materials calculated by Troy Barbee at LLNL.

The Synchrotron Beamline

The x-ray beamline, the synchronized laser system, spectrometers, and time-resolved detectors are all in place at the ALS. This beamline was funded through support of the ALS and a NSF Academic Research Infrastructure grant funded in 1996. The beamline is currently focused on studies of time-resolved x-ray diffraction of melting solids under the direction of the PI, Professor Roger Falcone. The beamline operates 24 hours per day, 5 days per week, and is not fully utilized; there is nominally 10% time available for the proposed experiments over the proposed grant period.

The ALS bending magnet beamline (designated 10.3.2) emits a broad spectrum of radiation with an average power of 50 W, extending from the visible to about 12 KeV with the electron energy in the ring of 1.9 GeV. Experiments can be performed with the ALS operating in a double-bunch mode, for which the average electron beam current is 40 mA and the light pulse repetition rate is 3 MHz. Alternatively, the ring is operated in a "camshaft" mode with a single, circulating 20 mA electron pulse (yielding high-power light pulses at a repetition rate of 1.5 MHz), followed by a series of 288 low-current pulses yielding light with an effective burst repetition rate of 500 MHz. The divergence of the synchrotron beam is about 0.3 mrad (vertical) and the experiment is contained in a shielded hutch 30 m from the ring. Broadband radiation is dispersed by either crystals or spectrographs, depending on the spectral region of interest. In order to maximize the signal seen by the detector and focus the x-ray light, bent crystals or curved grazing mirrors are employed for light collection. We observe several thousand photons per 100-ps pulse, in a fractional bandwidth of 10^{-4}, in virtually all regions of the spectrum, which is sufficient for well-resolved absorption spectroscopy. We are currently installing a 70-cm long, 5-cm wide, high-quality grazing (toroidal) mirror to produce a 200 μm x-ray spot in the experimental hutch, a one-to-one image of the emission from the electron bunch in the storage ring. The mirror has a spectral bandwidth extending up to 12 KeV and is expected to increase collected light levels by a factor of 10 to 100.

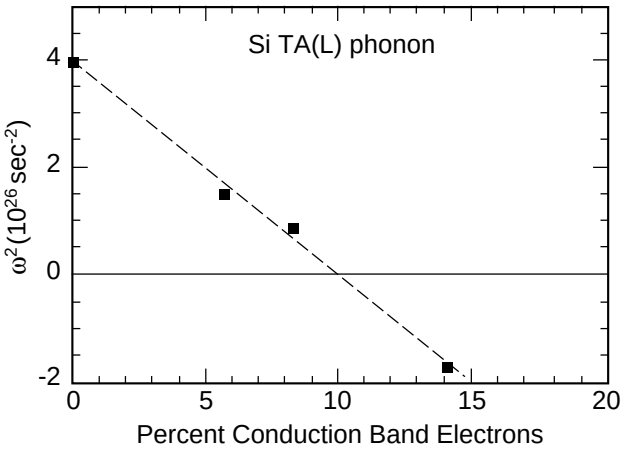

Figure 1. First principles calculations of the phonon frequency squared, ω^2, as a function of the fraction of electrons excited into the conduction band, are shown for the transverse acoustic L-point phonon ($q = \pi/a$ (111)) *in silicon. When 10% of the electrons have been excited into conduction band, a structural instability occurs; this is indicated by $\omega^2 < 0$. (The dashed line is a guide for the eye.)*

The 800-nm laser system consists of a Ti:Al_2O_3 laser oscillator pumped by a frequency-doubled Nd-laser and a Ti:Al_2O_3 regenerative amplifier system operating at a repetition rate of up to 1 KHz. The pulse duration is approximately 100 fs, and the pulse energy is about 1 mJ. Alternatively, the laser can be operated at pulsed energies of up to 100 mJ in single-shot mode, more than enough to heat sample foils to plasma condition. Synchronization of the laser pulses with the synchrotron pulses is achieved by locking the laser-oscillator repetition frequency (set by the oscillator cavity length) to the master clock of the ALS. The jitter between the laser and the synchrotron pulses is less than 5 ps. Using the x-ray streak camera we can detect single synchrotron pulses. The resulting initial measurements of the ALS pulse duration, using dispersed light from a crystal, show the expected 80 ps pulse from the storage ring.

References

1. Larsson, J., *et al*, "Ultrafast X-Ray Diffraction Using a Streak-Camera in an Averaging Mode", *Opt. Lett.*, **22**, 1012 1997.

2. Stampfli, P. and Bennerman, K. H., *Phys. Rev.*, **B49**, 7299, 1994 and refs. within.

Study of the Role of Coherent Phonons and Shock Waves on Energy Transfer Processes in Femtosecond Laser-Induced Melting of Solids

UC Principal Investigator: *Professor Harry W. K. Tom, UC-Riverside*
LLNL Principal Investigator: *Choong-shik Yoo*
Post-Doc: *Hong-Bing Jiang, UC-Riverside*
Students: *Hidong Kwok, Jingyan Guo, UC-Riverside*

The Goal of MRI-Funded Work

The goal of the MRI-funded work was to study the interplay between coherent phonons and hot electrons in femtosecond laser-induced disorder and melting processes in semiconductors. The key question is: how can energy be rapidly transferred from the hot electrons to atomic motion to enable the lattice to disorder in only 100 fs after the laser pulse? This short time for disorder is inconsistent with typical electron-phonon energy relaxation rates. We specifically examine whether or not the creation of coherent longitudinal (LO)-phonons under femtosecond laser irradiation enhanced the electron-phonon energy exchange rate or enhanced pressure-induced or pressure-enhanced disorder processes. Studies are relevant and complementary to high-pressure studies of materials, especially studies by the LLNL PI on laser-heating and processing materials under static high pressure.

Summary of Results

We made two significant experimental observations: (1) observation of coherent LO-phonon-hole plasmon-coupled oscillations at the native oxide-covered GaAs(110) interface under femtosecond laser irradiation, and (2) femtosecond laser-induced damage of the GaAs(110)-relaxed (1X1) surface. The first was delivered as a contributed oral talk at the March 1998 APS meeting in Los Angeles, CA, by student K. C. Chou. Numerical analysis is being performed before publication. The second result has recently been submitted for publication in *Physical Review Letters*. All work was performed at UC-Riverside in the UC PI's laboratory. MRI funds were used for partial support for two graduate students, (Hidong Kwak and Keng Chang Chou) and for postdoctoral researcher Hongbing Jiang. Additional funds were obtained from NSF contract CHE-9707143.

Result #1: Technical accomplishment

We conducted time-resolved second-harmonic-generation (SHG) studies of the GaAs(110)-native oxide interface under conditions of intense femtosecond laser irradiation. The experimental setup and basic idea is described in our publication on coherent phonons on the (1X1) reconstructed surface of GaAs(110) in ultrahigh vacuum,[1] and at the GaAs(100)-native oxide surface.[2] The basic idea is that carriers injected by the femtosecond pump laser pulse rapidly screen the static depletion field. The lattice, which is initially strained by the piezoelectric effect, is then suddenly allowed to oscillate about its low-field equilibrium position. The motion of the lattice is called coherent phonons because all modes of low k-vector are excited in temporal phase, behaving as a single large amplitude phonon oscillation. Ippen[3] and Kurz[4] have pioneered the use of coherent phonons to study carrier-phonon interactions in bulk matter. In n-doped GaAs, the surface depletion field drives holes to the surface and electrons into the bulk. The coherent LO-phonon oscillation at the bulk LO-phonon frequency (8.8 THz) and the LO-phonon-electron plasmon- coupled mode frequency (varies from 7.5 to 8.0 THz as a function of electron density) has been detected in time-resolved linear reflectivity by coworkers of Kurz.[5] Here we use time-resolved SHG (the SHG from a time-delayed probe pulse overlapping the excited region) to probe the bulk LO-phonon oscillations in the topmost ~100 Angstroms of the interface where there is a high-density hole plasma.

In Figure 1, we show a typical time-resolved SHG signal vs. time delay between the arrival of the pump pulse (initiating the coherent phonon) and the probe pulse. The fundamental laser wavelength is 850 nm, and the SH is at 425 nm. SHG is interface sensitive due to dipole selection rules, nonlinear optical phase matching, and the absorption of the SH photons in bulk GaAs. An abrupt change at delay time ~0 is due to the injection of carriers and rapid field screening.

The oscillations, which are about 1% of the total SHG and 10% of the pump-induced change in SHG, are due to coherent phonon oscillations. The background is subtracted in the time domain, giving the rapidly varying oscillations in the left inset. The SH radiation is driven

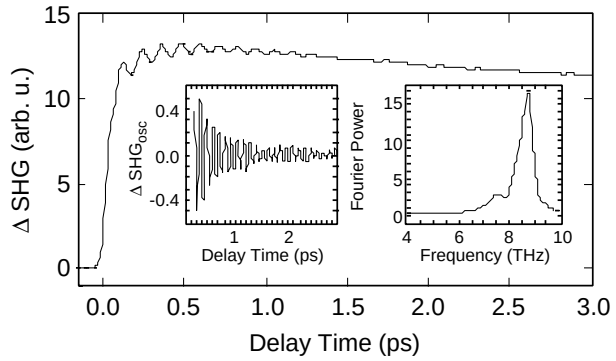

Figure 1. Pump-induced change in SHG vs. delay time from GaAs. Left inset shows SH oscillations after removing slowly varying SH background. Right inset shows Fourier power spectrum of oscillatory, SH data in left inset.

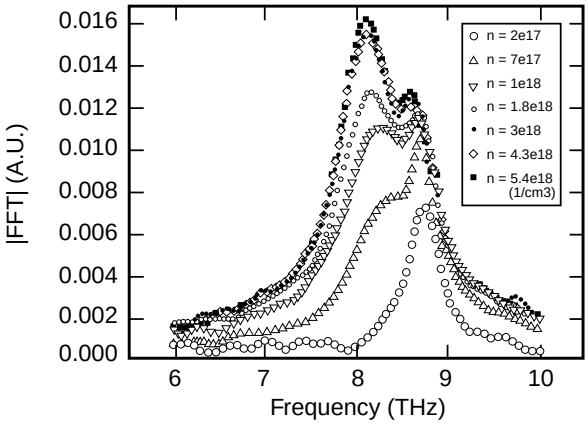

Figure 2. Fourier power spectrum of coherent phonons on GaAs(110)-native oxide interface for various injected carrier densities.

by the nonlinear polarization, which varies in time as:

$$P(2\omega,t) = \bar{\chi}^{(2)}(2\omega) + \frac{f\chi^{(2)}(2\omega)}{f\hat{Q}}\Big|_{Q=0} Q(t) + \chi^{(3)} E_{DC(t)} \sqrt{\quad} E(\omega)E(\omega),$$

where the first term is the usual second-order susceptibility, the second term is the change in the second-order susceptibility due to lattice displacement Q(t) through the hyper-Raman susceptibility, and the third term is the DC field-induced SH susceptibility that will vary in time as the DC field changes. The DC field and the lattice displacement are related through the piezoelectric effect. After the pump pulse, coherent excitation of the LO phonon follows free-induction decay, i.e., $Q(t) = Q_0 \cos(\omega_{ph} t + \phi)$, where Q_0, ω_{ph}, and ϕ are the initial amplitude, frequency and phase of the coherent oscillation. $E_{DC}(t)$ will have similar time dependence. We fit the data by iteratively fitting the time-domain data and the Fourier transform (frequency domain) of the time-domain data. It is easiest to display the Fourier transform (right inset). The phonon power spectrum is shown in Figure 2 for various injected carrier densities.

We see three features in the spectrum: bare LO phonon (ν_{LO}=8.76 THz), a very small-amplitude LO-phonon-electron plasmon coupled mode ($\nu < \nu_{TO}$ = 8.02 THz), and LO-phonon-hole plasmon-coupled mode *(8.0 < ν < 8.8 THz).* The first two are well characterized in previous work.[4,5] We concentrate here on the LO-phonon-hole plasmon-coupled mode. The LO-phonon and plasma-coupled mode frequencies are at the zeroes of the dielectric constant given by:

$$\varepsilon(\omega) = \varepsilon_\infty \left[1 - \frac{\omega_h}{\omega^2 + i\gamma_h\omega} + \frac{\omega_{LO}^2 - \omega_{TO}^2}{\omega_{TO}^2 + i\gamma_{LO}\omega - \omega^2}\right].$$

The hole plasma frequency is $\omega_h^2 = \frac{4\pi n_h e^2}{\varepsilon_\infty m_h^*}$, where n_h and $m_h^* = 0.34 m_e$ are the hole density and effective mass for holes, and $\varepsilon_\infty = 10.9$. $\omega_{LO,\,TO}$ are the longitudinal optical and transverse optical phonon angular frequencies. We may use well known values of $\nu_{LO} = 8.76$ THz and $\nu_{TO} = 8.02$ THz in the last term. Wan and Young,[6] measured the LO phonon-hole plasmon-coupled mode frequencies using Raman scattering in a series of bulk p-doped GaAs samples. They fit their data using $\gamma_{LO} = 0.15$ THz, and $\gamma_h = 15$ THz.

Detailed analysis is complicated by the spatial profile of the holes, which varies as a function of depth. In addition, the phonon amplitude is largest at the surface and drops almost to zero at the end of the depletion zone. We are currently modeling the results. However, we can note immediately that the highest 3 injected carrier densities give essentially the same result, thus indicating that the field is completely screened and no additional holes are accelerated to the surface. The n-doping is nominally 1.5 x 10^{18}/cm^3, so this is a reasonable result. At 1.8 x 10^{18}/cm^3 injected density, the injected carriers are just able to fully screen the field. At 1 x 10^{18}/cm^3 injected density, the field is not fully screened. Diffusion prevents the carriers from making an infinitely dense plasma at the surface. On the basis of the LO-phonon-hole plasmon-coupled mode frequency, we can estimate the peak density to be 6 x 10^{18}/cm^3 and the width to be about 1/6 the distance of the depletion region (260 Angstrom), which would be 43 Angstrom.

Result #1: Relevance to MRI-funded research goal

As we increased the laser intensity, we found that even at 10 times below the damage threshold there is strong coupling between the laser-injected hole plasma and the LO phonons at the surface. This means that the electron energy transfer rate is indeed larger than considered in the usual single-electron single-phonon scattering mechanism even at 10 times below the damage threshold. The coherent lattice motion produces a macroscopic polarization, which drives the carriers toward and away from the surface at the phonon frequency. This interaction reheats the holes (by reversing their direction) and thus allows holes to repeatedly scatter with phonons. The incoherent lattice motion will then heat up faster than expected from incoherent electron-phonon scattering. In addition to recovery of the piezoelectric energy of the depletion region, the depletion field itself drives carriers to high velocities, which can scatter with LO phonons efficiently. Finally, the restoring force for the lattice is changed by about 10% from 8.8 to 8.0 THz, so the barrier to disorder must be lowered by 20% (spring constant is proportional to square of frequency) accordingly. Femtosecond melting is still likely to be driven by high carrier density, lowering the barrier to disorder; however, coherent phonon excitation and plasmon-phonon coupling must play a significant role by reducing the barrier itself and by heating the lattice so it can more easily overcome the barrier.

Result #1: General scientific impact of this work

The impact on laser-heating and laser-processing of materials is that in addition to carrier-phonon interaction, one must also consider the effect of photo-injected carriers, carrier screening, and plasmon coupling, which can both heat the lattice motion and soften or weaken bonding energies and thereby lower barriers to reaction and phase transition. The dynamics of femtosecond laser-induced processing and phase transitions must take into account all sources of energy transfer.

This is the first nondestructive optical technique that can directly measure the hole density at the surface. The depletion field at the surface of n-type semiconductors drives holes to the surface, and typically one calculates this density because there are no nondestructive and time-resolved techniques that can measure the density right at the surface. These calculations are problematic as transport parameters such as mobility, diffusion constant, and recombination rates are not understood in the presence of high carrier density or high field. Linear reflectivity measures the average carrier density over the optical penetration depth, which can be 1000's of Angstrom. This experiment is performed with time-resolved second-harmonic generation and is most sensitive to the topmost 100 Angstrom. Because of the phonon-plasmon-coupled frequency, however, we have a calibrated measurement of the surface hole density. We use the measured phonon-plasmon-coupled mode frequencies in bulk p-doped semiconductors to calibrate our measurement. This is therefore a nondestructive time-resolved and independently calibrated technique for measuring hole densities near interfaces. We point out that this is the first time-resolved measurement of transient hole density profiles at surfaces and may have applications in the future related to semiconductor device geometries. We are currently studying transport in the depletion layers using numerical simulations and plan to use our measurements to deduce transport models and parameters in the high-field and high-hole-density limits. The latter are poorly understood despite their obvious importance in semiconductor devices.

This work is generally relevant to all ultra-fast laser-induced phenomena, showing clearly that energy transfer is very different when systems are far from equilibrium. For non-equilibrium systems, the individual dynamics must be included in any analysis of the energy transfer process. In the regime studied here, the detailed non-thermal distribution of both electrons and phonons effects the electron-phonon coupling.

Result #1: Relevance to other LLNL work

These studies are potentially relevant to theoretical studies of the carrier dynamics during intense laser heating and dielectric breakdown and are the study of solid density plasmas.

Result #2: Technical accomplishment

The second phenomena observed is femtosecond laser-induced surface damage induced by long-term exposure (10^{10}) to laser pulses at 1000 times less fluence than the single-shot damage threshold. We observed the reaction rate occur on the surface using time-resolved second-harmonic generation. We show below the SHG from the GaAs(110)-relaxed (1 x 1) reconstructed surface as it is continuously irradiated for several 1000 seconds. The laser train consists of 25 fs pulses at 860 nm, and the sample is n-doped with 1.5 x $10^{18}/cm^3$ Si. In panel A, the SHG is shown for 16 different fluences. In panel B, a reaction rate, k(F), is deduced as a function of fluence. The decay rate constant, k(F), is fit with a 6^{th} order polynomial in F and deconvolution of the Gaussian intensity profile of the laser

beam from the data. The fit results give the dashed lines in panel A. The crosses in panel B show the peak fluences in the experimental data of panel A.

We know that the change in SH is due to surface disorder and not bulk disorder, surface morphological damage, or chemical reaction. The surface-phonon spectrum is obtained using the technique of coherent surface phonon using time-resolved SHG.[1] The data show that the bulk LO phonon feature at 8.8 THz is unchanged during the damage process, and only the surface phonon peaks from 6.5-8.3 THz are modified (decreased) during damage. The surface reconstruction is fully restored with thermal annealing at 580oC which is also the temperature for annealing the surface under light argon sputtering. This suggests that the damage is confined to the 2-3 atomic layers of the reconstructed surface, but consists of more significant damage than just disorder or diffusion of the atoms.

We propose a new mechanism for damage in which fluctuations in the sub-damage threshold surface hole density create local regions of sufficiently high hole density to lower the potential barrier to disorder to ~k_BT. The potential barrier is reduced locally by similar physics in which femtosecond laser melting occurs globally. This is a very different mechanism from all existing proposed mechanisms of surface photoreaction in which laser light creates excited electronic systems that transfer energy to atomic motion and thereby heat atoms that can overcome the potential energy barrier. Using a fit of k(F) to a Poisson distribution about a mean value of the surface hole density, which we can estimate by a model based on the calculated density of states for the surface dangling bond hole band,[7] we find that the nonlinear fluence dependence is explained if we assume that significant reaction rate requires local

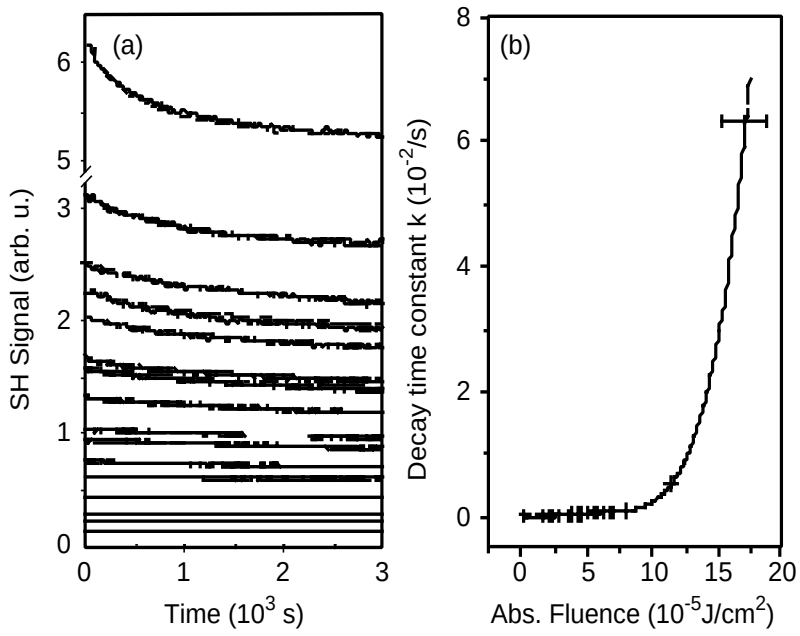

Figure 3. *(A) SH signal vs. time from (1 x 1)-relaxed GaAs(110) during irradiation by train of 25 fs pulses. Signals with higher amplitude obtained with higher fluence. (B) Decay rate k(F) vs. absorbed fluence/pulse obtained by fit to data in (A). Symbols indicate fluences used for curves in (A). Data (solid), Fit (dashed).*

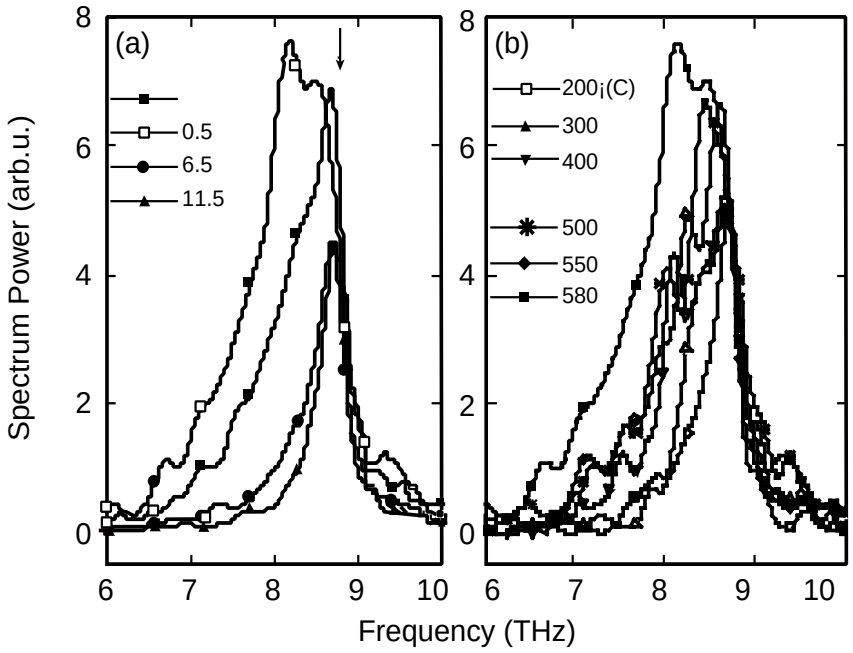

Figure 4. *(A) Coherent surface optical phonon power spectrum during laser damage with peak absorbed fluence of 110 μJ/cm^2. (B) Coherent surface optical phonon power spectrum after annealing at various temperatures. The spectra were taken at room temperature to allow for the temperature-dependent optical constants.*

fluctuations on the order of 2.3% occupation fraction. This number (2.3%) is comparable to the 5% mean density required for global transformation of the bulk in femtosecond disorder. Temperature dependence of the reaction rate gives us a barrier threshold of only 6 meV. This is two orders of magnitude lower than typical binding energy barriers and is consistent with our proposed mechanism in which a rare local fluctuation in the hole density induces the barrier to drop from ~1 eV to ~k_BT and then the reaction occurs efficiently due to the atomic motion in the thermal bath.

Result #2: Relevance to MRI-funded research goal

The new physics here is that electronic mechanisms of damage can occur due to fluctuations in the carrier density. We are used to the idea that thermal fluctuations drive chemical reactions; that is, a small fraction of atoms moving with high kinetic energy overcome the barrier. But when we consider electronically driven reactions or physical processes, we think in terms of global transitions. As in the Peierl's transition, we think of the entire lattice becoming unstable at once when the carrier density exceeds some critical point. Here, the experimental results are consistent with local carrier fluctuations causing a lattice instability (like a Jahn-Teller distortion around a self-trapped exciton). In this case, we argue that the data is consistent with about a 2% occupation density being sufficient for the local lattice instability. Even though the average density might be 10 times lower than that, there is a finite probability of the higher fluctuation. This concept applies to the femtosecond bulk phase transition as well as the surface transition. Electronically-induced bulk defect formation or damage may be occurring under femtosecond irradiation at levels far below the global transition threshold, but have escaped our notice.

Result #2: General scientific impact of this work

The science is relevant to mechanisms of damage to material surfaces/interfaces caused by long exposure to low-level pulsed lasers and also energetic electron or ion beams. Some particularly interesting applications are aging of optical component surfaces and semiconductor devices (for example, electron damage at the Si-SiO_2 interface). Because the reaction is produced under femtosecond laser exposure, and is detected by time-resolved second-harmonic, it may be possible that the dynamics of this interfacial reaction could be studied on the femtosecond time scale.

Result #2: Relevance to other LLNL work

The work is relevant to LLNL in conjunction with aging of optical components in the National Ignition Facility in which operation close to the single-shot damage threshold is contemplated. The work is relevant to all materials research concerned with aging effects.

Impact of Work on Continuing MRI Research

First, we answered many of the questions we initially raised about femtosecond melting. The first result showed that the phonon heating rate is indeed enhanced by the excitation of coherent phonons and the lattice is indeed hotter than expected by simply considering only the relaxation of electrons within the bands. The second project on surface disorder suggests that electronic disorder can proceed by creating low-barrier dynamical pathways even locally. This suggests that the "apparent" global threshold may simply occur when the density of local disorder is sufficiently high to create stresses in the remaining material to cause global disorder. This challenges our intuition about the local dynamics of this and other surface and bulk phase transitions.

Second, the results suggested that time-resolved studies of the phase transformation at standard pressure can not easily distinguish the interplay between pressure-induced and electronically-induced phase transitions, which was part of our original goal. The interplay between hot electrons and hot lattice motion is too complex even 10 times below damage threshold to sort these issues out. We therefore proposed a different series of experiments for MRI funding in calendar year 1998-99. We proposed that we study optical absorption, phase transition dynamics, and damage threshold of GaAs at different hydrostatic pressures just below and above a structural phase transition. The use of pressure to control static deformation of the electronic bands and the laser intensity to control the excited electronic density provide a new tool for studies of this kind. Presumably just below the phase transition, the pressure-induced effect will bias the system so a proportionately weaker laser-electronic excitation will drive a phase transition. By measuring the time-resolved spectroscopy of these systems near damage threshold, we hope to observe the bandgap collapse and recover as a function of time. We also hope to distinguish purely electronic from atomic-rearrangement-induced bandgap collapse. MRI funding in 1998-99 was approved. Experiments will be carried out in diamond anvil cells prepared in collaboration with Choong-shik Yoo.

References

1. Chang, Y.-M., Xu, L. and Tom, H. W. K., *Phys. Rev. Lett.* **78**, 4649, 1997.
2. Chang, Y.-M., Xu, L. and Tom, H. W. K., "Observation of Coherent Local Optical Phonons Localized at Buried Interfaces Using Time-Resolved SHG", to be published in *Phys. Rev. B*, May 15, 1999.
3. (a) Cheng, T. K., Brorson, S. D., Kazeroonian, A. S., Moodera, J. S., Dresselhaus, G., Dresselhaus M. S. and Ippen, E. P., *Appl. Phys. Lett.* **57**, 1004, 1990; (b) Zeiger, H. J., Vidal, J., Cheng, T. K., Ippen, E. P., Dresselhaus, G. and Dresselhaus, M. S., *Phys. Rev.* B**45**, 768, 1992.
4. Cho, G. C., Kutt, W. and Kurz, H., *Phys. Rev. Lett.* **65**, 764, 1990.
5. Cho, G. C., Dekorsy, T., Bakker, H. J. and Hovel, R., *et al.*, *Phys. Rev. Lett.* **77**, 4062, 1996.
6. Wan, K. and Young, J. F., *Phys. Rev. B* **41**, 10772, 1990.
7. Honke, R., Fritsch, J. and Pavone, P., *et al.*, *Phys. Rev. B* **53**, 9923, 1996.

Synthesis and Properties Modification of Novel f-electron Materials by Shock Compaction

UC Principal Investigator: *Professor M. Brian Maple, UC-San Diego*
LLNL Collaborator: *William J. Nellis*
Students: *Eric Bauer, Ricky Chau, Neil Dilley, UC-San Diego*

Abstract

We attempted to synthesize two filled skutterudites, $CeFe_4P_{12}$ and $GdFe_4P_{12}$, using the light-gas gun at LLNL with shock pressures of 200 and 400 kbar. Analysis by x-ray diffraction on these first trials indicates that the skutterudite structure was not formed. We have also performed shock compaction experiments on a rare earth borocarbide, $YPd_5B_3C0._3$, with shock pressures of 200, 300, and 400 kbar. The superconducting transition temperature remains the same at 21 K, but the amount of superconducting phase decreases with increasing shock pressure.

Goals

Our hope for these experiments was to synthesize new f-electron materials using shock compaction because of its high dynamic pressures (up to 1 Mbar) and fast quench rates (< 1 ms). The family of compounds known as filled skutterudites have the general formula LnT_4X_{12} (Ln = rare earth or actinide; T = Fe, Ru, Os; X = P, As, Sb), and show promise for use as thermoelectric devices. However, the skutterudite structure does not form for most of the heavy rare earth elements (Gd-Tm). We first attempted to synthesize $CeFe_4P_{12}$ (which has been made previously by conventional techniques) by shock compaction. In addition, we tried to form $GdFe_4P_{12}$ which, to our knowledge, has never been synthesized.

There has been renewed interest in exploring the interplay between superconductivity and magnetism with the discovery of the superconducting rare earth borocarbides. In particular, $YPd_5B_3C0_3$ has a superconducting transition temperature (T_c) of 23 K, which is one of the highest among intermetallic compounds. When prepared by arc melting, this material is found to contain a number of different phases including a metastable superconducting phase. There have been a number of conflicting reports as to the identity of this superconducting phase. Our goal was to isolate the phase responsible for superconductivity in a controlled fashion using shock compaction.

Results: Skutterudites

The pre-shocked skutterudite compounds were made at UC-San Diego by reacting RFe_4 (R = Ce or Gd) in an arc furnace with an argon atmosphere. These binary compounds were mixed with the correct amounts of FeP and P for the stoichiometry RFe_4P_{12} and then ground to a fine powder. The shock compaction experiments were performed at LLNL using the 7-m light-gas gun with shock pressures of 200 and 400 kbar.

The post-shocked materials at pressures of 200 and 400 kbar consisted of an amorphous phase with a considerable amount of unreacted phosphorous. Our analysis of these post-shocked compounds using x-ray diffraction at UCSD revealed that the skutterudite structure was not formed.

Rare Earth Borocarbides

An ingot of $YPd_5B_3C0_3$ was produced at UCSD by arc melting the elemental constituents in an arc furnace. The T_c was determined to be 21 K. The material was ground to a fine powder (< 20 μm) with a mechanical ball mill. The light-gas gun at LLNL was used for the shock compaction experiments with shock pressures of 200, 300, and 400 kbar.

For the two lowest shock pressures of 200 and 300 kbar, the two post-shocked samples formed dense powders of a similar appearance to the pre-shocked material. At 400 kbar, the borocarbide melted somewhat. X-ray diffraction measurements made at UCSD on the post-shocked materials showed evidence of phase changes, but we were unable to determine their exact nature due to the large number of different phases present. Measurements of dc magnetization using a SQUID magnetometer indicate that all of the post-shocked compounds have Tc's of around 21 K. These experiments also show that the volume fraction of superconducting phase decreases with increasing shock pressure. Electrical resistivity measurements, made using a standard four-wire technique, yield results that are similar to the magnetization studies in that they show that all of the post-

shocked materials have T_c's of 21 K, and the amount of superconducting phase decreases with increasing shock pressure. In addition, the residual resistivity increases with increasing shock pressure, suggesting an increase in the amount of disorder in the $YPd_5B_3C0_3$ samples with pressure.

Summary

In conclusion, we have performed shock compaction experiments to try to synthesize two filled skutterudites, $CeFe_4P_{12}$ and $GdFe_4P_{12}$. Our analysis indicates that we were unsuccessful in this regard. We also shock compacted $YPd_5B_3C0_3$ with pressures of 200, 300, and 400 kbar. We found that the amount of superconducting phase decreases with increasing shock pressure, and the compound also becomes more disordered.

Thermodynamic Measurements of High Energy Density Storage Materials

UC Principal Investigator: *Professor Frances Hellman, UC-San Diego*
LLNL Collaborator: *Hector Lorenzana*
Post-Doc: *Stefan Wohlert, UC-San-Diego*

The goal of this LLNL/UCSD collaborative research program is to develop and apply high temperature micro-calorimetric instrumentation and techniques to the determination of the energetic content of microgram quantities of novel materials. LLNL has a strong programmatic interest in the development of new materials with energetic properties. However, current synthesis capabilities at LLNL are limited to microgram quantities, much too small for typical conventional calorimeter systems. The measurement of the energetic content of these materials requires a novel and powerful approach to quantifying and characterizing thermodynamics of microscopic samples. The Hellman group at UCSD has well developed expertise and strong interest in thermodynamic measurements of thin film and other extremely low volume samples. Thus, we have sought to synergistically develop a micro-calorimetric system to address the common UCSD/LLNL need for a high-sensitivity high-precision calorimetric system for microgram-sized samples.

The development of novel high energy density materials (HEDM's) would be an important advancement for both LLNL missions as well as technological applications. Recently, the LLNL group has been studying the properties of materials synthesized at high pressures and high temperatures. One key property of programmatic interest is the energetic content of these new materials. The great difficulty in performing these measurements is that the LLNL group's synthesis techniques are limited to small samples (~micrograms) because of technical limitations of diamond anvil cell techniques. Recently, using the diamond anvil cell, the LLNL research group has synthesized a novel material derived from carbon monoxide at high pressure. Applying a broad range of spectroscopic probes, the LLNL group's measurements indicate that the recovered material is polymeric with strong potential as an energetic material. Ref. 1 discusses this material and shows infrared absorption spectrum of recovered solid polymerized CO at ambient conditions. It is critical that the efficacy of this material be evaluated before making the significant investment of resources necessary to establish large-volume press scale-up operations.

In the past year, using the MRI funding, the UCSD group has constructed a high-vacuum, small-sample differential thermal analysis system (DTA) based on Si-micromachined calorimeters. This MDTA (micro-DTA) provides orders of magnitude more sensitivity than existing high temperature systems and allows measurements of the enthalpy and release conditions for the microgram quantities of material. We have completed construction and preliminary testing of the new MDTA system. We now await a new post-doc (planned to begin in April) to begin calibration of the system and measurements in the MDTA of the materials prepared by the LLNL group.

In parallel with the calorimetry work at UCSD, the LLNL group has received some of the UCSD-fabricated Si-micromachined calorimeters to investigate details of handling procedures and techniques for effectively coupling their materials to these devices. These microcalorimeters will be used to measure the stored heat content of the materials made in Lorenzana's laboratory and the temperature/time for release of this stored heat (the time response of the microcalorimeters is sub-msec). We hope within six months to have completed a set of measurements on the materials made by the LLNL group.

References

1. Lipp, M. J., Evans, W. J., Baonza, V. G. and Lorenzana, H. E., *J. Low Temp. Phys.* **11**, 247-256, 1998.

APPENDIX A

SEMINARS
CONFERENCES
WORKSHOPS

FY97 Seminar

June 10, 1997 Roger Dorsinville	City College of New York	*Characterization of Third Order Nonlinear-optical Properties in Polymers*

FY98 Seminars

October 21, 1997 Prof. Lewis Rothberg	NSF Center for Photoinduced Charge Transfer, University of Rochester	*Organic Microcavity Light-Emitting Diodes†*
November 12, 1997 John Kinney	Chemistry and Materials Sciences, Lawrence Livermore Nat'l Laboratory	*Biomechanical Problems in Osteoporosis: What Causes Fracture?§*
December 3, 1997 Dennis Matthews	Medical Technologies Program, Lawrence Livermore Nat'l Laboratory	*Device Development within the Medical Technology Program§*
January 7, 1998 Mike McElfresh	Department of Physics, Purdue University	*Irreversibility Line in High Temperature Superconductors†*
January 14, 1998 Apostolos Doukas	Wellman Laboratories, Harvard Medical School	*Laser-Induced Pressure Waves in Medicine: A Method for Drug Delivery†*
February 11, 1998 Bill Goddard	Materials and Process Simulation Center, California Institute of Technology	*Atomistic Simulations of Materials with Applications to Ceramics, Semiconductors, Metal Alloys, Catalysts, Polymers, and Protein†**
February 25, 1998 Graham Bench	Health and Ecological Assessment Division/ Center for Accelerator Mass Spectrometry Lawrence Livermore Nat'l Laboratory	*Nuclear Microprobe Analysis of Biological Tissue§*
February 25, 1998 Ron Cohen	Carnegie Institution of Washington	*Transition Metal and Other Oxides at High Pressures: Magnetic and Structural Phase Transition†**

§ = Special seminar series on Biomaterials, Chair: J. De Yoreo † = General MRI Series, Chair: H. B. Radousky * = Co-hosted with UC-Davis

FY98 Seminars

March 4, 1998 Steve Garofalini	Rutgers University	*Molecular Dynamics Simulations of Glass Surfaces and Interface†**
March 11, 1998 Jim Sethna	Cornell University	*Hysteresis, Avalanches, and Barkhausen Noise†**
March 18,1998 Bernhard Rupp	Biology and Biotechnology Research Prog., Lawrence Livermore Nat'l Laboratory	*Modern Phasing Techniques in Advanced Macromolecular Crystallography§*
April 1, 1998 Rich London	Laser Programs, Lawrence Livermore Nat'l Laboratory	*Laser-Tissue Interaction Modeling§*
April 8, 1998 Paul Alivisatos	UC-Berkeley	*Semiconductor Nanocrystals†*
April 15, 1998 Karin Hollerbach	Institute for Scientific Computing Research, Lawrence Livermore Nat'l Laboratory	*Finite Element Modelling of Joint Biomechanics§*
April 29, 1998 Gregory Carmen	Mechanical Engineering and Aerospace Engineering, UC-Los Angeles	*An Overview of Research in Active (Smart) Materials at UCLA: Piezoelectrics, Magnetostrictive Composites, Shape Memory Alloys†*
June 3, 1998 Rod Balhorn	Biology and Biotechnology Research Prog., Lawrence Livermore Nat'l Laboratory	*Application of New Physical and Chemical Imaging Techniques to the Analysis of Individual Cells and Cell Populations§*
September 24, 1998 Mike McElfresh	Purdue University	*Dependence of the Vortex-Solid Phase Transition of $YBa_2Cu_3O_7$-d Thin Films on Oxygen Toichiometry: Evidence for a Universal Phase Transition†*

§ = Special seminar series on Biomaterials, Chair: J. DeYoreo † = General MRI Series, Chair: H. B. Radousky * = Co-hosted with UC-Davis

FY99 Seminars

October 7, 1998 Dave Wilson	Biology and Biotechnology Research Prog., Lawrence Livermore Nat'l Laboratory	*Specific Recognition and Processing of DNA by a Human Protein*††
October 14, 1998 Susan M. Kauzlarich	Department of Chemistry, UC-Davis	*Zintl Salts for the Solution Synthesis of Surface-Stabilized Si and Ge Nanoclusters*††
October 20, 1998 Ron Loehman	Advanced Materials Laboratory, Sandia National Laboratories, Albuquerque	*Interfacial Reactions in Ceramics with Applications to Composites, Ceramic Joining, and Electronic Devices*††
October 21, 1998 James De Yoreo	Chemistry and Materials Sciences, Lawrence Livermore Nat'l Laboratory	*Exploring the Growth and Dissolution of Crystal Surfaces at the Nanometer Scale*††
October 23, 1998 Eric J. Amis	National Institute of Standards and Technology, Gaithersburg, Maryland	*Dendrimers: Macromolecules of Unique Dimensions*††
October 28, 1998 Tom Breunig	Department of Restorative Dentistry, UC-San Francisco	*Structure and Properties of Cortical Bone*††
November 4, 1998 Umar Mohideen	Department of Physics, UC-Los Angeles	*The Weirdness of the Quantum Vacuum: An Experimental Exploration Through the Casimir Force*††
November 11, 1998 Karl-Heinz Ernst	Swiss Federal Laboratories for Materials Testing and Research (EMPA), Switzerland	*Nanostructured Chiral Surface*
November 18, 1998 David W. Deamer	Department of Chemistry, UC-Santa Cruz	*Nanopore Characterization of Single Polynucleotide Molecules: Potential for Ultra-Rapid Sequencing*††
December 9, 1998 Frances Hellman	UC-San Diego	*Giant Negative Magnetoresistance in Amorphous Rare Earth-Silicon Alloys*††

§ = Special seminar series on High Pressure, Chair: W. J. Nellis † = General MRI Series, Chair: H. B. Radousky * = Co-hosted with UC-Davis

FY99 Seminars

December 16, 1998 Rick Kaner	Department of Chemistry, UC-Los Angeles	*Rapid Solid-State Synthesis of Materials* ††
January 15, 1999 Mildred Dresselhaus	Massachusetts Institute of Technology	*The Remarkable Structure and Properties of Carbon Nanotubes* †
January 27, 1999 Gang-yu Liu	Department of Chemistry, Wayne State University, Detroit, MI	*Patterning Protein Molecules on Surfaces Using Scanning Probe Lithography* ††
February 2, 1999 John Neaton	Cornell University	*Is Lithium a Paired Insulator at High Densities?* §§
February 3, 1999 Ching Y. Fong	Physics Department, UC-Davis	*A Quantum Monte Carlo Study of the Exchange-Correlation Hole in Silicon Atom and System-Averaged Correlation Holes of Second Row Atoms* ††
February 8, 1999 Louis Terminello	Department of Applied Sciences, Lawrence Livermore Nat'l Laboratory	*Materials Characterization Using Soft X-Ray Synchrotron Radiation* ††
February 16, 1999 Ricky Chau	Physics Department, Lawrence Livermore Nat'l Laboratory	*Electrical Conductivities of Water at 20-180 GPa in Comparison with those of Hydrogen and* CH_2 §§
March 9, 1999 Larry Fried	Chemistry and Materials Sciences, Chemical Sciences Division, Lawrence Livermore Nat'l Laboratory	*Supercritical Molecular Fluids Under High Pressure* §§
March 10, 1999 John Pask, Gus Hart	UC-Davis	John Pask – *A Real-Space, Finite-Element Approach to Large-Scale Electronic-Structure Calculations* Gus Hart – *Electronic Structure of PtSi and IrSi* ††
March 17, 1999 Philip Sterne	UC-Davis and Lawrence Livermore Nat'l Laboratory	*Materials Research with Positron Annihilation* ††

§§ = Special seminar series on High Pressure, Chair: W. J. Nellis † = General MRI Series, Chair: H. B. Radousky †† = General MRI Series, Chair: R. Agbaria

FY99 Seminars

March 30, 1999 Chong-shik Yoo	Physics Department, Lawrence Livermore Nat'l Laboratory	*High-Pressure Chemistry of Carbon Dioxide* §§
March 31, 1999 Carel Boekema	San Jose State Univ.	*Plausible d-Wave Symmetry in Cuprate Superconductors: A Maximum-Entropy Muon-Spin-Resonance Study of R123 Vortex States* ††
April 1, 1999 Lukas Eng	Institute of Applied Photophysics, TU Dresden, D-01069 Dresden, Germany	*Inspection and Manipulation of Ferroelectrics on the Nanometer Scale*††
April 14, 1999 Sergei Stishov	Los Alamos Nat'l Laboratory, Institute of HP Physics, Moscow, Russia	*Isotopic Effects in Solids at High Pressures* §§
May 10, 1999 Peter Celliers	Medical Technology Program, Lawrence Livermore Nat'l Laboratory	*Shock Transformation of Liquid Deuterium into a Metallic Fluid* §§
May 11, 1999 Art Ruoff	Cornell University	*Mbar Pressures: From Metallic Oxygen to Molecular Li* §§
May 18, 1999 Gene Haller	UC-Berkeley	*Semiconductors at Large Hydrostatic Pressures* §§
June 2, 1999 Alex Hodges	Physics Department, University of Cincinnati	*Exciton Spin Relaxation in ZnSe-Based Dilute Magnetic Semiconductor Heterostructures* ††
June 15, 1999 Bill Nellis	Physics Department, Lawrence Livermore Nat'l Laboratory	*Metallization of Fluid Hydrogen at 1.4 Mbar* §§
June 17, 1999 Shane Aaron Catledge	Dept. of Materials and Mechanical Eng., Univ. of Alabama at Birmingham	*Advanced Techniques in Chemical Vapor Deposition (CVD) Processing of Diamond Films–Applications in High Pressure Science* ††
July 1, 1999 Kevin Roberts	Centre for Molecular and Interface Eng., Dept. of Mechanical and Chemical Eng., Heriot-Watt University, Edinburgh	*Probing the Structure of Habit Modifying Additives in Molecular Ionic Crystals using Synchrotron Radiation Techniques*

§§ = Special seminar series on High Pressure, Chair: W. J. Nellis † = General MRI Series, Chair: H. B. Radousky †† = General MRI Series, Chair: R. Agbaria

FY 98 Conferences/Workshops	# Attendees	Coordinator
Nov 11-13, 1997 **POSITRON CONFERENCE** **Lawrence Livermore Nat'l Laboratory** ***Materials Research Institute*** **Publication:** *Applications and Advances of Positron Beam Spectroscopy*: Appendix A, Nov 5-7, 1997, UCRL-130205.	30	Rich Howell, *Physics, LLNL*
June 8-10, 1998 **TRI-LAB COURSE: DISLOCATIONS IN MATERIALS** **Hilton Hotel – Pleasanton, CA**	50	Wayne King, *Chemistry and Materials Science, LLNL*
June 11-12, 1998 **NIST/LLNL WORKSHOP ON WORK HARDENING AND DISLOCATION PATTERNING IN METALS** **Hilton Hotel – Pleasanton, CA**	30	Wayne King, *Chemistry and Materials Science* Robb Thomson, Lyle Levine, *National Institute of Standards and Technology*
June 28 -July 3, 1998 **INTERNATIONAL WORKSHOP ON ELECTRONS CORRELATIONS AND MATERIALS PROPERTIES** **Crete, Greece** **Publication:** *Electron Correlations and Materials Properties* (Klewer Academic/Plenum Publishers, New York, 1999).	42	Tony Gonis, *Chemistry and Materials Science* Nick Kiousiss, *Cal. State Northridge*

FY 99 Conferences/Workshops	# Attendees	Coordinator
April 1-2, 1999 **GRAIN BOUNDARY ENGINEERING WORKSHOP** **Sheraton Hotel – Pleasanton, CA**	12	Wayne King, *Chemistry and Materials Science LLNL*
Sept 13-14, 1999 **CLC NOVEL MATERIALS WORKSHOP** **Lawrence Livermore Nat'l Laboratory** ***Materials Research Institute***	75	Harry Radousky *Materials Research Institute, LLNL* Shirley Chiang, *UC-Davis* Susan Kauzlarich, *UC-Davis*

APPENDIX B

FACULTY AND STUDENTS

VISITING PROFESSORS IN RESIDENCE AT THE MRI

PROFESSORS	LLNL CONTACT(S)	TOPICS
Prof. Carel Boekema (On Sabbatical) *San Jose St. Univ.*	Harry Radousky, *Materials Research Institute*	***Rare Earth Magnetism***
Prof. Tom Breunig, *UC-San Francisco*	John Kinney, *Chemistry and Materials Science*	***Cortical Bone***
Prof. Nicolas Kiousiss, *Cal. State Northridge*	Tony Gonis, *Chemistry and Materials Science* Harry Radousky, *Materials Research Institute* Andy McMahan, *Physics* Stavros Demos, *Institute for Laser Science Applications*	***Rare Earth Magnetism/Optical Materials***
Prof. Richard Scalettar (On Sabbatical) *UC-Davis*	Andy McMahan, *Physics* Malvin Kalos, *Defense and Nuclear Technologies*	***Magnetism***
Prof. Harry Tom, *UC-Riverside*	Ming Yan, *Chemistry and Materials Science* C. S. Yoo, *Physics* Harry Radousky, *Materials Research Institute* J. De Yoreo, *Chemistry and Materials Science* Stavros Demos, *Institute for Laser Science Applications*	***Optical Materials/ High Pressure***

GRADUATE STUDENTS IN RESIDENCE AT THE MRI

Names	LLNL Contacts	Thesis Advisor	Dissertation Title	Next Position
Matt Enjalran, *Physics Dept., UC-Davis*	Malvin Kalos, *Defense Nuclear Technologies*	Richard Scalettar, *UC-Davis*	*Monte Carlo Studies of Frustrated Layered Magnets and Disordered Strongly Correlated Fermi Systems*	PhD expected Summer 2000
Gus Hart, *Physics Dept., UC-Davis*	John Klepeis, *Physics*	Barry Klein, *UC-Davis*	*Electronic Structure Studies of Materials Properties and Stability in Transition Metal-Metalloid Compounds*	Post-Doc at Natl. Renewable Energy Lab., Golden, CO
John Pask, *Physics Dept., UC-Davis*	*Phil Sterne, Physics*	Barry Klein, *UC-Davis*	*Finite-Element Method for Large-Scale Electronic Structure Calculations*	Post-Doc at Naval Research Lab., Washington DC
Mike Paskowitz, *Materials Science, UC-Davis*	Bill Nellis, *Physics*	Subash Risbud, *UC-Davis*	*NanoCrystalline Si Produced by Shock Compression*	PhD expected August, 2000
Boyd Taylor, *Chemistry, UC-Davis*	Howard Lee, *Defense Nuclear Technologies*	Susan Kauzlarich, *UC-Davis*	*Spectroscopy of Nanocrystals*	Post-Doc at Lawrence Livermore Nat'l Laboratory

GRADUATE STUDENTS ASSOCIATED WITH THE MRI

Name/School	LLNL Contacts	Thesis Advisor	Project Title	Current Position
Adrian Allen, *Univ. of Oxford*	Bruce Remington, *Laser Programs*	Justin Wark, *Univ. of Oxford*	*Extreme States of Matter on Nova*	Student
Eric Bauer, *UC-San Diego*	William Nellis, *H Division, Physics*	M. Brian Maple, *UC-San Diego*	*Synthesis and Properties Modification of Novel f-electron Materials by Shock Compaction*	Student
Ricky Chau, *UC-San Diego*	William Nellis, *H Division, Physics*	M. Brian Maple, *UC-San Diego*	*Synthesis and Properties Modification of Novel f-electron Materials by Shock Compaction*	Post-Doc., H Division ***Lawrence Livermore Nat'l Laboratory***
Neil Dilley, *UC-San Diego*	William Nellis, *H Division, Physics*	M. Brian Maple, *UC-San Diego*	*Synthesis and Properties Modification of Novel f-electron Materials by Shock Compaction*	Quantum Design, San Diego
Jingyan Guo, *UC-Riverside*	Choong-shik Yoo, *H Division, Physics*	Harry Tom, *UC-Riverside*	*Study of the Role of Coherent Phonons and Shock Waves on Energy Transfer Processes in Femtosecond Laser-Induced Melting of Solids*	Newport Research Corp., Irvine, CA
Mirko Hattass, *Goethe Univ. Frankfurt*	Alex Hamza, *Chemistry and Materials Sciences*	Horst Schmidt-Boecking, *Goethe Univ. Frankfurt*	*Novel Approaches to Surface Analysis and Materials Engineering Using Highly Charged Ions*	Student
Hidong Kwok, *UC-Riverside*	Choong-shik Yoo, *H Division, Physics*	Harry Tom, *UC-Riverside*	*Study of the Role of Coherent Phonons and Shock Waves on Energy Transfer Processes in Femtosecond Laser-Induced Melting of Solids*	Post-Doc., Columbia University
Aaron Lindenburg, *UC-Berkeley*	Troy Barbee, III, *H Division, Physics*	Roger Falcone, *UC-Berkeley*	*Optically-Induced Structural Changes in Materials*	Student
Andrew Loveridge, *Univ. of Oxford*	Bruce Remington, *Laser Programs*	Justin Wark, *Univ. of Oxford*	*Extreme States of Matter on Nova*	Student
Tzy Jiun (Mark) Luo, *UC-Davis*	James De Yoreo, *Chemistry and Materials Sciences*	G. Taynas Palmore, *UC-Davis*	*Device Miniaturization Through Self-Assembly: An In-Situ AFM study of Molecular Scaffolds*	Graduated
Guillamme Machicoane, *Univ. of Paris*	Alex Hamza, *Chemistry and Materials Sciences*	Jean-Pierre Briand, *Univ. of Paris*	*Novel Approaches to Surface Analysis and Materials Engineering Using Highly Charged Ions*	Student

GRADUATE STUDENTS ASSOCIATED WITH THE MRI

Name/School	LLNL Contacts	Thesis Advisor	Project Title	Current Position
Tracie Martin, *UC-Davis*	James De Yoreo, *Chemistry and Materials Sciences*	G. Taynas Palmore *UC-Davis*	*Device Miniaturization Through Self-Assembly: An In-Situ AFM Study of Molecular Scaffolds*	Graduated
Rudy Martinez *UC-Los Angeles*	Tomas Diaz De La Rubia, *Chemistry and Materials Sciences*	Nasr M. Ghoniem *UC-Los Angeles*	*Dislocation Dynamics Simulations of Deformation Hardening in BCC Metals*	Student
Daniel Mayeri, *UC-Davis*	Howard Lee, *Defense and Nuclear Technologies*	Susan Kauzlarich *UC-Davis*	*The Study of Photoluminescence and Device Applications of Si Quantum Dots*	Intel Corp., Portland, OR
Mary McBride, *UC-Davis*	James De Yoreo, *Chemistry and Materials Sciences*	G. Taynas Palmore *UC-Davis*	*Device Miniaturization Through Self-Assembly: An In-Situ AFM Study of Molecular Scaffolds*	Post-Doc., ***Lawrence Livermore Nat'l Laboratory***
Mike Newman, *Univ. of Conn.*	Alex Hamza, *Chemistry and Materials Sciences*	Win Smith *Univ. of Conn.*	*Novel Approaches to Surface Analysis and Materials Engineering Using Highly Charged Ions*	Student
Thomas Niedermayr, *Univ of Paris*	Alex Hamza, *Chemistry and Materials Sciences*	Jean-Pierre Briand *Univ of Paris*	*Novel Approaches to Surface Analysis and Materials Engineering Using Highly Charged Ions*	Student
John Pask, *UC-Davis*	Philip Sterne, Richard Howell, *H Division, Physics*	Barry Klein *UC-Davis*	*New Theoretical Framework for Positron Annihilation Characteristics*	Post-Doc., National Renewable Energy Lab
Mike Paskowitz, *UC-Davis*	Howard Lee, *Defense and Nuclear Technologies*	Subash Risbud *UC-Davis*	*Nanocrystalline Si Produced by Shock Compression*	Student
Christiane Ruehlicke, *Univ. of Bielefeld, Germany*	Alex Hamza, *Chemistry and Materials Sciences*	Prof. Hipplet *Univ. of Bielefeld, Germany*	*Novel Approaches to Surface Analysis and Materials Engineering Using Highly Charged Ions*	Graduated
Boyd Taylor, *UC-Davis*	Howard Lee, *Defense and Nuclear Technologies*	Susan Kauzlarich *UC-Davis*	*Fundamental Studies and Applications of Semiconductor Nanocrystals*	Post-Doc., ***Lawrence Livermore Nat'l Laboratory***
T.J. Yang, *UC-Riverside*	Ming Yan, *Chemistry and Materials Sciences*	Umar Mohideen *UC-Riverside*	*Nanoscale Study of Strain and Strain Dynamics in Laser Materials and Nonlinear Optical Materials*	Post-Doc., Cal. Tech.

UNDERGRADUATE STUDENTS ASSOCIATED WITH THE MRI

Name/School	LLNL Contacts	Thesis Advisor	Project Title	Current Position
Dave Gamble, *Univ. Of Pacific*	Alex Hamza, *Chemistry and Materials Sciences*	*Junior*	*Novel Approaches to Surface Analysis and Materials Engineering Using Highly Charged Ions*	Student
Marcus Schneider, *Cal Poly, San Luis Obispo*	Alex Hamza, *Chemistry and Materials Sciences*	*Senior*	*Novel Approaches to Surface Analysis and Materials Engineering Using Highly Charged Ions*	Student

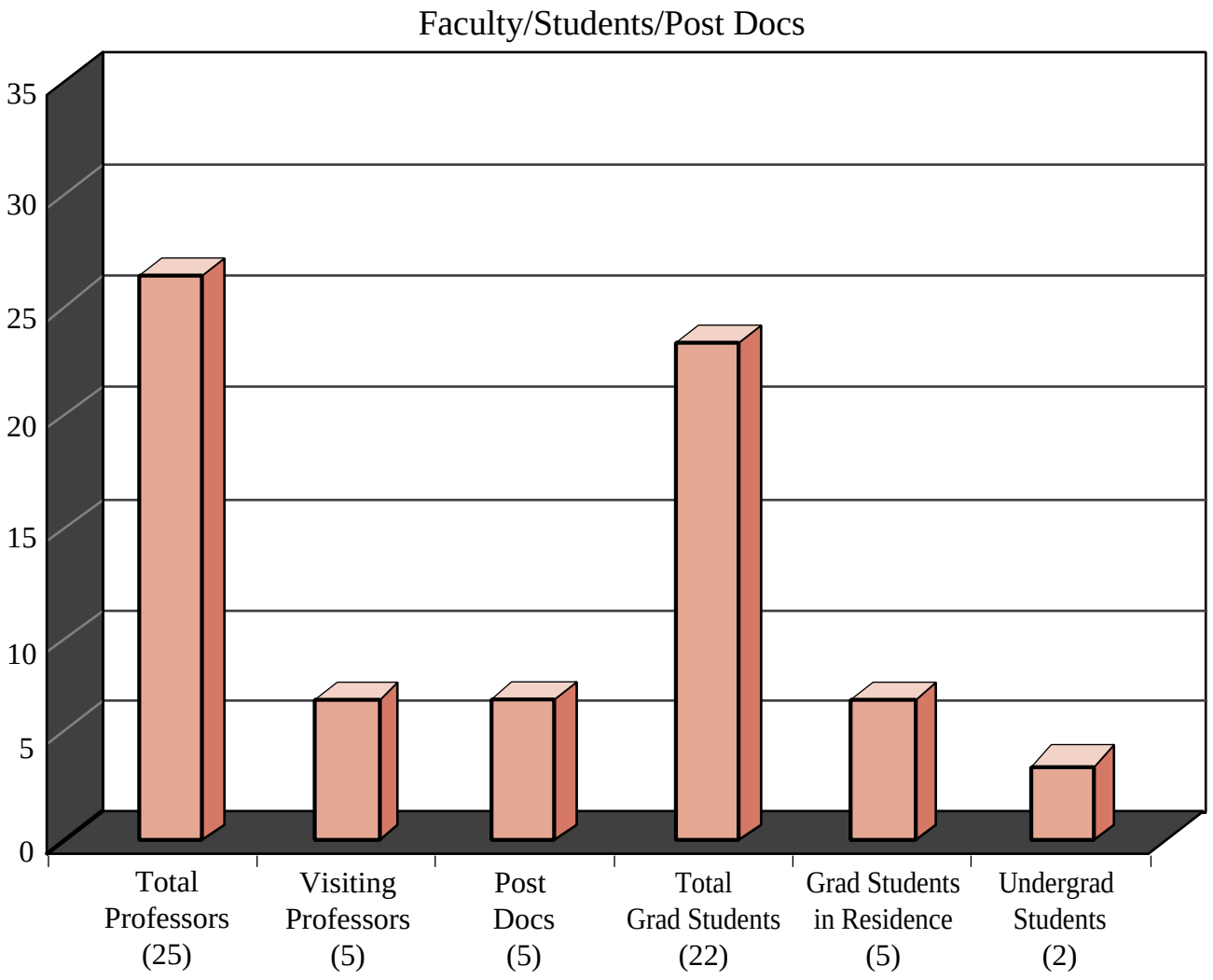
Faculty/Students/Post Docs
35
30
25
20
15
10
5
0
Total Professors (25)
Visiting Professors (5)
Post Docs (5)
Total Grad Students (22)
Grad Students in Residence (5)
Undergrad Students (2)

APPENDIX C

FY98-99 University Collaborative Research Project (UCRP) Awards

FY98 University Collaborative Research Project (UCRP) Awards

UC Campus	Campus Investigators	LLNL Collaborators	Project Title
UC-Berkeley	Roger Falcone, *Department of Physics*	Troy Barbee, *Physics*	***Optically-Induced Structural Changes in Materials***
UC-Davis	Philip Sterne, *Department of Physics*	Richard Howell, *Physics*	***New Theoretical Framework for Computing Positron Annihilation Characteristics***
UC-Davis	G. Taynas Palmore, *Department of Chemistry*	James De Yoreo, *Chemistry and Materials Sciences*	***Device Miniaturization Through Self-Assembly: An In-Situ AFM Study of Molecular Scaffolds***
UC-Davis	Susan Kauzlarich, *Department of Chemistry*	Howard Lee, *Physics*	***The Study of Photoluminescence and Device Applications of Si Quantum Dots***
UC-Los Angeles	Nasr Ghoniem, *Mech. & Aero Eng. Department*	Tomas Diaz De La Rubia, *Chemistry and Materials Sciences*	***Dislocation Dynamics Simulation of Radiation Hardening***
UC-Riverside	Harry Tom, *Department of Physics*	Choong-shik Yoo, *Physics*	***Study of the Role of Coherent Phonons and Shock Waves on Energy Transfer Processes During Femto Second Laser-Induced Melting of Solids***
UC-Riverside	Umar Mohideen, *Department of Physics*	Ming Yan, *Chemistry and Materials Sciences*	***Nanoscale Study of Strain and Strain Dynamics in Laser Materials and Nonlinear Optical Materials***
UC-San Diego	M. Brian Maple, *Inst. for Pure and Applied Physical Sciences*	William Nellis, *Physics*	***Synthesis and Properties Modification of Novel f-electron Materials by Shock Compaction***
UC-San Diego	Frances Hellman, *Department of Physics*	Hector Lorenzana, *Physics*	***Thermodynamic Measurements of High Energy Density Storage Materials***
UC-San Francisco	Thomas Breunig, *Department of Restorative Dentistry*	John Kinney, *Chemistry and Materials Sciences*	***Micromechanical Modeling of Cortical Bone Deformation***

FY99 University Collaborative Research Project (UCRP) Awards

UC Campus	Campus Investigators	LLNL Collaborators	Project Title
UC-Berkeley	Ray Jeanloz, *Department of Geology and Geophysics*	Jeff Nguyen, *Physics*	***High Pressure Synthesis and Characterization of Carbon Nitrides***
UC-Davis	G. Taynas Palmore, *Department of Chemistry*	James De Yoreo, *Chemistry and Materials Sciences*	***Device Miniaturization Through Self-Assembly: An In-Situ AFM Study of Molecular Scaffolds***
UC-Davis	Susan Kauzlarich, *Department of Chemistry*	Howard Lee, *Physics*	***The Study of Photoluminescence in Monodispersed Alkly-Terminated Si Nanoclusters***
UC-Davis	Philip Sterne, *Department of Physics*	Richard Howell, *Physics*	***New Theoretical Framework for Computing Positron Annihilation***
UC-Los Angeles	Nasr Ghoniem, *Mech. and Aero Eng. Department*	Tomas Diaz De La Rubia, *Chemistry and Materials Sciences*	***Dislocation Dynamics Simulations of Deformation Hardening in FCC Metals***
UC-Los Angeles	Richard Kaner *Department of Chemistry*	Hector Lorenzana, *Physics*	***Rapid Synthesis of Materials at High Pressures***
UC-Los Angeles	Greg Carman, *Mech. and Aero Eng. Department*	Troy Barbee, III, *Physics*	***Measuring the Thermal-Mechanical Properties of Multi-Layered Thin Films***
UC-Riverside	Harry Tom, *Department of Physics*	Choong-shik Yoo, *Physics*	***Study of Femtosecond Laser-Heating, Damage and Melting of Semiconductors Under High Pressure***
UC-Riverside	Umar Mohideen, *Department of Physics*	Ming Yan, *Chemistry and Materials Sciences*	***Nanoscale Study of Strain and Strain Dynamics in Laser Material and Nonlinear Optical Materials***
UC-San Diego	Ian Schuller, *Department of Physics*	Jim Tobin, *Chemistry and Materials Sciences*	***Magnetic Circular Dichrosim in Half Metallic Magnets***
UC-San Diego	Bimal Kad, *Applied Mechanics and Engineerimg Science*	Adam Schwartz, *Chemistry and Materials Sciences*	***Experimental Correlations of Deformation Strain Gradients and Grain Boundary Character Distribution (GBCD)***

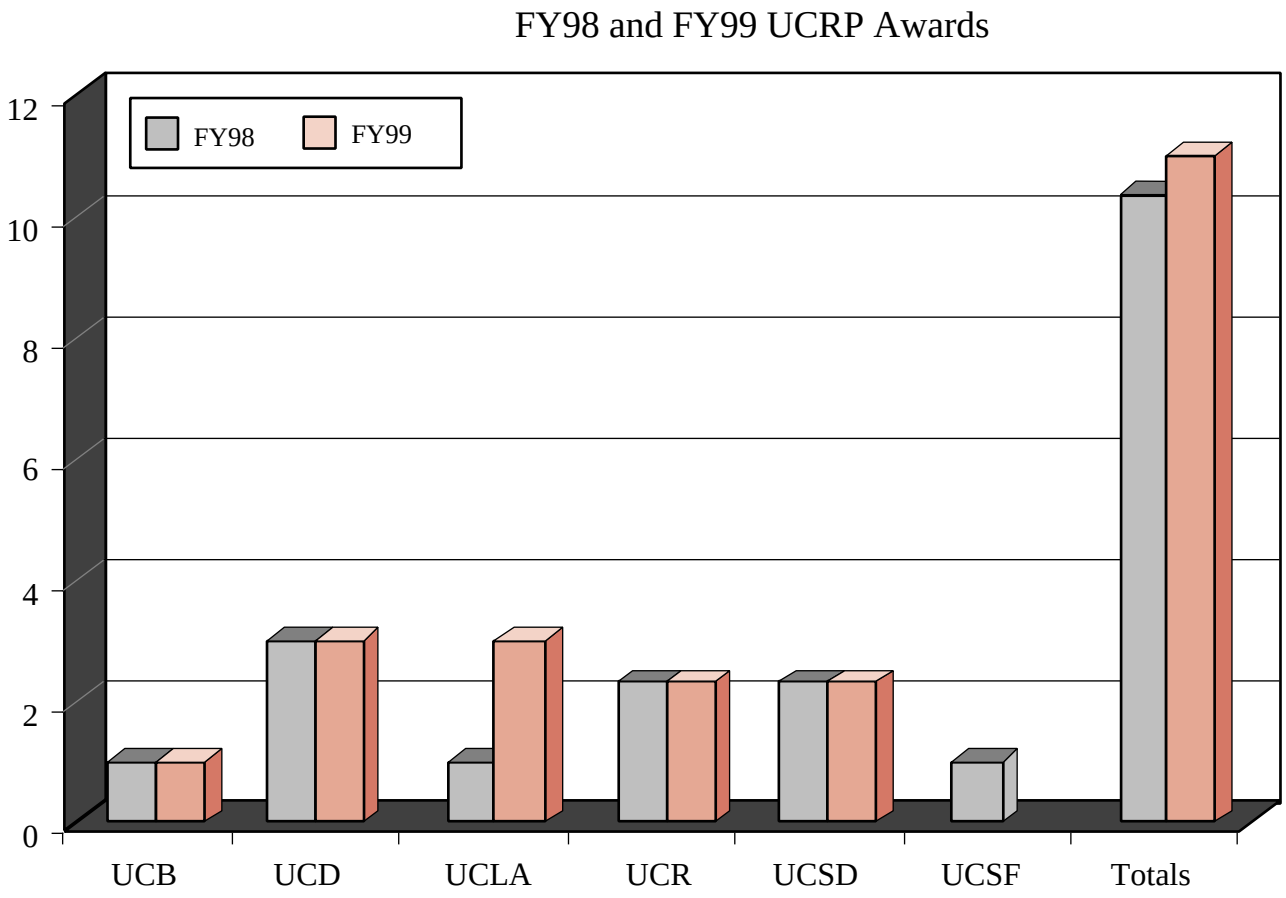
FY98 and FY99 UCRP Awards
FY98
FY99
12
10
8
6
4
2
0
UCB
UCD
UCLA
UCR
UCSD
UCSF
Totals

APPENDIX D

PUBLICATIONS

JOURNAL ARTICLES

Chang, Y.-M., Xu, L. and Tom, H. W. K., "Observation of Coherent Local Optical Phonons Localized at Buried Interfaces Using Time-Resolved SHG", to be published in *Phys. Rev. B*, May 15, 1999.

Chang, Y.-M., Xu, L. and Tom, H. W. K., "Observation of Local-Interfacial Optical Phonons at Buried Interfaces Using Time-Resolved Second-Harmonic Generation", *Phys. Sci. Rev.* (Condense Matter), **59**, (19), APS through AIP, pp.12220-3, 18 references, May 15,1999.

Chin, D. N., Palmore, G. T. R. and Whitesides, G. M., "Predicting the Crystalline Packing Arrangements of Molecules that Form Hydrogen-Bonded Tapes", *J. Am. Chem. Soc.*, **121**, 2113, 1999.

Cynn, H. and Yoo, C., "Equation of State of Tantalum to 174 GPa", *Phys. Rev. B*, **59**, 1999.

Cynn, H., Yoo, C. and Sheffield, S., "Phase Transition and Decomposition of 90% Hydrogen Peroxide at High Pressures", *J. Chem. Phys.*, **110**, 1999.

Demos, S. G., Wang, W. B. and Alfano, R. R., "Imaging Objects Hidden in Scattering Media with Fluorescence Polarization Preservation of Contrast Agents, Applied Optics", **V37**, N4:792-797, February 1, 1998.

Ghoniem, N. M., Singh, B. N., Sun, L. and De La Rubia, T., "Interaction and Accumulation of Glissile Defect Clusters Near Dislocations", to be published, *J. Nucl. Matter*, 1999.

Ghoniem, N. M., "Curved Parametric Segments for the Stress Field of 3-D Dislocation Loops", *Transactions of the ASME J. of Eng. Mat. and Tech.*, **121**, (2), (*Multi-Scale Modeling of Deformation and Fracture*, Washington D.C., USA, 27-30 Sept. 1998). *ASME*, p.136-42. 16 references, April 1999.

Ghoniem, N. M and Sun, L. Z., "Fast-Sum Method for the Elastic Field of Three-Dimensional Dislocation Ensembles", *Phys. Rev. B* (Condensed Matter), **60**, (1), APS through AIP, p. 128-40, 49 references, July 1999.

Hamza, A. V., Schenkel, T., Barnes, A. V. and Schneider, D. H., *Journal of Vacuum Science and Technology*, A **17**, 303, 1999.

Hamza, A. V., Schenkel, T. and Barnes, A. V., "Dependence of Cluster Ion Emission from Uranium Oxide Surfaces on the Charge State of the Incident Slow Highly Charged Ion". *European Phys. J. D*, **6**, (1), EDP Sciences; Springer-Verlag, p.83-7. 26 references, April 1999.

Isaak, D., Carnes, J., Anderson, O. and Cynn, H., "Elasticity of TiO_2 Rutile to 1800K", *Phys. Chem. Minerals*, **26**, 1998.

Kalantar, D. H., Chandler, E. A., Colvin, J. D., Lee, R., Remington, B. A., Weber, S. V., Wiley, L. G., Failor, B. H., Hauer, A., Wark, J. S., Loveridge, A., Meyers, M. A., and Ravichandran, G., "Transient X-ray Diffraction Used to Diagnose Shock Compressed Si Crystals on the Nova Laser", *Rev. Sci. Instrum.* **70**, 629, Jan. 1999.

Kalantar, D. H., Remington, B. A., Chandler, E. A., Colvin, J. D., Gold, D., Mikaelian, K., Weber, S.V., Wiley, L.G., Wark, J. S., Hauer, A. A. and Meyers, M. A., "High Pressure Solid State Experiments on the Nova Laser", *LLNL ICF Quarterly Report*, UCRL-LR-105821-98-3, p.101, Aug. 1998.

Kioussis, N., Turchi, P., Gonis, A., Price, D. and Cooper, B. R., "Electronic Structure Properties of the α and δ Phases of Pu", to be submitted to *Phys. Rev.* B**,** Summer 2000.

Lee, H. W. H., Thielen, P. A., Delgado, G. R., Kauzlarich, S. M., Taylor, B. R., Mayeri, D. and Yang, C-S., "Femtosecond Pump-Probe Spectroscopy of Silicon and Germanium Nanocrystals, in Nonlinear Optics '98". *Materials, Fundamentals and Applications* (New York, NY), p. 200, 1998.

Leppert, V. J., Zhang, C. J., Lee, H. W. H., Kennedy, I. M., and Risbud, S. H., "Observation of Quantum Confined Excited States of GaN Nanocrystals", *Appl. Phys. Lett.*, **72**, 3035, 1998.

Lipp, M. J., Evans, W. J., Baonza, V. G., and Lorenzana, H. E., "Thermodynamic Measurements of High Energy Density Storage Materials", *J. of Low Temp. Phys.* **11**, 247-256, 1998.

Palacin, S., Chin, D. N., Simanek, E. E., MacDonald, J. C., Whitesides, G. M., McBride, M. T. and Palmore, G. T. R., "Hydrogen-Bonded Tapes Based on Symmetrically Substituted Diketopiperazines: A Robust Structural Motif for the Engineering of Molecular Solids", *J. Am. Chem. Soc.*, **119**, 11807, 1997.

Palmore, G. T. R., Luo, T. J., Martin, T. L., McBride-Wieser, M. T., Voong, N. T., Land, T. A. and DeYoreo, J. J., "Using the AFM to Study the Assembly of Molecular Solids Transactions", *Am. Cryst. Assoc.*, **33**, 45, 1998.

Palmore, G. T. R. and MacDonald, J. C., "The Role of Amides in Functional Supramolecular Aggregates and Structures in The Amide Linkage: Selected Structural Aspects in Chemistry, Biochemistry and Materials Science", Eds. Greenberg, A., Breneman, C. and Liebman, J., Wiley, New York, in press, 1999.

Palmore, G. T. R. and McBride, M. T., "Engineering Layers in Molecular Solids With the Cyclic Dipeptide of S-Aspartic Acid", *Chem. Comm.*, **145**, 1998.

Pask, J. E., Klein, B. M., Fong, C. Y. and Sterne, P., "Calculation of Positron Observables Using a Finite-Element-Based Approach", *Appl. Surface Sci.*, **149**, 238, UCRL-JC-131338, 1999.

Pask, J. E., Klein, B. M., Fong, C. Y. and Sterne, P. A., "Real-space Local Polynomial Basis for Solid-state Electronic Structure Calculations: A Finite-element Approach", *Phys. Rev. B*, **59**, 12352, UCRL-JC-132360, 1999.

Rühlicke, C., Schneider, D., Schneider, M., Dubois, R. D. and Balhorn, R., *Nanotechnology*, **9**, 251, 1998.

Schenkel, T., Barnes, A. V., Hamza, A. V. and Schneider, D. H., *European Physical J.*, D, **1**, 297, 1998.

Schenkel, T., Barnes, A. V., Hamza, A. V., Banks, J. C., Doyle, B. L. and Schneider, D. H., *Phys. Rev. Lett.*, **80**, 4325, 1998.

Schenkel, T., Barnes, A. V., Hamza, A. V., Banks, J. C., Doyle, B. L. and Schneider, D. H., *Phys. Rev. Lett.*, **81**, 2590, 1998.

Schenkel, T., Schneider, M., Hattass, M., Newman, M. W., Barnes, A. V., Hamza, A. V. and Schneider, D. H., *J. of Vacuum Sci. Technology B*, **16**, 3298, 1998.

Schenkel, T., Hamza, A. V., Barnes, A. V., Schneider, D. H., Walsh, D. S. and Doyle, B. L., , *J. of Vacuum Sci. Technology A*,**16**, 1384, 1998.

Singh A., Mao H., Shu J. and Hemley R., "Estimation of Single-Crystal Elastic Moduli from Polycrystalline X-ray Diffraction at High Pressure Application to FeO and Iron", *Phys. Rev. Lett.*, **80,** 1998.

Smith, C. A., Lee, H. W. H., Risbud, S. H. and Cooke, J. D., "Ultraviolet-Blue Emission and Electron-Hole States in ZnSe Quantum Dots", *Appl. Phys. Lett.*, **75**, 1688, 1999.

Taylor, B. R., Kauzlarich, S. M., Delgado, G. R. and Lee, H. W. H., "Synthesis and Characterization of Quantum Confined Ge Nanocrystals", *Chem. Mat.*, **11**, 2493, 1999.

Taylor, B. R., Kauzlarich, S. M., Lee, H. W. H. and Delgado, G. R., "Solution Synthesis and Optical Investigation of Germanium Nanocrystals", *Chem. of Mat.*, **10**, 22, 1998.

Turchi, P. E., Gonis, A., Kioussis, N., Price, D. L. and Cooper, B. R., "Electronic Structure of Pu and its Alloys, in Plutonium Futures", *The Science*, p. 313, 1997.

Turchi, P. E., Gonis, A., Kioussis, N., Price, D. L. and Cooper, B. R., "Correlation Effects on Stability in Pu Metal and its Alloys, to Appear in Correlation Effects and Materials Properties", Ed. A. Gonis, N. Kioussis, and M. Ciftan (Plenum, New York, 1999).

Wang, W. B., Demos, S. G., Ali, J. and Zhang, G., "Visibility Enhancement of Fluorescent Objects Hidden in Animal Tissues Using Spectral Fluorescence Difference Method, Optics Communications", V**147**, N1-3:11-15, February 1, 1998.

Yan, M, Wang, L., Siekhaus, W., Kozlowski, M., Yang T. J. and Mohideen, U., SPIE vol. 3244, p. 268, *Proceedings of Laser Induced Damage in Materials*, 1997.

Yang, Y., Leppert, V. J., Risbud, S. H., Twamley, B. and others, "Blue Luminesence from Amorphous GaN Nanoparticles Synthesized In Situ in a Polymer", *Appl. Phys. Lett.*, V74 N16:2262-2264, April 19, 1999.

Yang, Y., Leppert, V. J., Risbud, S. H., Twamley, B., Power, P. P. and Lee, H. W. H., "Blue Luminescence from GaN Nanoparticles Synthesized In Situ in a Block Copolymer", *Appl. Phys. Lett.*, **74**, 2262, 1999.

Yang, C. S., Bley, R. A., Mayeri, D., Kauzlarich, S. M., Lee, H. W. H. and Delgado, G. R., "Synthesis of Alkyl-Terminated Silicon Nanoclusters by a Solution Route", *J. Am. Chem. Soc.*, **121**, 5191, 1999.

PROCEEDINGS/PRESENTATIONS

Fall 1997

Mayeri, D., Yang, C.-S., Kauzlarich, S. M., Delgado, G. D and Lee, H. W. H.; *Synthesis and Characterization of Luminescent Silicon Nanoclusters Terminated With Organic Ligands*, presented at the ACS National Meeting, Las Vegas.

Mayeri, D., Kauzlarich, S. M., Delgado, G. D. and Lee, H. W. H., *Synthesis and Characterization of Luminescent Silicon Nanoclusters Terminated With Organic Ligands*, presented at the CLC Meeting, Los Alamos.

Mayeri, D., Yang, C.-S., Kauzlarich, S. M., Delgado, G. D. and Lee, H. W. H., *Size Control and Blue Luminescence of Silicon Nanoclusters Terminated With Organic Ligands*, presented at the MRS National Meeting, Boston.

November 1997

Palmore, G. T. R., McBride, M. T., Picciotto, E. A. and Reynoso-Paz, C. M., *Physical-Organic Studies of Molecular Solids: Hydrogen-Bonded Tapes and Layers from Diketopiperazines*, Fifth Chemical Congress of North America, Cancun, Quintana Roo, Mexico.

De Yoreo, J. J., Land, T. A., Orme, C., McBride, M.T. and Palmore, G.T.R.; *Studying the Surface Morphology and Growth Dynamics of Solution-Based Crystals Using Atomic Force Microscopy*, Institute for Molecular and Atomic Physics, Amsterdam, The Netherlands.

Howell, R. H., Jean, J., Lin, K. G., Poat, J., Pickett, W., Tong, S. Y. and West, R., *Applications and Advances of Positron Beam Spectroscopy*: Appendix A, Nov 5-7, 1997, UCRL-130205.

December 1997

Lee, H. W. H., Delgado, G. D., Kauzlarich, S. M., Bley, R. A., Taylor, B. R., Mayeri, D. and Yang, C.-S., *Quantum Confinement and Trapping in Group IV Si and Ge Nanocrystals*, presented at the Materials Research Society Fall Meeting, Boston, MA, invited.

March 1998

Lee, H. W. H., Delgado, G. D., Kauzlarich, and Taylor, B. R., *Power Dependent Optical Spectroscopy of Si and Ge Nanocrystals—Implications for the Origin of Light Emission*, presented at the American Physical Society March Meeting, Los Angeles, CA.

Palmore, G. T. R., *Engineering the Structure of Molecular Solids*, Department of Chemistry, University of Nebraska, Lincoln.

Pask, J. E., Klein, B. M. and Fong, C. Y., *Real-Space Approach to Ab Initio Solid State Electronic Structure Calculation Based on the Finite Element Method*, talk at the American Physical Society March Meeting, Los Angeles, CA.

May 1998

Kalantar, D. H., Remington, B. A., Chandler, E. A., Colvin, J. D., Weber, S. V. and Wiley, L. G., *X-Ray Driven Solid-State Hydrodynamic Instability Experiments on the Nova Laser*, presented at the 25th ECLIM, Formia, Italy.

Kalantar, D. H., Chandler, E. A., Colvin, J. D., Lee, R., Remington, B. A., Weber, S. V., Wiley, L. G., Failor, B. H., Hauer, A., Wark, J. S., Meyers, M. A. and Ravichandran, G., *Transient X-Ray Diffraction of Shock-Compressed Crystals Using the Nova Laser*, presented at the MAR 98 Meeting of the APS.

Kalantar, D. H., Chandler, E. A., Colvin, J. D., Weber, S. V., Wiley, L. G., Remington, B. A., Wark, S., Failor, B. H., Hauer, A., Meyers, M. A. and Ravichandran, G., *Transient X-Ray Diffraction Used to Diagnose Shock-Compressed Si Crystals on the Nova Laser*, presented at the 25th ECLIM, Formia, Italy.

Pask, J. E., Klein, B. M. and Fong, C. Y., *Real-Space Approach to Ab Initio Solid-State Electronic Structure Calculation Based on the Finite Element Method*, poster at the Electronic Structure 1998 Conference, Philadelphia, PA.

June 1998

Gonis, A., Kioussis, N. and Ciftan, M., *Electron Correlations and Materials Properties* (Klewer Academic/Plenum Publishers, New York, 1999). International Workshop on Electrons Correlations and Materials Properties, Crete.

July 1998

Palmore, G. T. R., McBride, M. T., Olmstead, M. M., Land T. A. and De Yoreo, J. J., *In-situ Atomic Force Microscopy Studies of the Growth of Crystals of 2,5-Diketopiperazine*, American Crystallographic Association Meeting, Washington DC,

Kauzlarich, S. M., *Zintl Salts for the Solution Synthesis of Surface-Stabilized Si and Ge Nanoclusters*, presented at the American Chemical Society Meeting, Boston, MA, plenary speaker.

August 1998

Yang, C-S., Kauzlarich, S. M., Lee, H. W. H. and Delgado, G. R., *Synthesis and Characterization of Small Silicon Nanoclusters Terminated with Alkyls*, presented at the American Chemical Society Meeting, Boston, MA.

September 1998

Sterne, P. A., Pask, J. E., and Klein, B. M., *Calculation of Positron Observables Using a Finite-Element-Based Approach*, presented at the Eighth International Workshop on Slow Positron Beam Techniques.

November 1998

Breunig, T. M., *Micromechanical Modeling of Cortical Bone Deformation*, presented to the faculty and residents of the Orthopedic Surgery Department at UC-San Francisco.

Cynn, H. and Yoo, H., *Synchrotron, Neutron, and Laboratory Source Crystallography at High Pressure: Experiments, Theory and Related Techniques*, IUCr-HP98, Argonne Nat'l Laboratory, USA.

1998 ANNUAL REPORT

Materials Research Institute

Dr. Harry B. Radousky, Acting Director,
e-mail: radousky1@llnl.gov

Telephone: (925) 422-4478 • Fax: (925) 422-3519
Web page: http://www.llnl.gov:80/urp/MRI/mri.html

Lawrence Livermore National Laboratory
P.O.Box 808, Mail Stop L-413, Livermore, CA 94551